Generation of Frequency Tunable Laser Sidebands in the THz Region

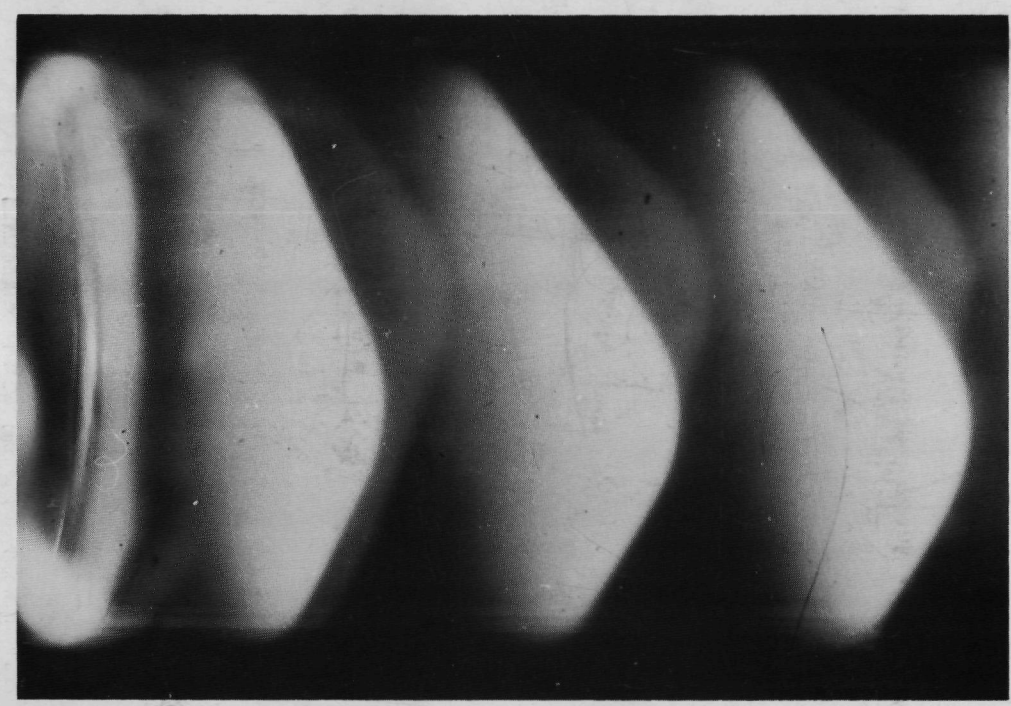

D. D. Bićanić

Krips Repro – Meppel

Generation of Frequency Tunable Laser Sidebands in the THz Region

Promotor: Prof. Dr. A. Dymanus

Generation of Frequency Tunable Laser Sidebands in the THz Region

PROEFSCHRIFT

TER VERKRIJGING VAN DE GRAAD VAN DOCTOR IN DE WISKUNDE EN NATUURWETENSCHAPPEN AAN DE KATHOLIEKE UNIVERSITEIT TE NIJMEGEN, OP GEZAG VAN DE RECTOR MAGNIFICUS PROF. DR. A. J. H. VENDRIK, VOLGENS BESLUIT VAN HET COLLEGE VAN DECANEN IN HET OPENBAAR TE VERDEDIGEN OP WOENSDAG 20 DECEMBER 1978 DES NAMIDDAGS TE 2 UUR PRECIES

door

DANE DANIJEL BIĆANIĆ

geboren te Zagreb (Kroatie), Joegoslavië

1978

Druk: Krips Repro Meppel

"Everything comes if the man will only wait",Benjamin Disraeli
Tancred (1847)

To

Vesna
Iva
Timi

and my parents
who all biased
me.

Contents

Author's foreword

It was a rare privelege for a foreigner like myself, to get first acquanted with The Netherlands in 1964. My father, a passionate admirer of the Dutch polders and my mother, both worked hard to enable for me a three months summer training with the Afdeling Onderzoek of the Koninklijke Nederlandse Heidemaatschappij in Arnhem. While enjoying the warm hospitality of Mr. and Mrs. Eshuis those Arnhem days, nothing seemed less probable than my own graduation almost fifteen years later at practically the same place .....

These thoughts repeatedly crossed my mind during the preparation of the "boekje", and this short preface serves to express my sincere gratitude to all of those who participated in the project the results of which are described in this thesis. True ..... an promovendus never does all his graduate work alone, but the nature of my own experiment in particular, required inevitable and very intense communication with number of skilled individuals, each specialist in his own field. It was mainly through their patience, enthousiasm, extensive knowledge and substantial effort, that the final goal of this project has been successfully achieved. We all worked very closely together and influence one another, and I need hardly to say how indebted am I to all the members of this "TUNABLE SIDE-BAND". I hope that remembering them all in a drawing created by Mr. John Slippens does them at least some satisfaction and justice.

My thanks further extends (not in the order of significance) to Ir. Marius Kaptein, Mr. Paul Walraven, Mr. Henk Verschoor, Ing. Jos van Bommel, Mr. Jaap van Langen, Mr. Jacques Holten, Mr. Huub Spruyt, and Ing. Adolph Dicke (Botany) and Mr. Jan Geertsen from various Technical Departments for their ever ready stand-by assistance.

Special appreciation is reserved for:

i) all inhabitants who have been populating the room N2094 in the past years (an island of laughing) in particular to Dr. Ben Zuidberg who whiskered me from the insulated layer into the barrier, and for his most valuable help in the last stage of the experiment;

ii) thick bearded, open minded and of joyous nature, Mr. Eugen van Leeuwen, for the friendship developed through many, often contraversial conversations, his deep insight in solving many difficult technical problems and from whom I have learned a great deal;

iii) Mr. Frans de Boer, who made all components of long and short laser, for his frequently demonstrated high professional skill, pride of workmanship, numerous advices and almost proverbial modesty;

iv) my successor, Drs. Erik van den Heuvel, who impressed me by his sense of genuine, coherent search for clear understanding of the problems, and for kindly generating some experimental data during the completition of the thesis. I wish him every success in pursuing the work I might have initiated;

v) Mr. Leo Hendriks and Mr. John Slippens who were always kind enough, and never turned down my appeals to make "just one more, the very last drawing";

vi) Dr. Reinhard Ulrich from Max-Planck Institut für Festkörperforschung in Stuttgart, West Germany, for constructing the metal mest filter and most stimulating collaboration;

vii) colleagues Dr. Brian Prewer and Dr. Jerry Brunt (EMI Electronics Ltd. Wells, England), Dr. James Small and Dr. Harold Fetterman (Lincoln Laboratory, Massachussets Institute of Technology, Lexington, USA), Dr. Clifford Bradley (National Physical Laboratory, Teddington, England), Dr. Jerry Wrixon (University of Cork, Ireland), Prof. Koji Mizuno (Tohoku University, Sendai, Japan) and Dr. Olek Wittlin (Polish Academy of Sciences, Warsaw, Poland) who either provided Schottky barrier diodes or contributed otherwise via number of important suggestions throughout the past years;

viii) Dr. Bob Parent and Mrs. Lies Remers-Dreuning who patiently and meticulously revised and typed the manuscript, so that all remaining errors can be claimed as my own work, and to

ix) Drs. Ben Westermann and Prof. Anica Jušič (Medical Faculty, University of Zagreb, Yugoslavia) whose distinctive guidance, understanding and moral support helped me to comprehend that the conservation of energy truly exists.

I acknowledge also deepest appreciation to my ever restless, prudent and affectionate parents who gave me a happy youth and required drive, implanted optimistic life spirits and taught me to be concerned about those around me, and whose direct share in completing this thesis is unmeasurable.

At last, but at most, thanks to my wife Vesna, not only for a tireless care, concern and support she has offered in every possible way, but much more for sacrifying unselfishly her own talents and ambitions in order to make this possible. Together we have undertaken this adventure, and learned to know the narrow passband character of fascinating graduate student life.

And finally, thanks to Iva and Timotej, our intensely radiating sum and difference frequency children, who were also generated in the course of this experiment, and to whom I promise never to write another "boekje" again ...


ONTVERP
Peter Claus
Peter v Dijk
John Holtkamp
LETTERS


TUNABLE SIDE-BAND
Hans Pfeiffer
Ben Zuidberg
BAK

CHAPTER 1

Introduction

1.1 Historical remarks and the goal of this project

There is no generally adopted definition of the extent of submillimeter portion of the electromagnetic spectrum. Most experimentalists, including us, quote it as the wavelength range extending from 100 μm to 1000 μm (frequency range 300 GHz to 3 THz). This part of the electromagnetic spectrum, linking the infrared to microwaves, has been only partly explored in the past, mainly due to the paucity of strong radiation sources and detectors operating efficiency at the submillimeter wavelengths. Radiation emitted by traditional, incandescent hot body source is too feeble for all practical purposes.

Submillimeter waves have nevertheless been attracting scientists ever since 1923 (GLA 24, NIC 23). During the World War II, and in the postwar years, short-wave generators such as radar, klystron and carcinotrons have been invented and further perfected. With the time, steadily shorter wavelengths have been reached by these sources. Radiation provided by such generators had ideal properties for the experimentalist: highly monochromatic, easily tunable and modulated both in amplitude and frequency, and large output power. High resolution microwave spectroscopy performed with these sources enabled precise and systematic study of structure and properties of a large number of molecules.

However, further extension of this direct power generation beyond one millimeter mark had proved a difficult task. As the turn of the fifth decade, Prof. Walter Gordy and his collaborators at Duke University, Durham, North Carolina, USA began to investigate semiconductor diode devices as generators of higher harmonics of the klystron radiation. With this indirect generation method, well known microwave techniques could be extended to

higher frequencies resulting in the surmounting of the submillimeter barrier (1 mm) in 1964 (GOR 64). Important contributions to the submillimeter spectroscopy came out of this laboratory during the last fifteen years (HUI 66, DIJ 71, ZUI 77).

Many applications require tunable coherent submillimeter radiation but even the harmonic generation becomes unapplicable at very high frequencies because of very low output power, and the quest for a novel, more powerful submillimeter sources went on. The advent of strong infrared lasers (CO_2) changed drastically the situation. A rather common concept for generating tunable submillimeter radiation was to use two of such strong lasers operating at slightly different frequencies and mix their radiation in a non-linear crystal to produce difference frequency in the submillimeter region. Zernike and Berman (ZER 65) were historically first to report detection of submillimeter output near 100 μm by mixing a large number of modes of a Nd: glass laser pulse in quartz crystal. In crystals lacking the center of symmetry, large dielectric non-linear polarization with magnitude proportional to the product of the applied fields can be induced. This non-linear polarization, can in principle permit the launching of substantial radiation at frequencies given as linear combination of the interacting frequencies. Such quadratic effects were of course unattainable with ordinary, non-coherent sources, because of low electric field intensities. Radiation of strong infrared lasers, however, when focussed to a small area can produce fields approaching the strength of the internal ("built-in", cohesive) fields in the matter ($\sim 10^9$ V/cm).

Infrared lasers are powerful, highly monochromatic sources, but unfortunately of practically zero tunability. Never-

theless, these lasers were used in various geometrical schemes, relying on the non-linear properties of the crystals, to generate radiation tunable over a wide range. For detailed literature survey, interested reader is referred to recent review and papers (SHE 76, SHE 77, KUH 74).

In recent years, following the advent of the first HCN submillimeter laser of Gebbie (GEB 64) development of other submillimeter lasers has become an rapidly growing and expanding activity. Shortly after optically pumped lasers, transversely excited lasers, waveguide lasers ... to name a few emerged. Large number of submillimeter wavelengths is currently available to experimentalists; their number increasing virtually continuously (RAD 75, ROS 76).

In the last decade considerable amount of research work aimed to the achievement of the submillimeter emission from the millimeter end has been performed. Advances in fabrication techniques resulted in development of semiconductor, metal-dielectric-metal, monolitic and integrated junctions of small contact area with promising properties both for generation and detection at submillimeter wavelengths. Initially, these devices were used as detectors and later as mixers in frequency stabilization and measurement of submillimeter lasers (HOC 67, BRA 72). Thin film technology has made possible production of small area printed junctions possessing high non-linearity, and good frequency response up to 1 THz (SMA 74). Improvements in the material quality and lithographic techniques also contributed to development of Schottky barrier diode (SB) that first rivaled and eventually surpassed its well known counterpart, the point contact (PC) diode. The usefulness of a Schottky barrier diode both in mixing and video mode has been confirmed experi-

mentally at frequency as high as 4 THz (HOD 77). Few experiments have been tried to obtain submillimeter radiation by frequency mixing of two CO_2 lasers (or of an HCN laser and a microwave source) in various kind of diodes (SAN 72, SMA 73, GUS 74), but the generated signals were too weak and only step tunable, so that no spectroscopic application could be made.

The primary goal of this project (*) undertaken late in 1972 was to develop a strong and tunable submillimeter source for high resolution spectroscopic research over a broad frequency range. This goal has indeed been achieved by producing tunable sidebands via frequency mixing of submillimeter HCN laser and klystron in a point contact (PC) or Schottky barrier (SB) diode acting as non-linear element. In doing so, is the extent of tunability range of the klystron transferred into the submillimeter range. Prominent advantage of this technique, when compared to direct harmonic generation at these frequencies, is evident by the fact that powers in the reradiated sidebands were sufficiently strong ($\sim 10^{-7}$W) to allow high resolution spectroscopy ($\sim$ 2 MHz linedith at $\sim$ 1 THz) on hydrogen sulphide (H_2S)

(*) Throughout this thesis, frequency of radiation will be given in GHz. Occasionally, when thought appropriate, corresponding wavelength in microns (μm) or in wavenumbers (cm^{-1}) will be given in parenthesis. Following relationships enable quick conversion between different quantities (an arrow means "is equivalent to"):

100 μm → 100 cm → 3000 GHz.

in (800 - 1037) GHz range. Observations of absorption lines, the first ever performed with this high resolution technique, present the evidence that essentially microwave methods can be used successfully even at frequencies exceeding 1 THz.

The thesis is divided into five chapters. Chapter 1, besides giving a short historical survey and stating the goal of this project, also deals with two experimental methods suggested for submillimeter sideband generation using a laser and a klystron source: (1) mixing in bulk media and (2) mixing in point-contact devices. Originally, the intention was to attempt the generation by mixing in non-linear crystals, but low conversion efficiency, resulting in estimated expected power level of 10^{-11} W (see Sect. 1.2.2) made this approach not applicable. Only the basic description of the generation method using point-contact devices as non-linear element is presented in Chapt. 1. Details are discussed, in extenso, in Chapt. 4.

Because, the expected power in the generated sidebands is directly proportional to the output power of the interacting sources, it was necessary to build a strong and stable submillimeter laser. Chapter 2 is devoted to the constructional and operational details of an elaborate 8 m HCN laser design using Michelson interferometric coupler and operating in continuous wave mode. All experiments that have been performed (with an 4 m HCN laser) in order to get the highest possible laser output are discussed in Chapt. 3. Large number of media have been investigated, some also with hydrogen gas added to the basic laser fuel. The chapter is completed by construction and performance data of a pulsed 4 m HCN laser, and the experimental results obtained with 4 m continuous wave HCN laser using a confocal resonator and hole output coupler.

Chapter 4 is fully concerned with the point-contact devices used in the sideband generation experiment. Description of all components of the spectrometer is given followed by survey of experimental results. Finally, measurements on absorption lines of SO_2 and H_2S gases are discussed. Closing remarks concerning present state of art, outlook and suggestions that may lead to improved performance of developed technique are summarized in Chapt. 5.

1.2 Mixing in bulk crystals

1.2.1 The non-linear polarization

When a crystal which lacks the symmetry center is subjected to an alternating electric field, the time polarization density $\vec{P}$ which results from the induced distortion of the internal electric charge will not be exactly proportional to the applied electric field $\vec{E}$. The relationship between these two quantities can be written as (SHE 77):

$$\vec{P} = \varepsilon_0 \underset{\sim}{\chi} (\vec{E}) \cdot \vec{E} \qquad (1.1)$$

where $\underset{\sim}{\chi}(\vec{E})$ is the field dependent susceptibility and ε_0 is the permitivity of the free space. For intense electric field, it is customary to expand this expression in terms of non-linear susceptibility tensors of different order:

$$\vec{P} = \varepsilon_0 [\ \underset{\sim}{\chi}^{(1)} . \vec{E} + \underset{\sim\sim}{\chi}^{(2)} : \vec{E}\,\vec{E} + \underset{\sim\sim\sim}{\chi}^{(3)} \vec{E}\,\vec{E}\,\vec{E} + \ldots\ ] \qquad (1.2)$$

where $\underset{\sim}{\chi}^{(1)}$ is the linear susceptibility tensor, and $\underset{\sim\sim}{\chi}^{(2)}$ and $\underset{\sim\sim\sim}{\chi}^{(3)}$ are quadratic and cubic non-linear susceptibility tensors respectively. Higher order terms in above equation are

small compared to the linear term except, of course, in very high fields. When the electric field consists of two components at different frequencies, the induced non-linear polarization can radiate at frequencies of the sum and difference and the overtones of the interacting frequencies. Hence, fraction of the incident energies used to create the non-linear polarization can be reradiated at number of different frequencies. The induced polarization at say, difference frequency ω_3 given as the frequency difference $\omega_1-\omega_2$ of driving fields is due to the $\underset{\sim}{\chi}^{(2)}$, and for the i-th component of $\vec{P}$ in Cartesian coordinates Boyd (BOY 71) gives the following expression:

$$P_i(\omega_3) = \varepsilon_o 2 \sum_{j,k} d_{ijk}^{(2)} E_j(\omega_1) E_k(\omega_2) \qquad (1.3).$$

In this equation $d_{ijk}^{(2)}$ is the ijk-th element of the non-linear susceptibility tensor and depends on the frequencies, temperature and the orientation of the crystal axes; E_j and E_k are the j-th and k-th component, respectively, of waves at frequencies given in parentheses. Under certain experimental conditions, depending on the three frequencies involved in the non-linear mixing process, the number of non-vanishing tensor elements in the above equation can be considerably reduced (KLE 62). As the subscripts j and k can be reversed due to the arbitrariness of the sequence in which the product is taken $d_{ijk}^{(2)} = d_{ikj}^{(2)}$, so that tensor components can be written in reduced (d_{il}) form with contracted notation 11 → 1, 22 → 2, 33 → 3, 23 and 32 → 4, 13 and 31 → 5 and finally 12 and 21 → 6 (NOW 75). Thus $d_{111}^{(2)} = d_{11}^{(2)}$, $d_{112}^{(2)} = d_{12}^{(2)}$, etc. Coefficients d_{il} describe intrinsic properties of the crystal. Equation (1.3) is often written in a different form (BOY 73):

$$P(\omega_3) = 2\varepsilon_o d_{eff} E(\omega_1) E(\omega_2) \qquad (1.3a)$$

in which E's represent scalar magnitides of the interacting fields and d_{eff} is the effective non-linear coefficient usually one or a combination of $d_{ijk}^{(2)}$ components depending on the crystal orientation. The advantage of this reduces the problem to one dimension, and that three dimensionality can easily be restored, if required. The appropriate relationships for d_{eff} have been calculated for different classes of crystal symmetry and can be found in standard references on non-linear optics (ZER 73, NYE 60, MID 65).

Before closing this section, it is useful to point out that non-linear sideband generation in bulk crystals can be thought of as arising from the mixing process of the carrier and modulating field through the non-linear susceptibility. In other words, the sidebands are associated with the phase modulation of the carrier, resulting from the alteration of the dielectric constant induced by the modulating field through the non-linear susceptibility coefficient.

1.2.2 Bulk crystal mixing experiment

Generation of submillimeter sidebands, the main goal of this research project, can in the principle be achieved by mixing the output of an HCN laser and a klystron in a suitable non-linear crystal. The principal requirement imposed on the non-linear crystal is to have large value for relevant non-linear coefficient and its transparency at all three frequencies involved in the non-linear interaction (the two interacting and the generated frequencies). For high conversion efficiency the interacting fields should be strong because the expected power at the sidebands is proportional to the product of the input powers and d_{eff} squared (SHE 77). Large d_{eff} value

is of particular importance in submillimeter mixing experiments because only moderate field strength that can be achieved with an HCN laser (when compared to the intense infrared lasers. To the best of our knowledge, the only experiment performed with an HCN laser as the input source in submillimeter bulk mixing is that of Bridges et al. (BRI 70), in which two HCN laser frequencies (964 GHz and GHz) with total output power of 100 mW were mixed in $LiNbO_3$ crystal to produce 5 x 10^{-15} W of radiation as the difference-frequency at 74 GHz.

Here we will propose an experimental arrangement for the generation of tunable submillimeter sidebands by mixing radiation of millimeter wave klystron ($\sim$ 70 GHz) with that of an HCN laser (890 GHz) in a $LiNbO_3$ loaded waveguide. This crystal material (3 m class symmetry) was chosen because of its well known non-linear properties in the submillimeter region (BOY 71). As all three frequencies (fundamentals and sideband frequency) are below the lattice absorption band (BOS 66, AGE 68), significant contribution of the ionic susceptibility to the non-linear coefficient can be expected (GAR 68).
The two interacting fields are coupled in the manner shown in Fig. 1.1. The radiation of the HCN laser, at angular frequency ω_1, is focused on the crystal with a lens, and enters the waveguide through the horn. The crystal fills the RG-99/U waveguide completely. The millimeter wave power at angular frequency ω_2, is fed through the directional coupler. The crystal is oriented with its optic axis parallel to the shorter dimension of the waveguide. Both incident fields are linearly polarized parallel to the optic axis of the crystal; the experimental situation which is easy to realize in practice. By convention, both waves are called extraordinary since the electric field

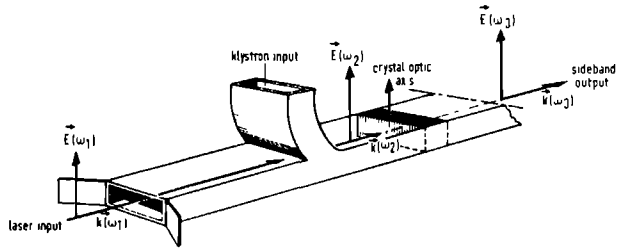

Fig. 1.1 Collinear frequency mixing of HCN laser and klystron radiation in $LiNbO_3$ loaded waveguide.

vectors are constrained in the plane formed by the optic axis and the propagation vectors. Conservation of momentum requires that the signal at ω_3 is also an extraordinary wave. This type of non-linear interaction is an example of collinear forward wave mixing, where the Kleinmann criterion is valid (KLE 62). However, phase matching which is important for efficient mixing with three extraordinary waves is not possible in this simple geometrical arrangement (ZER 73). The relevant, non-vanishing tensor component $d_{eff} = d_{33}$ which is fortunately quite large for $LiNbO_3$(BOY 71). For collinear mixing, the measure of residual momentum mismatch $\Delta k = (k_1 - k_2) - k_3$ is the reciprocal of the coherence l_{coh} length ($l_{coh} = \frac{\pi}{\Delta k}$) and can be evaluated from the crystal dispersion data. Coherence length is defined as the characteristic crystal thickness at which the generated output (in absence of absorption) reaches its first maximum. Since in our specific example, $\omega_2 \ll \omega_3 < \omega_1$ long coherence length are allowed, and long crystals can be used (this is important as crystal length squared enters the relationship for power at sideband frequency). By placing the crystal in the waveguide, the coherence length is increased (CHA 68).

The magnitude of the submillimeter sideband power at

The magnitude of the submillimeter sideband power at $\omega_3 = \omega_1 - \omega_2$ has been calculated following the method given by Chang et al. (CHA 68) for the frequency mixing of two focused laser beams in a waveguide loaded crystal. In MKS units this expression reads out:

$$P(\omega_3) = \frac{4}{3}\sqrt{\frac{\mu_o}{\epsilon_o}}\left[\frac{\omega_3(n_1\omega_1 - n_2\omega_2)^2}{c^3 n_1^2 n_2^2 K_{30}}\right](2\,d_{eff})^2\,P(\omega_2)\left(\frac{l^2}{a_1 b_1}\right) \quad (1.4)$$

with μ_o, c, l, a_1 and b_1 being the magnetic permeability speed of light, crystal length, waveguide width and height, respectively. The refractive indices, and input powers at appropriate angular frequencies are indicated by n_1, n_2, $P(\omega_1)$ and $P(\omega_2)$. The parameter K_{30} is given by (CHA 68)

$$K_{30} = \frac{\omega_3}{c}\sqrt{K_3 - \left(\frac{c\pi}{\omega_3 a_1}\right)^2} \quad (1.5)$$

where K_3 is a dielectric constant of the loaded waveguide. Equation (1.4) assumes that electrical fields $\vec{E}(\omega_1)$ and $\vec{E}(\omega_2)$ are both parallel to the vertical axis of the waveguide, and that both input beams are spatially identical Gaussian beams. Further assumptions involve requirement impossed on the coupling coefficient $\pi W^2 << a_1 b_1$ (W is the beam radius), $l < l_{coh}$ and propagation of difference-frequency in the fundamental mode. Not all of these requirements are met in the experiment shown in Fig. 1.1. Assuming 500 mW microwave power and 50 mW HCN laser power, and using the room temperature dispersion data for $LiNbO_3$ of Bosomworth (BOS 66), useful sideband output powers in the order of 10^{-11} W have been computed (BIC 74a). Based on data of Wittlin (WIT 76) and Bosomworth (BOS 66), reducing the crystal temperature to 80^oK would yield 80 times stronger signals maintaining the same geometrical arrangement of Fig. 1.1.

This figure for useful output accounts for internal transmission losses (Eq. (1.4) corrected with known values of absorption coefficient at three frequencies), but does not take in consideration surface reflection losses. In order to obtain more power at the sideband, all possible orientations of the fields with respect to the crystal should be studied (components d_{51} and d_{13} for $LiNbO_3$, both larger than d_{33} used in above example, could be used for instance. Varying the orientation of the driving fields with respect to the optic axis would also allow the phase matching by angle tuning ($LiNbO_3$ is birefringent).

The 10^{-11} W calculated sideband power should be regarded only as a rough estimate, and confidence in the number requires the performance of the actual bulk mixing experiment. It is however worth mentioning, that the discrepancy between the calculated value and the amount of sideband power obtained in practice is quite considerable in this type of experiments, sometimes even few order of magnitudes. This conclusion is based on author's study of literature data available for number of difficult mixing experiments performed with other laser sources and bulk media.

1.2.3 The choice of the non-linear crystal

In the previous sections $LiNbO_3$ was considered as the nonlinear crystal for the generation of the submillimeter sidebands. However, any crystal lacking inversion symmetry and transparent to in the region of interest, that possesses nonlinear properties such as large refractive index, low dispersion or considerable briefringence is a possible candidate. Further, relatively long crystals should be available. Because of the low output powers of the HCN laser and the millimeter wave klystron, high dammage treshold is not required.

Millimeter wave and in particular submillimeter wave data of interest for the mixing experiment described in Sect. 1.2.2 are scarce. In recent years the availability of various submillimeter sources has enabled the measurements of some of these quantities. An exhaustive literature study was carried out by the author to select the most promising non-linear crystals, and in certain cases crystal manufacturers were consulted (BIC 74a, BIC 74 b). A short survey of the most promising materials is given below.

$LiNbO_3$ Lithium metaniobate has been used as an electro-optical crystal for quite some time. Kaminow et al. (KAM 70) reported electro-optical modulation of an He-Ne laser beam at 4.74×10^2 THz (0.63 nm) with an HCN laser oscillating at 890 GHz. The power converted into the sideband was roughly 10^{-5} of the incident carrier power for each watt of submillimeter power. Lithium metaniobate has quite large non-linear coefficients ranging from $(10^{-7}-10^{-8})$m/V (BOY 71). It is practically transparent at millimeter wavelengths, but exhibits unfortunately considerable absorption in the submillimeter region particularly at room temperature (BOS 66). Refractive indices are quite large at three frequencies involved in the submillimeter mixing experiment described above, and dispersion is low in the same range. Recent measurements of Witlin (WIT 76) indicated considerable decrease of the absorption coefficient at reduced temperature.

$LiTaO_3$ Barker et al. (BAR 74) have determined the values of the dielectric constant at several temperature for $LiTaO_3$ which has the same symmetry as $LiNbO_3$. The absorption is also similar to that measured in $LiNbO_3$ with the exception of the extraordinary ray, for which a 2.5 times larger value for absorption coefficient has been observed. Cooling lowers the at-

tenuation but even at $15^{o}K$ the absorption coefficient is a few cm^{-1} near 40 cm^{-1} frequency. The value of the d_{33} coefficient is 2.5 times larger than that of $LiNbO_3$(BOY 71).

CdS Cadmium sulphide has 6 mm symmetry. Values of refractive index and the absorption coefficient at relevant frequencies for the submillimeter mixing experiment are not very well known. There is considerable lack of agreement among the absorption data published for this material (YAJ 70). At microwave frequencies data of Boyd (BOY 71) and unpublished results of Tacke (TAC 75) are available. Refractive index is 3.0 for wavelengths close to and higher than 500 μm (BER 63). A fully compensated crystal bar of CdS (to eliminate charge carrier absorption) purchased from Cleveland Crystals Inc. might be a good choice for the non-linear material in the contemplated mixing experiment.

$ZnGeP_2$ Ternary chalcopyrite ($\bar{4}2m$ symmetry) has been intensively studied in recent years because of its acentricity and large refractive index by Isomura (ISO 75), who kindly provided single crystal bar for our laboratory. Some non-linear infrared properties have been studied by Boyd (BOY 72).

GaAs Gallium arsenide has been one of the most commonly used non-linear crystals in numerous experiments performed with CO_2 lasers. Most of them are described in book edited by Shen (SHE 77). Corcoran et al. (COR 70) produced tunable coherent signals in the infrared region by mixing a radiation of millimeter klystron and that of a CO_2 laser in a GaAs loaded waveguide. Substantial quasi tunable sum and difference-frequency sidebands have been obtained by intracavity modulation of CO_2 laser with GaAs (BON 74). Dielectric properties of GaAs in the submillimeter region have been studied by Johnson et al. (JOH 69). Transmission at millimeter wavelengths is quite high and

the non-linear coefficient is relatively large (BOY 71). The restrahlen resonance frequency is 8.06 THz (37.2 μm).

Other materials such as CdTe, ZnSe, ZnS and ZnSe might be useful (DAN 74, HAT 73), but most of them are currently still under development. The same applies to the lithium iodate $LiIO_3$, proustite $Ag_3A_sS_3$ and to a few other ternary compounds. As only incomplete literature data is available no definite conclusion can be reached (NIK 77).

Based on the author's own calculation for several crystals, the expected sideband power will not exceed 10^{-11} W with the available input powers of the lasers and klystron (BIC 74b). This is unsufficient for the spectroscopic applications. The amount of power that would become available by using optimum geometry to meet the phase matching conditions is difficult to estimate reliably. However, the prospects for this type of experiment do not look favourable, and it was therefore necessary to consider the use of another kind of non-linear device, a metal-semiconductor diode, for the generation of tunable submillimeter sidebands.

1.3 Generation of tunable submillimeter sidebands using point contact (PC) and Schottky barrier (SB) diode

1.3.1 General remarks

In the past few sections we have discussed the generation of submillimeter frequency sidebands using acentric crystals as the non-linear media. A number of laser and millimeter resea - chers in the past years have tried frequency mixing experiments using diodes fabricated from advanced semiconductor materials in order to produce a monochromatic, frequency tunable source in the submillimeter band. In particular, the research group of

Prof. Ali Javan at the Massachusetts Institute of Technology, Lexington (USA) has been active in performing such experiments with various lasers and microwave klystrons (or radio frequency sources).

In an experiment designed for the achievement of the same goal as of this project, Dr. James Small from Prof. Javan's group (SMA 73) has mixed the 25 mW radiation of a HCN laser with that of a 70 GHz klystron in an open type point contact mixer. The radiation emitted from the diode was collected by a lens and collimated to a parallel beam. The detection was performed at a distance of about 1 m away. With the heterodyne technique faint sideband signals of approximately 10^{-10} W were observed. An attempt to detect the mixing producs directly using a diffraction grating to separate the sidebands from the forward scattered laser radiation was not successful despite the availability of a He cooled detector capable of detecting 10^{-13} W at 300 μm. Insufficient supression of the fundamental laser power was recognized as the major cause of the failure. Construction of Fabry-Perot filters using metal meshes has been initiated to achieve higher rejection, but to the best of author's knowledge no data has yet been reported. In an outgrowth of this experiment, Fetterman et al. (FET 78) using essentially a new mixer design, obtained tunable submillimeter radiation.

Sanchez (SAN 72) was the first to report the usefulness of the metal-oxide-metal (MOM) diode as the mixer of CO_2 laser radiation and that of klystron. He obtained weak amount of ($\sim 5 \times 10^{-11}$ W) difference-frequency sideband power. In another experiment reverse to that of Sanchez, Gustafson and Bridges (GUS 74) reported detection of low power ($\sim 10^{-11}$ W) millimeter

radiation obtained as difference-frequency wave by mixing two pulsed CO_2 lasers in a MOM diode.

The Nijmegen group with which the author was associated has a long tradition in millimeter and submillimeter wave spectroscopic work (HUI 66, DIJ 71, ZUI 77) using point contact diodes in harmonic generation and superheterodyne experiments. It therefore seemed quite appropriate to proceed with this research project along this familiar line. The use of a diode (formed by a metalic antenna-whisker in contact with a semiconductor surface) as mixer is based on the non-linear dependence between the current (I) and the voltage (V). In the frequency domain, a mixer can be thought of as a device with one or more input frequencies f_{inp} that determine the output frequency f_{out}. The output frequencies at the mixer terminal are given as the linear algebraic combination of f_{inp}'s:

$$f_{out} = z_1 f_{inp_1} + z_2 f_{inp_2} + \ldots z_i f_{inp_i} \qquad (1.6)$$

where z_i can take one of the integer values 0, $\pm$ 1, $\pm$ 2 ... etc. The order of mixing is defined as the sum of the absolute values of z_i (this definition also includes rectification, namely $f_{out} = 0$). The production of frequency tunable sidebands by mixing the fundamental frequencies of the laser and klystron is according to the above definition a second order non-linear process.

In general, the coupling of the radiation field at a certain frequency to the diode will result in the development of an alternating voltage across the diode at the same frequency. Due to the inherent, non-linear nature of the I-V dependence, the current flowing through the diode will not be linearly related to the applied voltage, and it is easy to demonstrate

that this results in a current flowing through the diode that has also frequency components at harmonic frequencies. Similarly, when two sources of radiation, such as a laser and a klystron are coupled to the diode, it can be shown that the total current will have components at their sum and difference frequencies (ORL 64, GRE 66). Such a current component at a specific sideband frequency can then excite the propagating currents in the whisker, that consequently emits the radiation at the sideband frequency.

1.3.2 Direct (video) technique for generation and detection of submillimeter sidebands

The basic lay-out of the experimental apparatus developed here for the generation of frequency tunable submillimeter radiation at both klystron sidebands of an HCN laser carrier frequency using point contact devices is shown in Fig. 1.2. The non-linear device, a PC or a SB diode in irradiated simultaneously by the radiation from the HCN laser (say at 890 GHz) and that of that of microwave klystron at $\sim$ 70 GHz. The klystron frequency is chosen arbitrary to produce 10 % frequency shift of the sidebands, but in principle lower or higher frequencies can be used. The most fundamental requirement for achieving good mixing in the diode (of proper dimension) is, of course, to couple both radiations efficiently into the diode mount. The most efficient mixer configuration for the purposes of this experiment has not been indisputably established (Sect. 4.3.1 and Chapt. 5). However, using three arm mixer, essentially a quasi optical modification of the familiar cross waveguide microwave mixer, we have successfully demonstrated frequency synthesis and obtained usable amounts of tunable sidebands power

with the apparatus shown in Fig. 1.2.

In addition to the efficient coupling of the interacting radiations, there is also a problem of separating the reradiate sideband one wants to use from other frequency components that are simultaneously generated. The fundamental laser frequency accounts for the dominant of the reradiated power. Some of this power is genuinely reradiated from the whisker; the rest is "leakage" formed by the radiation scattered by the whisker that leaks from one waveguide into another within the mixer mount. This leakage was anticipated to be a serious problem when weak sideband signals must be detected. Consequently, the use of a filtering device, capable of 10^6 - 10^7 power rejection at the 890 GHz fundamental laser frequency, but transparent to the sideband was thought necessary. In practice this was realized by using a series combination of grating monochromator and metal mesh filter.

The reradiated beam of composite frequencies generated in the diode (consisting of unmixed 890 Hz laser carrier and sidebands offset by 70 GHz) leaves the mixer and enters the monochromator where it is first expanded and collimated by the parabolic horn (Sect. 4.3.2 and Sect. 4.3.3). After striking the properly positioned grating, the diffracted beam is collected by F/1.6 optics mirror and focussed onto the output slit of the monochromator in front of which the metal mesh filter was mounted (Sects. 4.3.4, 4.3.5 and 4.3.6). To aid in frequency selective discrimination, a Fabry-Perot interferometer could be added to the system. In such way, sufficient spatial and frequency filtration was obtained. The desired sideband radiation is transmitted through the absorption cell containing the gaseous sample under study, and fed to a sensitive detector for further pro-

cessing. In the initial search for sidebands amplitude, on-off modulation of microwave power was utilized together with phase sensitive detection. Later in the course of the experiment, other modulation techniques, such as mixer external bias modulation could be used optionally. For accurate frequency measurements the klystron was stabilized by means of down conversion to a standard crystal oscillator (Sect. 4.8.2). High resolution absorption spectroscopy in THz region of SO_2 and H_2S has been carried out in the Doppler limited region with this experimental system (Sects. 4.8.2, 4.8.3, 4.11).

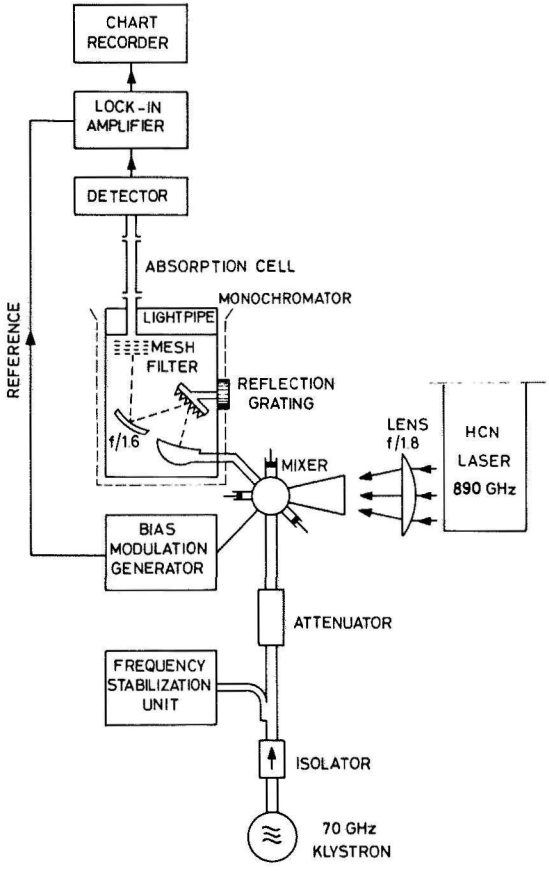

Fig. 1.2 The experimental set-up used for the generation and reradiation of continuously tunable submillimeter sidebands by frequency mixing of laser and klystron radiation in metal-semiconductor diode.

C H A P T E R 2

ENGINEERING DETAILS AND THE HARDWARE OF THE 8 M SUBMILLIMETER HCN LASER

2.1 Introduction

In the previous sections it has been frequently stated that the construction of a high output power submillimeter laser was required for the efficient sideband generation.

The hydrogen cyanide, HCN laser was chosen because of its highest gain. The present free-running and single mode 8 m laser designed to produce continuous wave monochromatic radiation at 890 GHz (337 μm), is the result of the gradual evolution of 4 m long HCN laser constructed by Evenson and his colleagues at National Bureau of Standards at Boulder, Colorado, USA (EVE 71, WEL 71). The excitation of this molecular laser was achieved by the longitudinal glow d.c. discharge pumping of the gaseous mixture (that contains H, C and N atoms) flowing at the low rate. The mechanism of the laser action has been discussed by Lide and Maki (LID 67).

Basic design characteristics of the 8 m laser are shown in Fig. 2.1. The semiconfocal resonator is formed by the spherical mirror with curvature radius of 16 m and the plane mirror separated by 8 m. Vacon 12 invar spacers are used to control the cavity length. Both mirrors are placed inside the evacuated laser plasma tube with inner diameter of 140 mm. The discharge tube has a double wall that can be used as oil jacket. Both electrodes, the cathode (kept at high negative potential) and the anode (grounded) are placed in separate sections of the glass tubing having the same diameter as the plasma tube. Initially, the intention was to close the plasma tube with an 6 mm thich round TPX window, and to stabilize the long laser by means of the piezoelectric translator placed outside the vacuum envelope. This translator carrying the spherical mirror assembly is not shown in Fig. 2.1. However, at the later stage of the experiment,

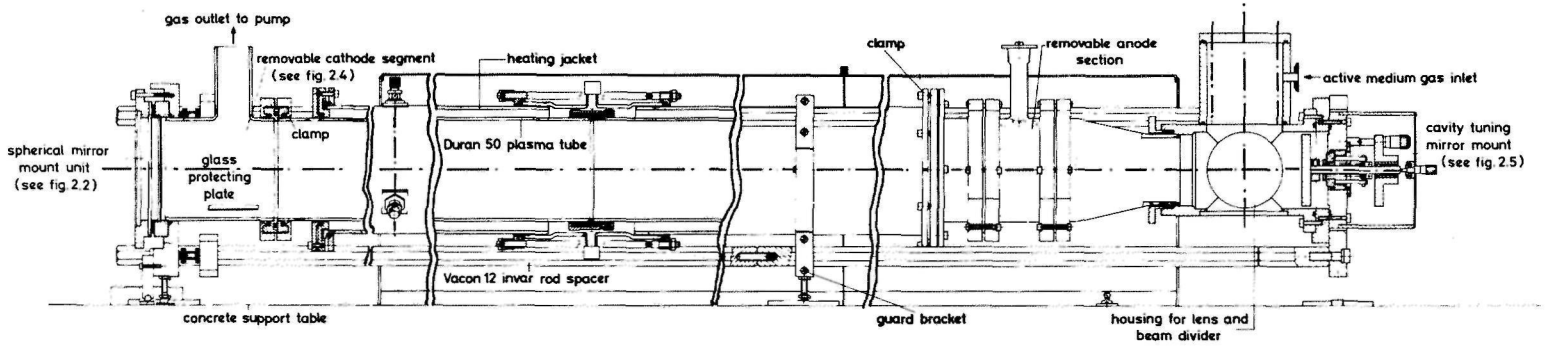

Fig. 2.1 A d.c. longitudinally excited 8 m HCN laser operating in continuous wave mode.

the spherical mirror was mounted in the vacuum and connected to the plasma tube via a large teflon bellows shown in Fig. 2.2. The laser output power is extracted by the variable Michelson interferometric coupler using a 59 μm polyethylene beam splitter positioned at 45^{o} with respect to the resonator axis. Maximum laser power at 890 GHz was about 100 mW under optimal discharge conditions. A continuous wave 4 m HCN laser was operated first here in Nijmegen, and most of the experimental results discussed in Chap. 3 were obtained with this laser. The 8 m laser benefited from the experience gathered with its shorter counterpart, and has only been used in the final stage of this research project.

Constructional and operational details of all hardware components that differ from those used by Evenson are described below. A number of figures illustrating parts of the apparatus are also included. Finally, longitudinal and transverse mode structure has been evaluated for the present laser resonator.

2.2 Laser hardware

2.2.1 Laser plasma tube

Duran 50(Pyrex) glass manufactured by Scott Jena Glaswerk (Mainz, West Germany) has been chosen as the material for the laser plasma tube because of its satisfactory performance with 4 m laser. This borosilicate glass was used because of the moderate power requirements of the glow discharge laser, and hence resistance to thermal shocks was not an prerequisite. Its mean linear thermal expansion coefficient is $3.3 \times 10^{-6}/^{o}C$ in 20^{o}-$300^{o}C$ range. To ensure single mode operation and to have resonator with substantially loss-free optical characteristics, the inner diameter of the plasma tube was found by scaling up

the original design of Evenson. In selecting the thickness, heavy (or medium) wall tubing was prefered to light wall tubing, because the rate of cooling was found to have influence on laser output power (VAN 76). Operation at increased temperature also extends the effective tube lifetime due to the reduced deposition rate of paracyanogen polymer crust at high temperatures (BEL 73).

Due to the considerable difficulties in producing and transporting at 8 m long plasma tube, two 4 m long segments were constructed and joined by means of a clamp. These tubes, were in turn made of 2 m long sections joined together in a glass lathe machine. At all stages of production, the tubing was controlled for uniform bore size with a polished tungsten mandrel. After cooling, the entire structure was critically inspected for residual diameter abberations and for indications of potentially weak spots.

The assembled plasma tube rested on eight equally spaced aluminum guard bracketts. Each of these was provided with three adjustable pins terminated by teflon heads in order to facilitate lateral and vertical centering of the tube, and to provide support. During alignement this construction proved useful. The optical length of the plasma tube was controlled by four Vacon 12 invar spacers that passed through the guard bracketts and joined the two end plates carrying the mirror mounts. Vacon 12 rods 2 m long and of octagonal cross sectional form were supplied by Drijfhout & Zoon's Amsterdam. Basic constituents of Vacon 12 are nickel 28%, 18% cobalt and remaining iron. Physical properties of interest are: density 8.3 g/cm^3; specific resistance 0.45 $\Omega mm^2/m$ at 20^oC, and average linear thermal expansion coefficient $5.3 \times 10^{-6}/^oC$ in 20^o-200^oC range. The choice of Vacon 12 was a compromise made between moderate linear thermal

expansion coefficient value and low cost (in comparison to suprainvar metal alloy and ceramics such as Cervit and Zerodur). However in the course of the experiment, periods of several hours were normally required to eliminate thermal drifts and to obtain constants laser output. For gross stability of laser output, thermal drifts and consequently shifts of cavity length should be kept within the amplification bandwidth of the Doppler broadened gain profile of the laser transition (HEA 68). The estimated lower limit of long term stability is one part in 10^6 if the laser plasma temperature is assumed to be 400^oK. Application of various possible stabilization techniques is certainly worth consideration in order to avoid the annoyance of frequent resonator detuning. Since the glass tube experiences elevated temperatures due to its contact with the hot gas medium, the design featured a large teflon bellows which permitted free thermal expansion of the glass envelope. The teflon bellows, shown in Fig. 2.2, was placed between the glass section carrying the cathode and the spherical mirror mount.

The entire laser rested on a 9 m long concrete bench. The heavy weight of the structure (installed in situ) provide good vibrational isolation.

Although the arrangement of electrodes was similar to that used by Evenson, their mounting was redesigned to allow easy access. Excessive cathode sputtering and leaks were problems that were frequently encountered in the short laser an required cleaning, sand blasting and occasionally reprocessing the entire cathode. A 150 mm long segment of Duran 50 tubing of the same diameter as the remaining plasma tube (i.d. 140 mm) was inserted between the teflon bellows and cathode termination of the main plasma tube. A glass appendage 105 mm long and 45 mm inner diameter was smelted to this Duran 50 segment at right angles to

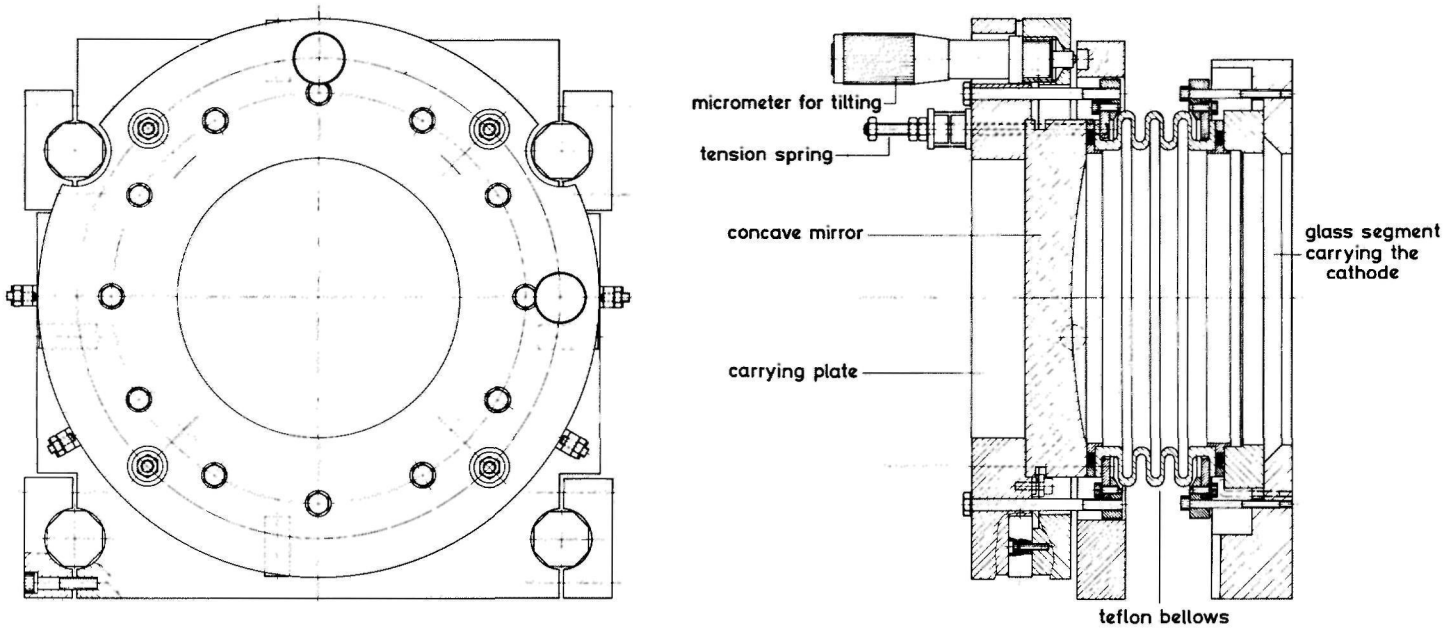

Fig. 2.2 Spherical mirror mount with tilt adjustment screws and teflon bellows.

accomodate the cathode. Either end of the glass segment was fitted with an "o" ring seal, so that it could be easily mounted or demounted without dismantling the entire laser tube. A similar design was adopted for the stainless steel anode to allow its easy removal for cleaning. For transients from glow to arc discharge causing the macroscopical dammage to the material surface, such design proved satisfactory. Another advantage was that the occurrence of irreparable cracks in the glass that caused rejection of the entire laser tube in the past was only a minor problem, as the defected section could be replaced by a prefabricated spare.

The chemical reactions that produce the laser active medium also form a brownish paracyanogen layer on the interior surface of the plasma tube lowers the laser output power.

The deposition rate of translucent polymer crust was inhomogeneous along the tube being highest at the anode side (gas inlet) and decreasing towards the cathode end (gas exhaust). This deposition gradually degrades the optical qualities of the intracavity components and lowers the laser output power. In particular, those components which are kept at a lower temperature than the discharge section (mirrors, beam splitter) are worst affected, and frequent cleaning is necessary because the deposited layer is strongly absorbing at submillimeter frequencies. Fortunately, soaking the optical components in a solution of mild soap or Alconox (cleaning agent) was sufficient to remove the deposit. The contamination rate could be reduced by maintaining the walls at a higher temperature. This was done by enclosing the plasma tube (along the entire tube length) within an aluminum shield. Alternatively, maintaining pure methane discharge for prolonged time produced decontamination of laser tube. Periodic application of these techniques provided a long effec-

tive lifetime of the plasma tube, exceeding practically 3000 hours, before the paracyanogen flakes began to peel off and dismantling of the laser became necessary .

Higher wall temperature is obtainable with the oil jacket that can be mounted around the main plasma tube. Temperature of the tube could be controlled by silicone oil flowing through the jacket. This additional feature was incorporated to enable further research on the previously reported results that increased power and indefinite tube lifetime were possible at higher temperatures (BEL 73, VAN 76). However, at the time of writing no experiments been performed with this thermal jacket on the 8 m laser. However, investigations with the same system on the short laser showed that temperatures higher than $160^{o}C$ measured by a bimetal thermometer could not be achieved, even if the laser was operated at high currents and pressure values. Mainly for the reasons of ease and simplicity, long laser is presently used with a 1 mm thick aluminum shield. The temperature measured externally, directly on the plasma tube near the anode ring section was 90^{o} - $100^{o}C$ under typical operating conditions. The inner wall temperature is unknown, but it was estimated to be 20^{o} - $30^{o}C$ higher under the same circumstances. All temperature readings (by Rueger V-104 bimetal thermometer) were taken above the stainless steel anode in presence of polymer crust which might have affected the measurement in some way.

2.2.2 Vacuum system

The large resonator volume (approximately 140 liters) and relatively low flow rates normally reported in the literature for continuously operated HCN lasers were important in making the proper pump choice. A Leybold-Heraus DK 50 rotary pump

(capacity 300 liters/min) used without cold trap was selected. The vacuum system could be pumped down to the modest pressure of 5×10^{-3} Torr after long pumping time which was found quite adequate. Accurate measurements of gas pressure ranging from 0.1 - 1.5 Torr were performed with a Balzers TPG 022 Pirani manometer. Typical working pressure of the HCN laser was 0.4 - 1 Torr. Because of unknown correction factors for all gaseous media that very studied, comparison of measured values with the readings obtained by an absolute gauge was required. An Mc Leod or oil manometer could be valved into the system at any desired time for that purpose. Experience showed that air should by all means be prevented from coming into the contact with the interior of laser tube, particulary if the latter is hot, as this will cause oxidation of surfaces and accelerate the tube contamination.

Direction of gas flow was reversed from that used by Evenson. An increase in output power by 15% and an improved stability have been observed under the same working conditions with this modification. In the present design, gas is pumped out through the 17 mm diameter central hole drilled in the cathode. As the cathode is kept at a negative potential, well insulated a connection between the pump and the electrode was required. Heavy duty PVC tubing of 63 mm outer diameter and 4.7 mm wall thickness was chosen for that purpose. Total length of the tubing was about 13 m. Such a long distance was required to prevent a discharge striking between the cathode and the pump. The voltage necessary to sustain a glow discharge in the laser tube is dependent upon the product of the interelectrode separation b and the pressure p (LLE 67). A plot of the discharge voltage as a function of b x p, known as the Paschen law, shows a minimum at a particular value of b x p and hence an optimum

value of pressure at which a relatively smooth breakdown will occur for given gas and the electrode separation. At both lower and higher pressures, larger electric fields are required for the discharge to strike. Before striking the discharge,the pressure in the laser tube was about 0.25 Torr (so b x p = 200 Torr cm). Due to the direction of pumping, the pressure in the PVC pumping line was always somewhat less than that in the laser plasma tube. Therefore, in order to prevent the product b x p in the pumping line to assume a value at which the discharge would strike between the cathode and the pump (instead of being constrained within the plasma tube), a very long PVC tubing was used. When two possible paths are accidentally made comparable, discharge in the plasma tube may be extinguished. It was initially discovered that a layer of paracyanogen was deposited along the length of the PVC pumping line. This was apparently due to the discharge striking between the cathode and the pump. The problem was solved by placing the Saunders-Edwards flow regulating valve in the pumping line immediately before the pump. This increased the pressure in the pumping line to a value at which the discharge would preferentially strike between the cathode and the anode.

2.2.3 Discharge characteristics and power supply

The gas plasma tube was excited with a direct current Cober Electronics 1631 - 1768 A power supply capable of 0-12 kV and 0-1.2 A. Ten 270 Ω, 350 W Rozenthal ballast resistors, in series with the power supply and mounted in an fan cooled case, provided reasonable current stability and protection against transients from glow to arc discharge in the laser tube. The laser discharge exhibited usual self sustained, low pressure,

normal glow characteristics. Apart from the dark zones near the electrodes, clearly visible positive column occupied the largest part of the discharge. The general appearance of the discharge is pink. Under certain conditions, the positive column showed striations a visible structure consisting of bright and dark bands in regular succession. The presence of striations was found important in order to obtain stable frequency output of the HCN laser (BRA 72). Various types of striations were encountered. Sometimes the luminous bands were thin and sharply defined and separated by dark bands of much greater width. Changing the discharge parameters could cause a broadening of the bright bands and the appearance of blurred edges. Occasionally, bright strias showed up in pairs, closely coupled to each other and separated by a dark space. Striations were always convex towards the cathode and could one be seen within narrow limits of pressure and current, and even minute changes produced their wandering in the plasma tube. Formation of the striations began at the cathode side (direction of pumping) and then slowly moved towards the gas inlet near the anode side. A Leybold 17317 variable leak valve that could be set in the range from 1×10^{-4} to 50 Torr lit/s was connected to gas inlet to facilitate formation of the steady discharge in this part of plasma tube. Extensive experimental studies with striated discharges helped in establishing typical working conditions of the 8 m laser: 8 kV, 0.8 A, 0.65 Torr hot tube (externally about $95^{o}C$) and a low flow rate of gaseous mixture. These conditions guaranteed ample power output and stable discharge. Considerable deviations from these values led initially to rapid fluctuations in the appearance of the discharge followed by the formation of a highly unstable fishbone like structure that destroyed the column. Unfortunately, lack of time did not allow more work with this relatively little studied phenomenon (THO 33).

The most important quality of the laser medium, its gain factor, is closely related to the discharge parameters. As virtually any mixture that contains H, C and N atoms in some proportion will produce lasing action, difficulties in finding the "best medium" are considerable. Early experimental investigations to determine the unsaturated gain characteristics of the laser at 890 GHz indicated large variations even for mixtures of similar compositions (STA 69). Ammonia and methane mixtures were extensively studied by Svich and Dyubko (SVI 71). Gain characteristics for a methane-nitrogen medium was experimentaly determined by Birch (BIR 73). His data suggested that gain under optimum conditions is inversely proportional to the radius of the discharge tube. Gain factors of 0.028 m^{-1} and 0.037 m^{-1} for striated and unstriated discharge respectively were obtained for a plasma tube with inner diameter of 150 mm. This is close to the size of the plasma tube of our HCN laser. The figure 0.028 m^{-1} suggests a gain of approximately 20 % per single pass (usable discharge length is 7.3 m) for the 8 m HCN laser in the crude approximation assuming loss-free system. This is however not true at submillimeter wavelengths, and the above quoted value is lower than theoretically anticipated (see also Sect. 3.4).

2.2.4 Gas mixing system

Since the laser operated on a flowing mixture, a gas mixing system which controls the composition, pressure and the flow of constituents has been constructed (LEU 76). The present design shown in Fig. 2.3 is a reliable, low cost unit that permits quick interchanging of gases and continuous monitoring of individual flow rates. The unit consists of three identical

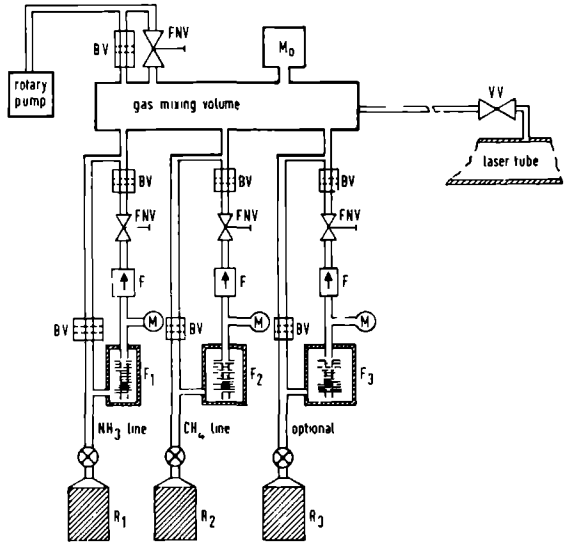

Fig. 2.3 The gas mixing unit used with the 8 m HCN laser. BV two-way Whitey ball valve; FNV Cayon ultrafine flow metering valve; F - Nupro filter; VV - Leybold Heraus 17317 variable leak valve; M_0 - Edwards absolute gauge Capsulon; M - Econosto manometer; R_1, R_2, R_3 gas supply reservoirs; F_1 Porter B-125-10 flowmeter (51 cm^3/min air @ STP); F_2 Porter B-125-6 flowmeter (35 cm^3/min air @ STP); F_3 optional Porter flowmeter B-125-20 (90 cm^3min air @ STP).
(Quoted rates are maximum ones, referring to 150 mm, (full flowmeter scale) deflection).

tubing vacuum manifolds that lead to an $\sim$ 800 cm^3 buffer container where actual gas mixing takes place. Each manifold had a simple absolute manometer indicating pressure in the reservoir, and a metering needle valve for ultrafine flow rate control. In addition a vertically mounted 150 mm long flowmeter

made by Porter Instruments, and a two way ball valve (on-off service) were added to each manifolds. The flowmeter consisted of single tapered glass tube with a spherical float. Depending on the flow rate to be measured carboloy, glass or tantalum floats were used. Maximal air quantity at STP for three flowmeters is specified in Fig. 2.3. Standard accuracy of the flowmeter was five percent of the maximum scale. Readings were corrected with the sizing factor for each gas used, and the reproducibility of measurements was very good. Each line was connected directly to a single stage Edwards Speedivac pump 1SC150B via an separate bypass system. Gases were admitted to the buffer container at a selected flow rate and mixed to a predetermined ratio. An absolute Edwards Capsulon gauge monitored the pressure in the buffer cylinder. A constant pressure was maintained within the buffer chamber by adjusting the needle valve that connected the chamber to a rotary pump. The gas mixture was led to the laser tube through a 12 mm inner diameter flexible hose terminated by calibrated Leybold Heraus 17317 leak valve. Flow rate resetability was very good due to suplementary on/off valve that could be opened or closed independently of the selected setting on the leak valve.

The non-toxic gases used to synthesize the hydrogen cyanide molecule in the electrical discharge were of normal commercial purity. On few occasions gases such as dymethylamine or dyethylether (supplied by Matheson Gas Products) were of higher purity.

2.2.5 The electrodes

As mentioned in Sect. 2.2.1, the cathode was mounted in separate glass section between the teflon bellows and the main plasma tube. Constructional details of the revised cathode are

shown in Fig. 2.4. The cathode was constructed from hard copper tubing with the following dimensions: length 250 mm, inner diameter 17 mm and wall thickness 1.5 mm. Attempts to reduce the wall thickness to 1 mm resulted in a weak structure susceptible to mechanical dammage. The cathode, placed in a 100 mm long section of non-flared glass, was sealed to the surrounding glass envelope via a copper collar with two "o" ring seals. This insured the accurate centering of the cathode and prevented the cathode from touching the glass. Experience with the 4 m laser had shown that contact between the glass and the cathode led to the breakages (cracks, blisters) of the glass tube.

A transparent plastic cage was mounted around the cathode to prevent anyone inadvertently touching the electrode. The cathode is cooled along its entire length by running tap water at a low flow rate. An insulating teflon cylinder 120 mm long with inner diameter 25 mm and NW 25 flanges on either end, was used to link the cathode to the heavy duty PVC pumping line. High temperature resistant expoxy was used to glue the flange tubing inside the wider PVC tube. The depth to which the cathode could be inserted in the laser tube could be varied by means of an adjustable clamp. A reasonably smooth, reliable and clean operation was achieved by processing the cathode every 2000 hours in the following sequence: sand blasting, sulphuric acid bath, polishing and final treatment of the cathode top with teflon spray. Reports in literature suggest lower degree of continual dissintegration and longer lifetime of chromium or nickel (COB 58) cathode. However, author's own experiments with a copper cathode coated with above materials did not confirm the expectations.

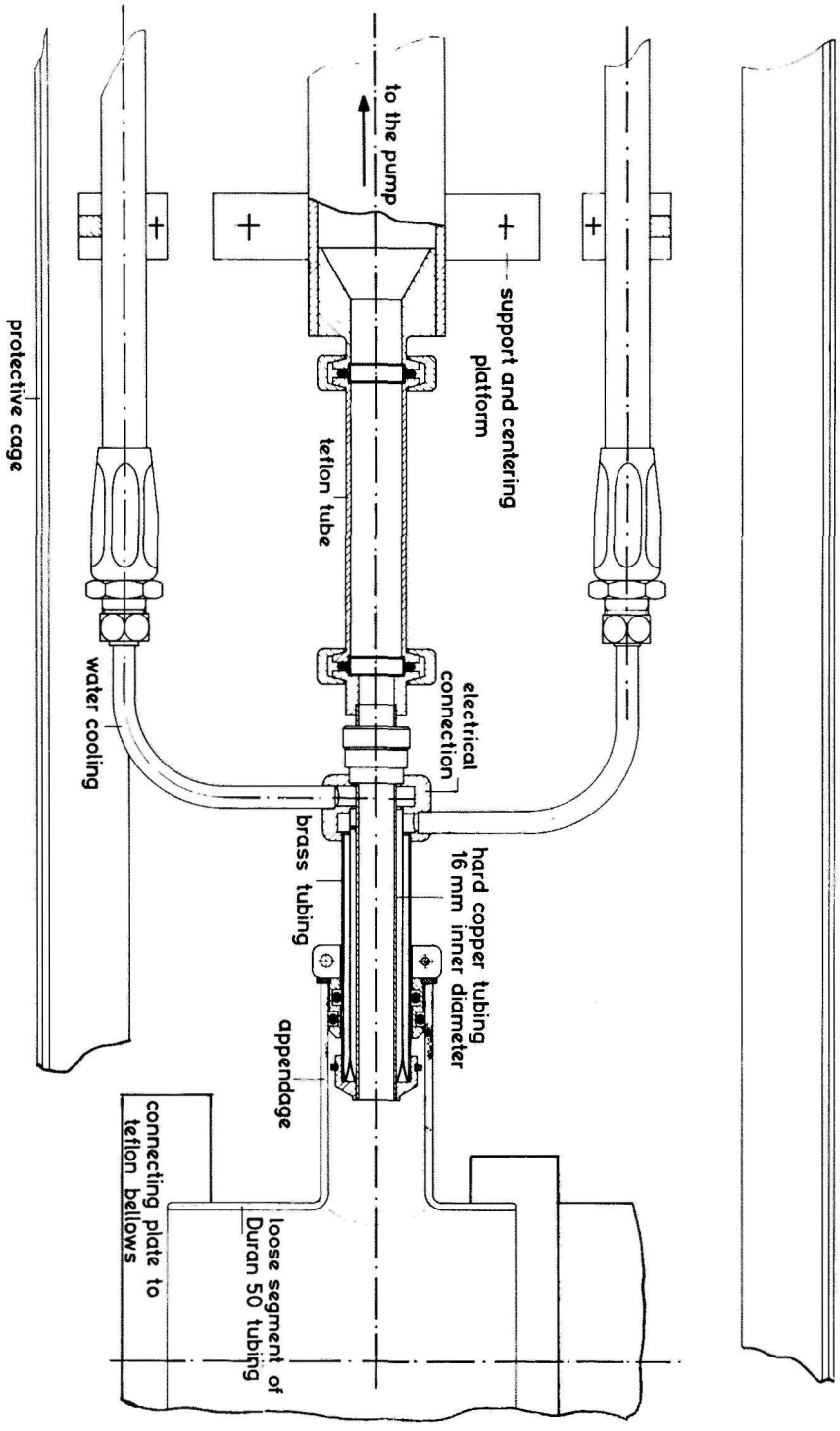

Fig. 2.4 Cathode design for 8 m HCN laser.

The anular anode for the laser was machined from stainless steel and had the highest attainable degree of surface flatness. This electrode was also placed in a separate section of Duran 50 tubing. The inner diameter of the tubing was close to the outer diameter of the anode. As surface imperfections and oxide layers produce large localized concentrations of electric field and lead to severe material dammage, the anode edges were made smooth and gently curved on both sides. Finally, the surfaces were carefully polished with diamond paste. When operated properly in striated regime, plasma occupied the region inside the ring, and the anode was not overheated. Grounding of the anode was accomplished through the side arm by means of a sealing cap provided with a contact spring.

2.3 Intracavity optical components

2.3.1 Lens and mirrors

Lenses were machined from commercial plastics such as white polyethylene and TPX (methylpentene polymer). Absorption coefficient for both materials is rather low in the submillimeter region and their resistance to heat is substantial (CHY 69). TPX is superior to high density polyethylene in hardness, mechanical strength and thermal stability, and exhibits practically no variation in refractive index from the submillimeter to the visible part of the electromagnetic spectrum. This latter property is of great advantage when visually aligning the long laser. Polyethylene has higher transmission but it is essentially opaque to visible radiation. TPX was obtained from ICI Ltd. London and a reflection of 3.5 % per single surface at normal incidence has been quoted (NOB 73). According to the same source 6 and 3.2 mm thick TPX plate will have 77.5 and

91 % average transmission at normal incidence.

Shape of the lens, served to focus the HCN laser output radiation was designed to obtain optimal performance with a single lens element. A polyethylene lens 100 mm in diameter and 220 mm focal length used at the initial stage of the experiment (with 4 m laser) was later replaced by a 70 mm diameter plano-concave TPX lens with 130 mm focal length. Such a F/1.8 lens, when irradiated at its aperture by a laser oscillating in the fundamental transverse mode produces an spot in the focal plane. In the absence of aberation, the size of the spot will be determined by diffraction. Thus, the linear radius a_1 of the spot size is given by the well known relationship:

$$a_1 = 1.22 \frac{f}{D} \lambda \qquad (2.1)$$

where f is the focal length, λ is the wavelength of the radiation and D is the lens diameter. The diameter of the image spot was chosen to match the dimension of the mixer horn at its throat (see Sect. 4.6.1) and of the circular waveguide accomodating the junction (1.5 mm diameter). Rough estimate of focal point location could be obtained with liquid crystal immersed in a cold water. The lens was mounted in an adapter that fitted the collar opening of the laser housing. Such arrangement was required because of difference in diameter between the selected F/1.8 lens and a round opening in the housing constructed to accept larger leuses.

Intracavity window losses have been eliminated by mounting all mirrors inside the plasma tube. The laser cavity was defined by a spherical concave mirror with 16 m radius of curvature and a plane mirror separated by 8 m.The radius of the reflecting mirror (both mirrors were of the same size) was equal to half the internal diameter of the plasma tube. In the present de-

sign, the spherical mirror mount was different from that used by Evenson. The flexibility necessary for tilting the mirror sufficiently for proper alignement was provided by the large teflon bellows that connected the plasma tube to the mirror assembly (see Fig. 2.2). The mirror could be accurately aligned with two micrometer driven mounts placed outside the vacuum. This is different from the design used with 4 m laser where external adjustement of the spherical mirror was achieved by squeezing the "o" ring on the plate carrying the mirror mount.

A similar approach has been followed in designing the two plane mirror assemblies on the other side of the plasma tube.

The two identical plane mirror with the beam splitter and lens served as Michelson interferometric output coupler. Figure 2.5 illustrates the constructing and mounting of the plane mirrors to laser plasma tube. All mirrors were made of high quality Pyrex glass. Plane mirrors were initially metalized with an aluminum layer and then coated with evaporated layers of chromium, gold and a protective quartz film. The spherical mirror possessed only a thermally sputtered gold coating and frequent renewing was required to maintain its high performance. The thickness of the gold coating on all mirrors was substantial (0.3 μm) as skin depth is large at long wavelengths (approximately 900 Å at 890 GHz). Quality of coating was regulary checked with bright filament lamp located behind the mirror in a room. No light transmitted through the mirror should be seen. Gold was preferred to other materials because of its slow tarnishing rate (KIM 70). Exact reflectivity data at submillimeter frequencies are not known, but an extrapolation of empirical relationship gives 99.5 percent reflectivity for gold at a frequency of 890 GHz (HAG 04, KIM 70). The protective quartz

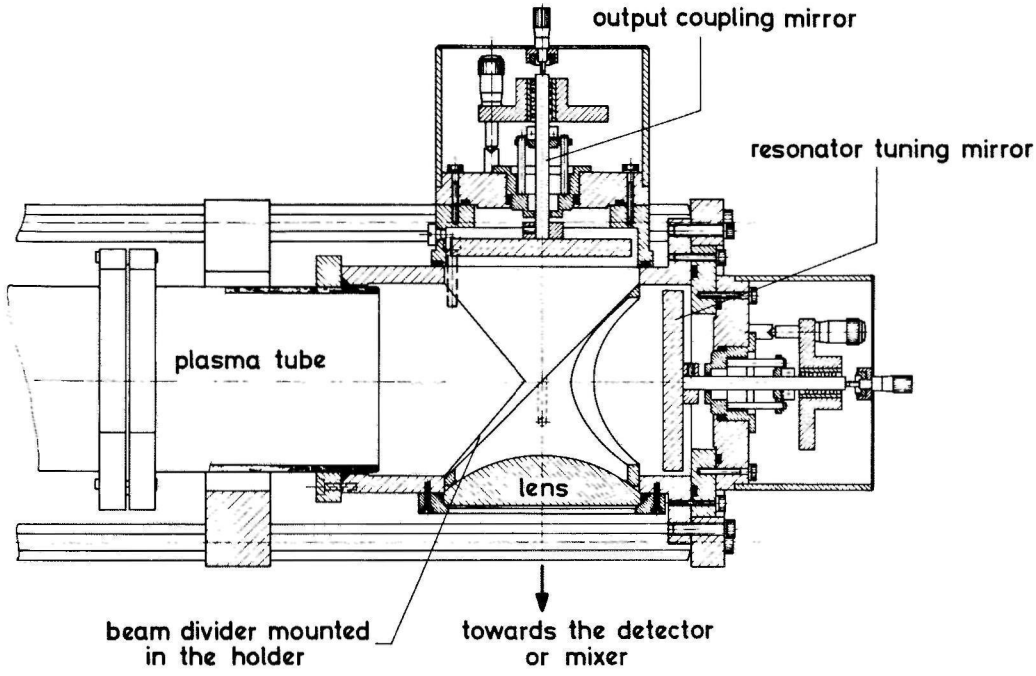

Fig. 2.5 Tuning and output coupling mirror of the laser. Beam divider and the lens are also shown.

coating was required in order to preserve a high degree of reflectivity despite frequent cleanings required to remove the paracyanogen deposit. Gently swabbing the mirror surface with the soap solution and then rinsing with distilled water and alcohol was normally sufficient. Mirrors were then carefully inspected for dirt, greasy spots and dust. Unfortunately, despite the considerable distance of both mirrors from either electrode, mirror contamination remained a significant problem as the relatively cooler surface of the mirrors presented an attractive region for condensation of impurities and metal vapours.

2.3.2 Beam splitter

It has become a common practice to use an uncoated thin transparent film of dielectric material as a beam divider in order to couple out the power of the HCN laser. In Michelson interferometric output coupling scheme illustrated in Fig. 2.5, the third mirror allows the fraction of power coupled out of the laser to be varied continuously from $0\text{-}4r^2$, where r^2 is the reflectivity of the film at each surface (BRA 72a). The surface of beam splitter should be made well flat without wedges or dents to ensure good interaction with the curvature of the wave front.

In submillimeter lasers diffractive losses are considerable but, nevertheless, power reflected by the beam divider represents the main loss factor in the cavity. To estimate the performance of various dielectric films, accurate optical data should be known at the specific wavelength of the laser emission. For this experiment polyethylene, polypropylene and Melinex (mylar) have been testes as beam splitter materials. Melinex sheets 6,13 and 50 μm thick obtained from ICI Ltd. London, have been used, and polypropylene material 28 μm thick was provided by our colleagues at National Physical Laboratory, Teddington, England. Most work has been done with 59 μm thick polyethylene. Beam splitters were all prepared following the same sequence: after being mounted in a specially designed stretcher providing uniform tension force in all directions for some hours, the film was glued to an aluminum frame with rubber cement. Blowing hot air across the mounted film generally improved the surface condition of material.

The Fresnel equations determine the amplitude coefficients for reflection and refraction at the interface of the beam splitter and gas medium, each characterized by its refractive index.

In general, the reflected power for a non-absorbing film is composed of two contributions, one with electric vector perpendicular to the plane of incidence ($\perp$ or s component) and the other with electric vector parallel to the plane of incidence ($\parallel$ or p component). Because the reflectivity of a beam splitter differs for the $\perp$ and $\parallel$ components an unpolarized beam will upon the passage through the interferometer be partly polarized. However, the reflection factor of a dielectric beam divider is complicated by multiple interference in the film. This problem has been discussed by several authors (CHB 65, JAM 67, LOE 67). The single amplitude reflection factor r for a perpendicular component is given by Chamberlain et al. (CHB 65):

$$r_{\perp} = R_{\perp}^{\frac{1}{2}} \frac{1 - \exp 2i\varphi}{1 - R_{\perp} \exp 2i\varphi} \qquad (2.2)$$

with dimensionless parameter φ given by:

$$\varphi = 2\pi d\, k\, n_1 \cos \theta_1 \qquad (2.3)\ .$$

In the above equation d is the thickness of the beam splitter, k is the wavenumber and $R_{\perp}$ represent single surface power reflectivity for perpendicular polarization. The refractive index n_1 of the beam splitter material is taken at wavenumber k_1, and θ_1 denotes the refractive angle. A similar expression with $R_{\parallel}$ instead of $R_{\perp}$ holds for the parallel component.
Surface power reflectivities can be found from:

$$R_{\perp} = \frac{\sin^2(\theta_o - \theta_1)}{\sin^2(\theta_o + \theta_1)} \qquad (2.4a)$$

and

$$R_{\parallel} = \frac{\tan^2(\theta_o - \theta_1)}{\tan^2(\theta_o + \theta_1)} \qquad (2.4b)$$

where θ_0 is the angle of incidence (measured with respect to the normal to the surface of the beam splitter). For a Michelson output coupler in this laser $\theta_0 = 45^o$. Apparently, the subscripts $\perp$ and $\parallel$ have been interchanged inadvertently in original paper of Chamberlain.

In Fig. 2.6 percent reflective loss (r^2 %) for both polarization directions at 45^o incidence is plotted versus the wavelength for materials used as beam splitters in this experiment. Refractive indices for polyethylene (1.461), polypropylene (1.5) and Melinex (1.69) were taken from data available in literature (CHY 71, LOE 67). The thickness of divider was 59 μm, 28 μm and 6 μm for polyethylene, polypropylene and Melinex respectively. Therefore above relationship for $R_\perp$ (and $R_\parallel$) which assumes a non-absorbing reflecting medium could be used. For Melinex beam splitters with thickness of 13 and 50 μm the situation is more complicated and Eqs. 2.4a and b are not adequate (FAH 61). At 890 GHz (29.7 cm^{-1}), the reflective loss $r_\perp^2$ for radiation polarized parallel to the plane of beam divider is larger than the total gain in the cavity. Consequently, the emergent laser beam will be polarized parallel to the plane of incidence. Because output coupling losses in the laser cavity are always greatest for the $\perp$ component (independently of the beam splitter material) the laser reaches threshold first with the $\parallel$ component, and accordingly laser output is $\parallel$ polarized.

As seen from Eq. 2.3, the parameter φ is directly proportional to the divider thickness d at a given frequency and angle of incidence. It can easily be shown that the thickness d_{opt} of the film resulting in maximum reflection out of the laser cavity is given by:

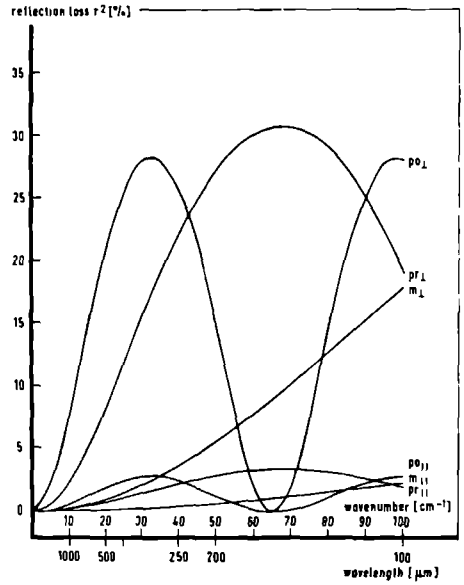

Fig. 2.6 Reflection loss (in percents) at 45^{o} incidence, in the plane parallel and perpendicular to that of beam divider for three materials used: polyethylene 59 μm (po), polypropylene 28 μm(pr) and melinex 6 μm(m) plotted versus the wavelength or wavenumber. The absorption in the beam splitter is ignored.

$$d_{opt} = \frac{\lambda}{4} \left(n_1^2 - \frac{1}{2}\right)^{-\frac{1}{2}} \qquad (2.5).$$

Substitution of $n_1 = 1.461$, and $\lambda = 337$ μm, yields $d_{opt} = 65.8$ μm for polyethylene material. No absorption loss data is available for polyethylene of this thickness, but Bradley et al. (BRA 72a) quote 0.025 per pass for 25 μm beam divider. The thickness closest to d_{opt} that could be found on the market was 59 μm. This beam splitter was used at both strong transitions of the HCN laser 890 GHz and 964 GHz (see Chapt. 4).

Finally, for reasons of completeness, the normalized transmission of the interferometer with a 59 μm thick polyethylene

film has been computed and plotted versus the wavenumber, as shown in Fig. 2.7. The values associated with the vertical axis can be regarded as the energy transmitted towards the detector (CHY 71). The plot is computed for || radiation polarized parallel to the plane of incidence, following the technique proposed by Loewenstein (LOE 67). Other authors termed it as beam efficiency, or depth of modulation fringes (LOE 67, JAM 67).

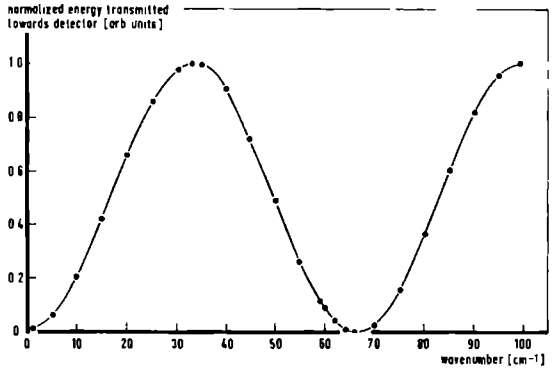

Fig. 2.7 Transmission of the interferometer for 59 μm polyethylene beam divider versus the wavenumber, at 45^{o} incidence. Maximum corresponds to transmission of 10.82 % for $r_{||}$ component.

As seen from above figure, transmission function is periodically dependent on frequency, with peak at wavenumber to be covered with this beam splitter.

2.4 Alignement of the laser resonator

Precise alignement has been carried out with a He-Ne laser emmiting the bright 6328 Å line with symmetrical intensity distribution and low divergence. Collimated beam of such laser defines for all practical purposes straight line across the inter-

mirror separation. Alignement began by removing the spherical mirror from its mount and placing a closely fitting round plastic disc into the plasma tube. The disc had a small pinhole on its center to allow the passage of laser light. Circular groove cut in the disc facilitated the making of a rigid connection with He-Ne laser, which was resting on three precision linear translators stacked atop each other. Such unit enabled stable and highly accurate translation in X, Y and Z direction. Incident laser beam, after passing through the hole in disc and being reflected at far plane mirror, usually hits the backside of disc somewhere off its center. Adjustment of the plane mirror will eventually result in the reflected beam passing back through the pinhole. The aligned plane mirror is then removed, and He-Ne laser unit is mounted in its place. With the spherical mirror remounted the procedure is simply repeated. Alignement could be improved by placing an additional round plate with a central pinhole in front of the distant mirror to be aligned. The output coupling mirror of the Michelson interferometer was aligned at the same time as plane mirror. The beam splitter was placed at 45^{o} to the optical axis, and laser light reflected from both mirrors was observed on a blank sheet of paper. When properly aligned, a single bright spot resulting from the superposition of two beams is seen in the focal plane of the TPX lens. Final alignement is completed by igniting the laser and adjusting the mirrors to maximize the laser output. This should be done after the laser discharge has been run for several hours and the laser is thermally reasonably stable.

2.5 Resonator characteristics of the 8 m HCN laser

Of the several possible variations, a plano-concave cavity

was chosen for the 8 m HCN laser resonator. The resonator consisted of a spherical concave mirror with curvature radius R_1 = 16 m and a plane mirror $R_2 = \infty$; both mirrors had diameters equal to that of plasma tube (140 mm). The properties of such semiconfocal resonator with $R_1 = 2\ L$ (where L is the intermirror separation) are equivalent to those of an ideal confocal system, when the flat mirror is large enough. The selected design represents a compromise between several factors such as mode volume, mode discrimination, diffraction loss, stability and alignement tolerance, that govern the performance of this low gain submillimeter laser. The basic objective of the cavity design was to obtain the maximum amount of monochromatic output power in the fundamental transverse mode of oscillation, TEM_{00q}. Operation in this mode is desireable for the purposes of this experiment (see Chapt. 4).

The far field diffraction angle of the emergent beam, which ultimately determines the efficiency of coupling into the point contact junction, is smallest for the TEM_{00q} mode. Also the diffraction loss is lowest for a given resonator in the TEM_{00q} mode. In the present design, fraction of maximal flux potentially available has been sacrified in order to relax the alignement tolerance. Since $L < R_1 << R_2$, the resonator is expected to be stable with a field distribution concentrated around the axis and with a diffraction loss exceeding that of confocal resonator (KOG 66).

The Fresnel number N is the critical parameter determining the diffractive loss in the laser cavity. As both mirrors are of equal radii a_m, one has (ROS 73):

$$N = a_m^2 / L\lambda \qquad (2.6).$$

Submillimeters lasers, contrary to their optical counterparts have much smaller N values; $N \sim 1$ is often found in the literature. For semiconfocal resonator twice the actual physical mirror separation has to be substituted for L in Eq. 2.6. The 4 m laser of Evenson had N = 0.92 with tube and mirror diameters of 100 mm. As the same Fresnel number at 337 μm is required for the 8 m laser, one finds a_m = 70.43 mm from Eq. 2.6. The closest tube diameter commercially available was Duran 50 with an outer diameter 145 mm and a wall thickness of 3 mm, giving an inner plasma tube diameter of approximately 140 mm, which is comparable with 2 a_m.

Spot size ω of the laser beam is its radius in a given plane, perpendicular to the axis of propagation. This important quantity is related to the intensity distribution of the transverse cross section of the beam (by convention it is chosen as the distance from the axis at which the power in TEM_{00q} mode drops to $1/e^2$ of its maximum). The spot size at the spherical and plane resonator mirrors, ω_1 and ω_2 respectively, are given by a general expression that is valid for an arbitrary resonator. (KOG 66). After some arithmetic manipulation one can show that.

$$\omega_1 \underset{R_2 \to \infty}{=} \sqrt[4]{(R_1 \lambda/\pi)^2 \, L/(R_1-L)} \qquad (2.7a),$$

and likewise

$$\omega_2 \underset{R_2 \to \infty}{=} \sqrt[4]{(\lambda/\pi)^2 \, L \, (R_1 - L)} \qquad (2.7b).$$

Substituting R_1 = 16 m, L = 8 m, yields ω_1 = 41.43 mm and

ω_2 = 29.29 mm for the spot sizes at the spherical and plane mirror respectively. Lengyel (LEN 66) suggested the use of plasma tube having the inner diameter three times larger than the spot diameter, if significant mode discrimination is desired. Since the gain of an HCN laser is inversely proportional to the tube radius squared (BIR 73) the inner diameter of the plasma tube ($\sim$ 140 mm) was chosen to be $\sim$ 2.5 ω_2.

The beam waist ω_o can be evaluated from the general expression of Kogelnik (KOG 66):

$$\omega_o = \sqrt[4]{(\lambda/\pi)^2 \frac{L(R_1-L)(R_2-L)(R_1+R_2-L)}{(R_1 + R_2 - 2L)^2}} \qquad (2.8).$$

For $R_2 \to \infty$, ω_o reduces to ω_2 and $t_1 = L$, $t_2 = 0$, where t_1 and t_2 denote the distance from the beam waist to concave and plane mirrors, respectively. Therefore for this HCN laser resonator beam waist is located at the plane mirror and equals the spot size ω_2 at the same mirror.

An approximate relationship for the mode volume V_M is given for near confocal configuration by Kotthaus (KOT 68):

$$V_M \approx L \pi \omega_1^2 \qquad (2.9)$$

and with known values for L and ω_1 of 8 m laser, V_M is 4.3×10^4 cm^3. For large power flux it is desireable to have volume of active medium V_L comparable to V_M, which is only true for plane parallel resonator. Because of very stringent alignement tolerance in addition to high diffractive loss, plane parallel resonator is not commonly used with submillimeter laser, and hence $V_M \sim 0.35\ V_L$ for the present resonator.

A simple criterion to distinguish between the low loss system capable of maintaining the radiation within the cavity from loosy resonators has been introduced by Boyd (BOY 64). For

stable resonator the product of two "g" factors g_1 and g_2 (where $g_i = 1 - L/R_i$) must be positive number between zero and one. As R_i is counted positive if mirror surface is concave $g_1 . g_2 = 0.5$ for our HCN laser resonator.

Once the Fresnel number of the resonator has been determined, the diffraction loss can easily be found from data published in literature (FOX 61). The diffraction loss in the cavity is defined as fractional energy lost per transit due to diffractional effects on the edges of the mirrors. For a confocal resonator with N = 0.92 a power loss 0.12 % per single pass is found for the dominant mode (FOX 61).This is much lower than the values of 2.4 and 18 percent for the higher order transverse modes, TEM_{10q} and TEM_{20q} quoted in the same reference. It is clear that diffraction loss (varying from mode to mode) allows mode discrimination, since unavoidable losses due to imperfect mirror reflectivities are the same for all modes. In view of the low gain factor of the HCN laser, diffraction losses play an important role in designing the laser to operate in the lowest mode.

2.5.1 Resonant condition for half-confocal laser resonator

The resonant frequencies of the cavity modes are dependent on resonator length and the mode numbers. For a TEM_{plq} mode in a general cavity with unequal curvature radii of two mirrors, the resonance frequency ν_{plg} is given by (KOG 66):

$$\nu_{p\,l\,q} = (c/2L)\left[\left(\frac{q + p + 2l + 1}{\pi}\right) \cos^{-1}\sqrt{(1-L/R_1)(1-L/R_2)}\right] \quad (2.10)$$

where c is the speed of light and L is the mirrors spacing.

For an semiconfocal cavity in which the concave mirror forms an image on the plane mirror, the above relationship can be further simplified by noticing that the $\cos^{-1}$ term satisfies the following degeneracy condition:

$$\cos^{-1} \sqrt{(1 - L/R_1)\ (1 - L/R_2)} = \pi/z \qquad (2.11)$$

with z being an integer; in this case z = 4. This means, that a ray launched in laser cavity makes four complete transversals before retracing its original path. For such a reentrant resonator; the oscillation condition for mode frequencies becomes:

$$\nu_{p\ l\ q} = (c/2L)(4q + p + 2l + 1) \qquad (2.10a).$$

For three lowest oscillation modes of 8 m laser resonator it follows:

$$\nu_{0\ 0\ q} = 18.75\ (q + \tfrac{1}{4})\ \text{MHz} \qquad (2.12a)$$
$$\nu_{1\ 0\ q} = 18.75\ (q + \tfrac{1}{2})\ \text{MHz} \qquad (2.12b)$$
$$\nu_{2\ 0\ q} = 18.75\ (q + 3/4)\text{MHz} \qquad (2.12c).$$

From these expressions, positions of higher order transverse modes can be found in terms of tuning distance c/2L between two axial modes. This frequency spacing $\Delta\nu_{ax}$ between the resonances of two modes with the same transverse configuration is only a function of the resonator length. For present design of the laser $\Delta\nu_{ax}$ is 18.75 MHz, so that TEM_{10q} mode is approximately 0.25 of the tuning distance between two successive modes of the same transverse configuration (see Sect. 3.5).

Quality factor of the HCN laser resonator was found to be in the order of 10^5-10^6 (BIĆ 75). Frequency pulling of the resonator by the output coupling plane mirror could be neglected because of the low Q factor (EVE 71).

It is useful to close this chapter with a few considerations about the linewidth of the laser emission. The chief contributions to the linewidth are Doppler and pressure broadening. At typical working pressure of the HCN laser ($\sim$ 0.5 Torr) full width $\Delta\nu_p$ at half maximum is 9.5 MHz due to pressure broadening. Full width at half maximum $\Delta\nu_D$ due to Doppler broadening is about 2.5 MHz for strongest laser transition and at 400^{o}K gas temperature. Total linewidth $\Delta\nu_T$ as the result of these contributions is estimated to be in the order of 10 MHz. The unique feature of submillimeter laser follows immediately if one realizes that axial mode separation $\Delta\nu_{ax}$ is several times larger than the Doppler broadened gain profile $\Delta\nu_T$. Since $\Delta\nu_{ax} > \Delta\nu_T$, the laser will operate in a single mode.

C H A P T E R 3

EXPERIMENTAL STUDIES WITH VARIOUS TYPES OF 4 M HCN LASER

3.1 Introduction

In the proceeding chapter the basic constructional and engineering details of the 8 m HCN laser have been discussed. Ever since the discovery of stimulated emission from HCN, this laser has been subject of numerous extensive experimental investigations. Most of this research effort was directed towards maximizing the output power of the HCN laser, which is the most powerful coherent source of submillimeter radiation that is available.

It has been pointed out in Chap. 1 that successful sideband generation requires the interacting radiations from the laser and klystron sources to be as intense as possible. Thus, an exhaustive study of the possibilities of obtaining higher laser output powers seemed indispensable even at the risk of considerable loss of time. This Chapter deals with these studies which were performed with a 4 m HCN laser. Relevant results were later applied to the operation of the 8 m laser.

In general, the output power P of the HCN laser depends on the composition of the gaseous mixture used as the active medium, its pressure p, flow rate Ψ, discharge current I, wall temperature of the laser tube T and degree of wall contamination (FUL 71, VAN 76). In order to get some quantitative insight into this dependence, a large number of measurements have been made. Throughout the measurements, the largely uncontrolable influence of wall contamination on the output power was disregarded, and only power-current-wall temperature (P-I-T) as well as power-pressure-temperature (P-p-T) dependence have been measured. Great attention has been paid to the reproducibility of the measurements. All studies were performed with a given constant gas mixture flow rate and a stable striated discharge. The

plasma tube was always allowed sufficient time to reach a thermal steady state condition .

3.2 Active medium

Initially, experimental studies of the composition of the active medium were concentrated on mixtures composed of methane. nitrogen, ammonia and air in various proportions (BIC74). The nature of the chemical reactions among these gases in the plasma is unknown, but it is believed to be very complex with many unstable intermediates involved in production of HCN molecule. With a few exceptions the gain factors for these mixtures are also not known.

The measurements were all performed under identical operating conditions, with the gas mixture admitted at the anode end of the laser tube, and pumped out from the cathode end. Reversal of the flow direction resulted in an approximate 15 % power reduction under otherwise comparable discharge conditions. A mass spectrometric analysis of plasma products was performed for the two alternative inlet/outlet systems. Remarkably enough, the evidence for the presence of HCN as well as may other products with molecular masses ranging between 2 and 50, was observed only when the mixture was admitted at the anode end. A possible qualitative explanation of this effect can be based on different electron energies at cathode and anode ends of the plasma tube, which in fact determines the abundance of dissociated products and ions. The direction of gas flow is then of influence for what the mass spectrometer will measure (HAR 73).

A 220 m focal length and 100 mm diameter F/2.2 polyethylene lens was used to focus the output laser radiation onto the entrance cone of Molectron P-3 pyroelectric detector which was

mechanically chopped at 120 Hz. The calibrated voltage responsivity of detector specified by the manufacturer is 15 mV/mW. An adapter attacked to a collar around the output lens on one side and accomodating the chopper and detector unit on the other side was designed (axes of lens and detector coincide). Phase sensitive detection was used in order to increase the sensitivity. A beam splitter made of polyethylene with an average thickness of 59 μm was used and the output coupling mirror was positioned to maximize the output power.

Figure 3.1 shows the relative laser output for 4:1 ammonia/methane mixture at constant pressure and flow rate plotted versus the discharge current. At low currents production of HCN and population inversion is small resulting in low output powers. Increase of the current produces larger output power, since the formation of HCN molecule is more effective due to the increased electron density in the positive column. Dissociated molecules do not recombine and the amount of "used up" gas is proportional to the current. At very high currents, presumably the dissociation of HCN itself becomes important leading to a reduction of gain and power.

Typical dependence of laser output power on the pressure of the active medium constant flow and current values is shown in Fig. 3.2. At low pressures, the amount of gas is insufficient to obtain lasing action and consequently no output is observed. Additional pressure increase results in lasing action. However, the curve flattens and begins to fall at higher pressures because discharge excitation is no longer adequate to compensate for the rapidly increasing collisional deexcitation.

At still higher pressure the measurements become appreciably more difficult to make because of transients from a stri-

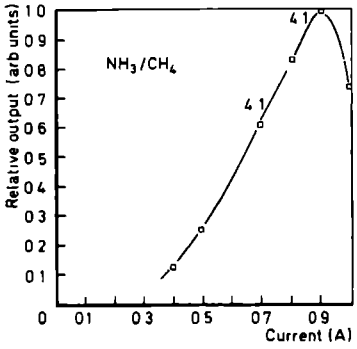

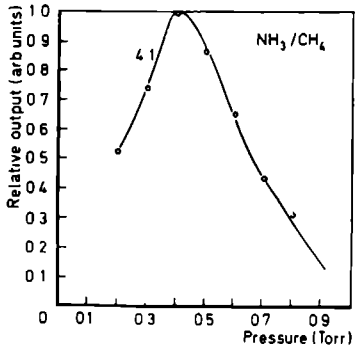

Fig. 3.1 Typical dependence of the laser output power with discharge current at constant pressure and gas flow rate for 4:1 ammonia/methane mixture.

Fig. 3.2 Output laser power versus pressure at constant current and flow rate. The active medium is a 4:1 ammonia/methane mixture.

ated to an unstriated discharge. These could not be totally eliminated within the voltage range available from the power supply.

At this point it should be noted that the high flow rates reported in our first paper (BIC 74) were inproperly monitored and are incorrect . This problem was avoided in the 8 m laser by using flowmeters from which the flow rates could be read off directly, before the gas mixture entered the plasma tube (see Sect. 2.2.4). Plots in Figs. 3.1 and 3.2 do not account for effect of the tube temperature on the output power (not known at the time).

Studies suggested that more power is available from ammonia and methane mixtures than from nitrogen and methane mixtures. The maximum output power from the 4 m laser oscillating in a TEM_{00q} mode on the 890 GHz transition was about 23 mW when a

4:1 ammonia/methane was used as the active medium. With a rapidly fluctuating unstable discharge, it was possible to obtain powers close to 40 mW. Other investigated mixture involved methane/air and methane/nitrogen. The power levels observed were largest for a 1:2 nitrogen/methane mixture and slightly lower for a 1:1 nitrogen/methane blend. The 4:1 methane/air and 2:1 nitrogen/methane produced output powers about 60% lower than 1:2 nitrogen/methane under the same discharge conditions. This is in agreement with gain data for the same mixtures, reported by Stafsudd and Yeh (STA 69).

3.3 Hydrogen as the buffer gas for active media and some new mixtures lasing in submillimeter band

In recent years, reports dealing with the use of helium or hydrogen as buffer gases in submillimeter lasers have appeared in the literature (VOL 72, YOS 74, VAN 76). Encouraged by large contraversy still prevailing in the literature a study was carried out to investigate the effect of hydrogen addition on laser output power from several active media. Details of the experimental set-up and results can be found in the reprint at the end of this chapter (BIC 75b).

Measurements were performed for several mixtures at one particular set of pressure and flow values, both chosen to ensure substantial output powers. With the exception of an ethylene/nitrogen mixture, all mixtures enriched by hydrogen exhibited a decrease in power. It appears, that hydrogen produces a power increase only for mixtures with relatively low hydrogen concentration. It seems that ammonia/methane mixtures possess, most likely, a near optimal hydrogen concentration. In the later stage of the experiment, we have studied a large variety

of gaseous mixtures consisting of dimethylamine, carbon monoxide, ethylene, acetylene diethylether, methane, nitrogen, ammonia adn others. The object of the study was to observe the power dependence of the laser output with discharge current at constant flow, pressure and tube temperature. Results are summarized in the publication reprinted at the end of this chapter (BIC 76). The most interesting result that emerged from these studies was the continuous power performance of 1:1 dymethylamine/ammonia and 1:1 ethylene/ammonia mixtures. Both mixtures were superior to the 4:1 ammonia/methane mixture. The increase in power was about 30% accross the entire current range (0.3A - 0.8 A) for 1:1 dymethylamine/ammonia mixture.

3.4 Optimum output coupling and estimate of total resonator loss

In the present laser design, a Michelson interferometer permits the continuous variation of the output power from $0 - 4r^2$ (see Sect. 2.3.2). The operation of the interferometric output coupler is illustrated in Fig. 3.3a. The laser output power (arbitrary units) is shown as a function of tuning position γ_0 or the output coupling mirror (or relative phase in units of laser emission wavelength) for several values of discharge currents. Recordings were made with the 4 m laser at constant pressure, low flow rate and a striated discharge. Relative output power under the same experimental conditions but at lower current values is shown in Fig. 3.3b. Both figures were recorded with an active medium of 4:1 ammonia/methane and a 59 μm polyethylene beam divider. From Fig. 3.3b it can be seen that for currents below 0.3 A the laser can be overcoupled to such an extent that oscillation is quenched. Treshold coupling

coefficient could be found by determining the intersection of power curves with the horizontal axis.

In order to determine the optimum coupling, we use the data plotted in Fig. 2.7 for a 59 μm beam splitter at 45^{o} incidence to 337 μm radiation, and evaluate coupling coefficient $t = 4\, r_{\parallel}^{2} \cos^{2}\gamma_{o}$, where γ_{o} is the relative phase of the output coupling mirror (see Fig. 3.4). Figures 3.3a and 3.3b illustrate that maximum output power is obtained at all discharge current at a γ_{o} of roughly $\pi/3.3$ this corresponds (see dotted line in Fig. 3.4)to a t_{opt} of 0.037.

Figure 3.3a also shows that displacement of the output coupling mirror through one quarter of the wavelength does not vary exactly the output power from zero to maximum. This is ascribed to irregularities in the beam splitter and to imperfect alignement which prevent destructive interference over the whole of the mode cross section.

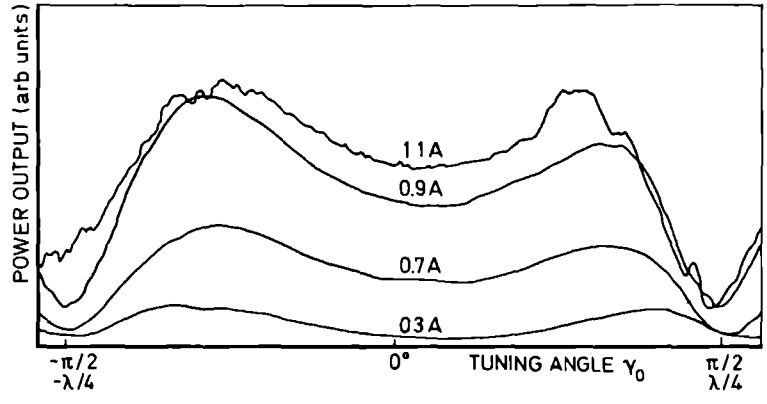

Fig. 3.3a Typical recorder trace of the power coupled out of HCN laser versus tuning position of the output coupling mirror γ_{o} for several current values.

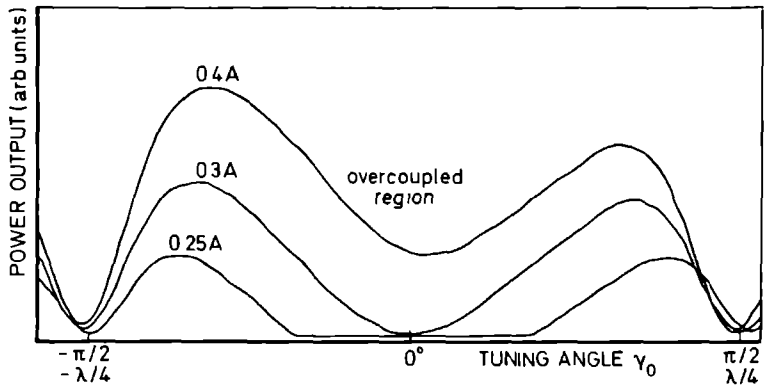

Fig. 3.3b Coupled out laser power versus the tuning mirror position γ_0 for low currents indicating overcoupled region. Remaining discharge parameters were the same as in Fig. 3.3a.

Knowledge of t_{opt} is very useful is very useful in determining the total resonator loss per round trip L_T. This quantity accounts for reflection and diffraction losses on both mirrors and the absorption loss in the beam divider. Using the approach of Bennett (BEN 62) it is easy to show that:

$$t_{opt} = \sqrt{G\,L_T} - L_T \qquad (3.1)$$

where G is the total unsaturated gain per round trip in the laser cavity. Birch (BIR 73) has found that a plasma tube with 100 mm inner diameter (0.02 mm^{-1})reciprocal radius and with discharge parameters and lasers mixture comparable to our own, has a gain factor of about 0.035 m^{-1}. For an 4 m HCN laser for instance, with usable discharge length of 3.6 m, this corresponds to a total round trip gain of G = 0.252 (for 8 m laser with reciprocal tube radius 0.014 mm^{-1}, the unsaturated gain is 0.026 m^{-1} and hence the total round trip gain equals 0.38).

Substituting t_{opt} = 0.037 from Fig. 3.4 (determined from the measured tuning curve for TEM_{00q} mode in Fig. 3.3a) and G=0.252 in the Eq. 3.1, total loss factor L_T of approximately 0.17 is obtained. A reasonable estimate for reflection loss per single reflection on a gold coated mirror is about 0.005 (BRA 72a , KIM 70) and diffraction loss for a semiconfocal resonator with N = 0.92 is about 0.04 per single pass (LEV 66). Since the sum of diffraction and reflection losses per round trip is 0.09, the absorption loss in the 59 μm polyethylene beam splitter must be 0.08 per round trip. There is no absorption loss data available in the literature for material of this thickness. However, Bradley (BRA 72a) reported 0.025 single pass loss for a 25 μm polyethylene beam divider at 118.6 μm.

In view of the above findings pertaining the diffraction and reflection losses it is interesting to evaluate what degree of coupling is suitable for a hole in the end mirror of the given laser resonator. Bradley (BRA 72a) has shown that for a hole diameter $2a_h < \omega$ (where ω is the spot size at the appropriate mirror containing the hole), the fractional power loss t through the hole can be written for the fundamental transverse mode of operation as:

$$t = 2\, a_h^2/\omega^2 \qquad (3.2).$$

If the 59 μm polyethylene beam splitter is removed from the plasma tube, and the 4 m HCN laser is operated at same discharge conditions (same value of unsaturated gain G), the losses other than transmission out of the system equal 0.09. The Eq. 3.1 yields t_{opt} of 0.0606 with G = 0.252 and L_T = 0.09. For the semiconfocal resonator the spot size ω_1 on the spherical mirror is $\sqrt{2}$ times larger than the spot size ω_2 on the plane mirror

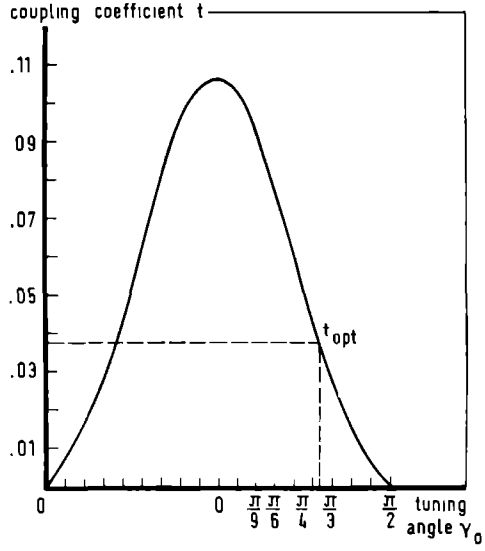

Fig. 3.4 Coupling coefficient for 59 μm polyethylene beam splitter at 337 μm laser emission wavelength plotted versus the tuning angle of the output coupling mirror.

(ω_1 = 29.3 mm and ω_2 = 20.7 mm for a given 4 m HCN laser from Eqs. 2.7a and 2.7b), and hence Eq. 3.2 yields a_h = 3.6 mm (with ω_2) and a_h = 5.1 mm with (ω_1) for the optimal hole radius.

3.5 Measurements of the transverse mode profiles and interferometry of the laser resonator

The transverse mode profile of the laser emission is closely linked to its resonator characteristics. There are basically two methods to examine the transverse mode structure or the intensity distribution of the laser output beam:

i) directly, by means of visual imaging (with a liquid crystal thermal imaging device), or

ii) scanning the beam perpendicularly to its axis with a detector sensitive to a small portion of the beam.

In the course of this experiment the transverse energy distribution of two lowest transverse modes TEM_{00q} and TEM_{10q}, have been determined by measuring the laser output power as a function of the radial distance from the beam axis using pyroelectric Molectron P-3 detector equipped with a polished brass cone (F/2, halfview angle 12^{o}, demagnification factor 5). Transmission of the cone is over 90 % at the wavelength range of interest. The polyethylene lens in the laser was removed, and replaced by 5 mm flat circular plate of the same material. Measurements were performed immediately behind the circular plate (the near field approximation). The detector and chopper unit were mounted on a massive platform resting on a precision laboratory scissor jack and two translational stages allowing continuous and accurate scanning in the horizontal and vertical planes.

Measured normalized profile of the TEM_{00q} transverse mode of the strongest laser transition is shown as function of radial distance in Fig. 3.5. This data allows an experimental determination of the spot size at the plane mirror, ω_2. As seen from Fig. 3.5 the measured value, 22 mm, is in good agreement with the calculated value, 20.7 mm, obtained by substituting L = 4 m, and R_1 = 8 m into Eq. 2.7b.

Figure 3.6 shows the transverse profile of the TEM_{10q} mode of the same laser transition A distinct minimum on the symmetry axis is clearly seen. The observed mode patterns are similar to those obtained by other investigators.

Single mode oscillation of the HCN laser permits an interferometric study of the laser emission. If one of the cavity mirrors is displaced continuously along its axis, an interferogram of the laser resonator is obtained. The following information

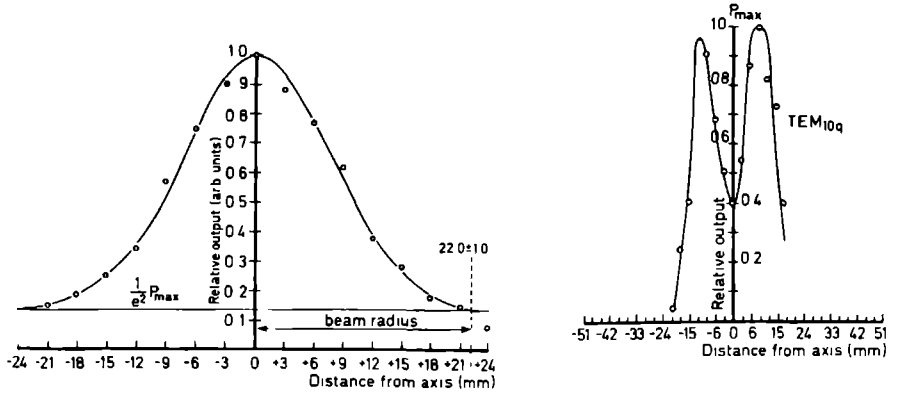

Fig. 3.5 Measured transverse TEM_{00q} mode profile of the 4 m c.w. HCN laser.

Fig. 3.6 Measured transverse TEM_{10q} mode profile of the 4 m c.w. HCN laser.

is obtained from such an interferogram:

i) a quick estimate of the wavelength of the laser emission by reading off the separation between consecutive peaks (on the micrometer head attached to the mirror) arising from the same transverse mode,

ii) an identification of oscillating modes.

Figure 3.7 is an example of an interferogram obtained with a 1:1 methane/air mixture at typical operating conditions of the 4 m laser. The plane mirror was driven with a precision Elkmehanic motor, the speed of which was adjusted to match the integration time of the lock-in aplifier. The plot of emission power versus resonator length displays clearly the presence of TEM_{00q} and TEM_{10q} modes for both 337 μm and 311 μm. The separation between the fundamental and the higher mode (0.38 of the tuning distance between two longitudinal modes 37.5 MHz) agrees

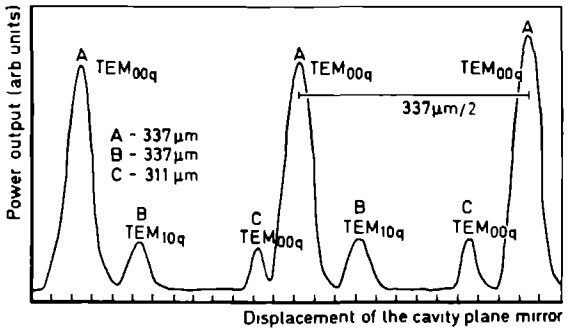

Fig. 3.7 Typical resonator interferogram obtained with the 4 m c.w. HCN laser.

well with that calculated by means of Eq. 2.10a. The ratio of observed intensities at 337 μm and 311 μm is approximately 3.5, which agrees fairly well with experimental gain data obtained by Svich for a stable striated discharge in a 1:1 air/methane mixture (SVI 71).

3.6 Transmission measurements of some plastic polymers

Absorption coefficients of several plastics have been measured at the frequency of the strongest transition, 890 GHz. Transmission measurements were performed by inserting a circular plate of the material under investigation at the entrance of the detector cone. Reflection measurements were not performed, but reflection loss per single surface were calculated (HAD 67). Refractive indices of most materials were taken from Chantry (CHY 71). Surface roughness was measured with a Bruel and Kjaer type 6102 meter and is shown in the first column of Table 3.1. Absorption coefficients corrected for reflection loss are also presented in the same Table and compared with other measurements.

trade name	roughness (μm)	thickness (cm)	measured external transmission	refractive index	computed reflection loss per single surface at normal incidence	calculated absorption coefficient at 890 GHz (Nepers/cm)					
						(CUB 51)	(BEC 70) *	(CHY 71) *	(KIM 70)	this work *	this work if reflection neglected
TPX polymethyl pentene	0.7	0.317	0.85	1.457	0.035	-	0.412	0.31	-	0.28	0.51
polystrene	0.8	0.096	0.76	1.5	0.04	2.66	-	2.22	2.14	2.01	2.86
teflon polytetrafluorethylene	2.1	0.25	0.86	1.391	0.027	1.23	0.393	0.5	-	0.39	0.61
white polyethylene	1.4	0.213	0.89	1.461	0.035	0.58	-	0.182	-	0.27	0.55
black polyethylene	1.2	0.166	0.6	assumed 1.5	0.04	5.8	6.94	-	5.32	2.59	3.08
white perspex (polymethyl methacrylate)	1.1	0.102	0.33	-	-	-	-	8.1	10.21	-	10.46

Measurements listed under the first two references (columns 8 and 9 of Table 3.1) have neglected surface reflection losses (CUB 51, BEC 70). The sizeable discrepancy for the absorption coefficient of black polyethylene can be explained by the different origin and composition of the material studied by various investigators (different percentage of carbon load in the polyethylene). In addition to these plastics, we have investigated a large number of other polymers, among which commercially available polyvinyl chloride was found the best attenuator at the 337 μm wavelength with an absorption coefficient of 21.7 Nepers/cm.

3.7 Pulsed 4 m HCN laser

It is well established fact that lasers operating in the pulsed mode can deliver very high peak powers. As high power was an prerequisite for successful non-linear sideband generation, a pulsed HCN laser was constructed (BIC 74c). The resonator and output coupling design were identical to that used with the continuously operating laser. Excitation of the plasma tube was achieved by means of a pulsed longitudinal electrical discharge through a flowing 1:1 ammonia/methane mixture. In order to obtain short pulse duration and high currents, 0.5 μ F Bosch capacitor capable of 20 kV d.c. was discharged accross the laser tube. The maximum total input energy of the capacitor at 12 kV was approximately 25 J. The electrical excitation scheme was designed for minimum inductance to provide large (few kA) and short (few μs) current pulses. Assuming internal laser resistance of approximately 10 Ω and capacitance of 0.5 μF the time constant is 5 μs. The total current pulse length will be of the order of 4-5 times the time constant. A schematic diagram

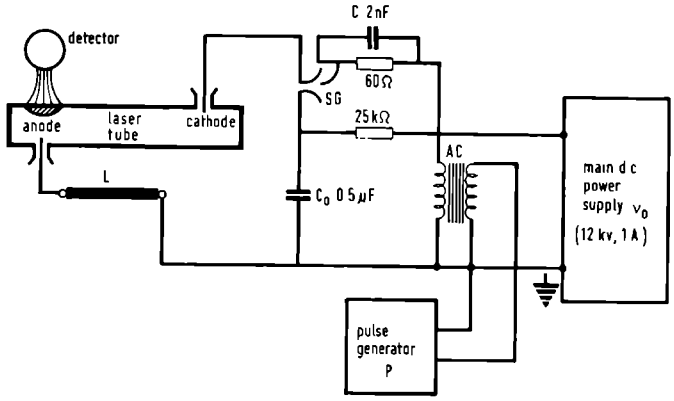

Fig. 3.8 The schematic diagram of the excitation electronics used to operate the pulsed HCN laser.

of the excitation electronics is shown in Fig. 3.8. At low rates (few pulses per second) the capacitor C_0 is charged to a voltage V_0 selected on the Cober power supply (typically a few kV) by means of the current flowing through the 25 kΩ resistor. The spark gap SG is open and the voltage at the cathode is zero. The secondary winding of the autocoil provides a large voltage sufficient to cause short circuiting of the capacitor C_0 which in turn shuts off the circuit. Energy stored in the capacitor is then discharged in short pulse accross the plasma tube. As soon as the voltage drops below a certain value, the spark gap opens once again, and the capacitor is recharged. It is desireable for the circuit consisting of the laser tube, spark gap and capacitor to posses a very low inductance to prevent the appearance of high voltage peaks due to rapid $\Delta i/\Delta t$ fluctuations. This condition was satisfied by 3.25 m long hollow copper cylinder 6 mm in diameter mounted above the laser tube along its length; the self-inductance L of such arrangement was few μH. Variable rate (0.5 - 35) Hz could be obtained by using a

pulse generator and a Schmitt 7413 trigger to fire the auto-coil (BIC 74d).

Initially point contact diodes (Si and GaAs) were used in conventional video detectors to measure the laser output in the pulsed mode. Radiation was focused on a copper horn leading to the diode junction. Progressive deterioration of the I-V contact characteristics has been observed with each successive pulse. This phenomenon is assumed to be due to pick-up from high current peaks, rather than substantial power densities.

Figures 3.9a and Fig. 3.9b shows oscilloscope traces of discharge current and laser emission pulse respectively versus time. The Molectron P-3 pyroelectric detector set at intermediate speed was used as the detector. The zero of the time base corresponds to the onset of the discharge pulse. Peak current has been determined by measuring the voltage drop accross a 0.0327 Ω resistor connected in the series with copper cylinder and the anode. The recording displayed in Fig. 3.9a was obtained at a capacitor voltage of 6.5 kV, repetition rate of 3 Hz, pressure of 0.7 Torr and low flow rate. The current peak pulse had a duration of about 10 μs and a maximum amplitude of 3.2 kA. The laser output pulse is about 50 μs long, but delayed 40 μs with respect to the onset of the discharge current pulse (Fig. 3.9b), indicating apparently the time interval needed to achieve population inversion and lasing action. Pulse lengths of 2 μs to 20 μs and delays before the onset of laser action of 10 μs to 28 μs at currents of 50 A to 180 A have been reported by Sochor and Branen (SOC 67). At very high peak currents, pulsed laser radiation 50 μs in duration and delayed 90 μs has been observed by Turner and Poehler (TUR 71).

It has been observed that power of the pulsed laser was

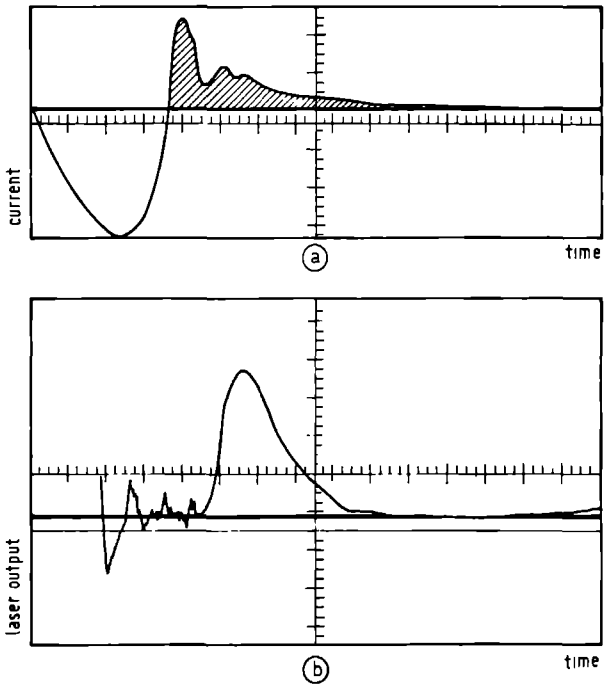

Fig. 3.9a and b) The time dependence of the laser discharge current pulse (horizontal 2 μs/cm vertical 1.53 kA/cm);

b) the oscillogram of the HCN laser output pulse indicating delay with respect to the offset of the current pulse (horizontal 20 μs/cm, vertical 10 V/cm). The results are obtained with 4:1 ammonia/methane mixture, at 0.5 Torr and repetition rate 2 Hz.

always obtained independently of the position of the resonator plane mirror. This is explained by time dependence of plasma refractive index during the discharge. Consequently, optical length of the cavity, defined as the product of refractive index and physical distance between the two resonator mirrors will change. This alteration of optical length can be comparable

to the mode spacing, and since two cavity modes sweep Doppler broadened gain profile, lasing can occur at any setting of cavity mirrors with practically negligible power fluctuations. Observations that support this explanation can also be found in work of Kon et al .(KON 67), who analyzed interferograms for pulsed laser with static filling.

Estimated peak power obtained with our 4 m HCN laser was about 15 W at 0.7 Torr, 3 Hz and low flow for 1:1 ammonia/methane mixture. However, accurate figures for observed power require the use of a faster detector. Further optimization of discharge parameters such as flow, gas composition, repetition rate and eventually resonator type itself should result in power levels on the order of 100 W. Such prediction is based on experimental results obtained by other investigators using comparable electrical input energies (YAM 68, SHA 72). Because of hazardous effects of radiatively induced currents on the diode, the work on the pulsed HCN laser was not continued.

3.8 4 m HCN laser with hole coupling

Extraction of laser power by means of a circular apperture in the center of the resonator mirror is a well established and effective coupling method. Partially transmitting dielectric coatings are not commonly used at submillimeter wavelengths, since a film thick enough to reflect most of the incident radiation would attenuate transmitted radiation.

The construction of the hole output coupler was undertaken to test its performance against the Michelson output coupler in laser cavities of comparable N. A near confocal configuration was chosen for such system. The design featured two identical aluminum spherical mirrors with 3.8 m radius of curvature sepa-

rated by 4 m. Mirror spacing is larger than confocal spacing in order to avoid unstable configuration and the resonator properties are practically equal to those of ideal confocal resonator. Fresnel number of the resonator was 1.2 at 337 μm, and the circular hole was drilled in the spherical mirror close to the cathode (BIC 75c).

The shape of the coupling hole is shown in Fig. 3.10. The acceptance angle 20^{o} was chosen deliberately to be much larger than the angle α_1 of the first order diffraction maximum, given by (TRA 72):

$$\alpha_1 = \text{arc sin } (1.22\ \lambda/d_{beam}) \qquad (3.3).$$

Here d_{beam} refers to the hole diameter so long as the aperture is smaller than the cross section of the emerging beam. Both mirrors were coated with a 3000 Å thick gold coating. In order to prevent potentially lethal shocks, the metal mirror was placed in an insulating perspex container that also accomodated the vacuum seals and a TPX lens. The assembled unit mounted on the laser is also shown in Fig. 3.10.

Field distribution and diffraction losses at reflectors of an asymmetric confocal resonator with an output hole in one mirror have been theoretically analyzed by Moran (MOR 70). The analysis was performed for low loss modes with the Fresnel number of the resonator ranging from 0.8 to 1.2. Moran's results indicate that the presence of the hole perturbs the field distribution. Distortion of the field distribution is more pronounced for low order modes and at larger Fresnel numbers. Stated differently, the TEM_{00q} mode will be more perturbed than TEM_{10q} mode at increased hole diameters (the same is also true for all modes exhibiting maxima at mirror center).

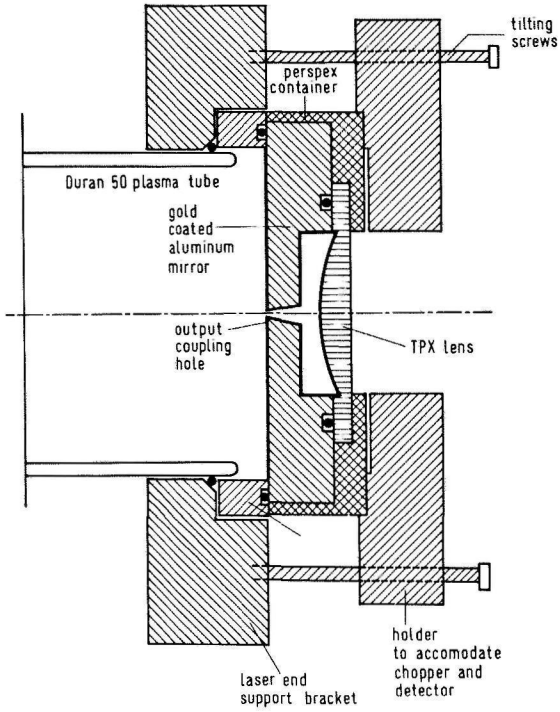

Fig. 3.10 The hole output coupler arrangement used with the 4 m HCN laser.

Average diffractive loss for low order modes in cylindrical confocal resonator with $0.4 \leqslant N \leqslant 1.6$ and hole Fresnel number N_o ($N_o = a_h^2/L\lambda$ with a_h being the hole radius) has been studied by Mc Nice and Derr (NIE 69). By introducing the concept of aperture efficiency, he has separated the energy lost around the edges of the mirrors (that does not constitute the useful output) from the energy propagated through the hole.

Figure 3.11 shows measured laser output power (in arbitrary units) plotted versus the hole diameter $2a_h$ for our near confocal, N=1.2, HCN laser resonator. Results are obtained under the following experimental conditions: current 0.9A, pressure 0.6 Torr, actual flow rate of 1:1 ammonia/methane mixture 11 lit/min of air at 20^oC and at given pressure, and tube temperature 105^oC.

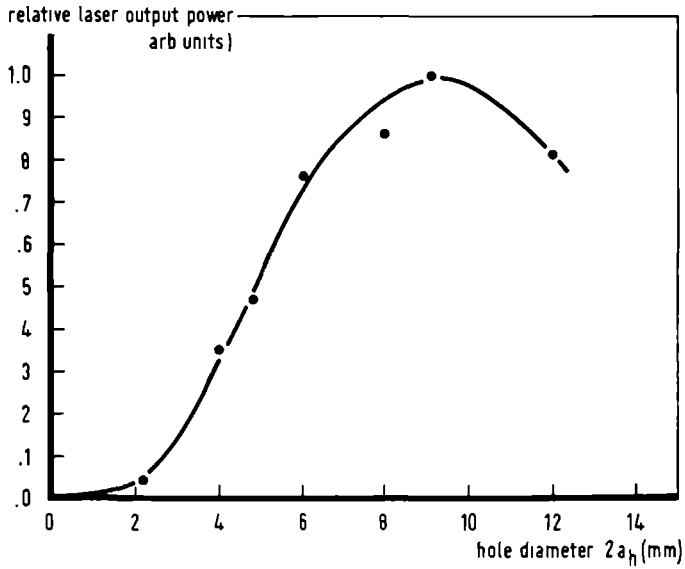

Fig. 3.11 Relative laser output power versus the hole diameter. The active medium is 1:1 ammonia/methane mixture.

It is seen in Fig. 3.11 that at small output hole diameters, the measured output power is proportional to the hole diameter. This is consistent with the theoretical predictions (NIE 69) because for small hole diameters the power loss in the fundamental mode is mainly due to diffraction around the edges of the mirrors. This is not true for increased hole diameters where the energy coupled out through the hole becomes a considerable fraction of the total resonator loss. The optimum coupling is obtained for the hole diameter $2a_h$ about 9.5 mm. At this value the area of the hole is approximately 1.25% of the total reflecting mirror area. A number of investigators have found optimum hole areas varying within 1 to 5 % of the mirrors area (KON 67, ONO 70, VOL 72, DYU 73).

It is of interest to discuss these results from Fig. 3.11 in view of considerations in Sect. 3.4. For almost confocal resonator with N = 1.2, diffractive loss per round trip is very low, 0.000015 and the reflection loss per round trip equals 0.01, so that a total loss is 0.01003. With G = 0.252 (see Sect. 3.4), and $\omega_1 = \omega_2 = 20.7$ mm, Eq. 3.1 gives $t_{opt} = 0.04$, and hence $a_h = 3$ mm from Eq. 3.2. The discrepancy between the calculated and measured values for the optimum hole coupling diameter is most likely due to the uncertainty in discerning the G and, in particular, L. The amount of laser power obtained at optimal hole diameter (Fig. 3.11) in confocal resonator (N=1.2) was about 30 % larger than maximum power observed with the 4 m HCN laser using semiconfocal cavity (N=0.92) under the comparable operating conditions and for the same diameter of the discharge tube. However, the polarization of the emergent laser beam is ambiguous. Because the availability of linearly polarized radiation from the laser is highly desireable for the sideband generation experiment (see Chapt. 4), the Michelson interferometric coupler utilizing 59 μm polyethylene beam splitter (see Sect. 2.3.2) was preferred to the hole coupling arrangement, even at risk of sacrifying some amount of power that was potentially obtainable.

Volume 15, number 2 OPTICS COMMUNICATIONS October 1975

THE EFFECT OF HYDROGEN ADDITION TO SOME HCN LASER ACTIVE MIXTURES ON THE C W OUTPUT POWER AT 337 μm

Dane D BICANIC and A DYMANUS
Fysisch Laboratorium Katholieke Universiteit Nijmegen The Netherlands

Received 27 June 1975

An experimental investigation has been carried out in order to find out the effect of hydrogen gas addition to the basic HCN laser fuel on the continuous output power of the laser at 337 μm The experiment has been performed by adding hydrogen to the striated discharge at a constant flow rate, pressure and external glass tube temperature and for stabilized currents ranging from 0 2 to 0 9 A With the exception of the ethylene–nitrogen mixture, the output power of the laser decreased for hydrogen enriched mixtures regardless of the magnitude of the hydrogen percentage added to the basic constituents However, the alteration of the chemical composition of the gaseous mixture led to the variable mode suppression at 337 μm for the fundamental transverse and the next higher mode

1 Introduction

Although hydrogen has been shown to act as the buffer gas in the water vapor laser, little is known about the effect of addition of hydrogen to the basic mixture consisting of gaseous compounds of C, H and N in the submillimeter HCN laser [1,2] At the present time, the HCN laser is still the most powerful source of submillimeter radiation, and a further increase of the output power level is highly desirable for many applications Adam has reported an increase in power by one order of magnitude, when hydrogen in 6 1 proportion was added to HCN in the TE HCN laser [3] The mass spectroscopic studies performed on the striated c w HCN laser positive column plasma, revealed a dominant production of H_2 among the other dissociated products [4–6] It has been observed, that the output laser power and the concentration of the mass number 2, both exhibit maxima at the same value of the discharge current, and that a laser inactive mixture could be made to lase if a proper amount of hydrogen is added to the discharge [5,7] Unlike hydrogen, the investigation of the presence of helium as buffer gas in the HCN laser active mixtures has been more thorough, though some contraversory still prevails in the available literature [8 11] Most investigators found that the laser output at 337 μm for He enriched mixtures increased to the certain pressure value Further addition caused reduction of the output power, and finally the laser action ceased An important feature of the He addition is the possibility of adjusting the optimum wall temperature, combining thus the high power output with clean tube operation [12]

This experiment has been undertaken in order to get more insight into the role that hydrogen as the buffer gas has on the output power of the continuously operating HCN laser Due to the complexity of the entire problem, the power measurements have been done at identical discharge conditions (namely the laser current, pressure, tube temperature and the total flow rate) for each mixture investigated

2 Experimental

The axial discharge HCN laser was 4 m long with gold coated mirrors, 10 cm in diameter, in a semi confocal arrangement ($R_1 = 8$ m, $R_2 = \infty$, $N = 0\,92$, where the R's refer to the curvature radii, and N is the Fresnel number of the resonator at 337 μm), and the interelectrode separation was 3 58 m The submillimeter radiation has been coupled out by means of a 59 μm thick polyethylene beam splitter positioned at 45° with respect to the laser axis [13] A schematic diagram of

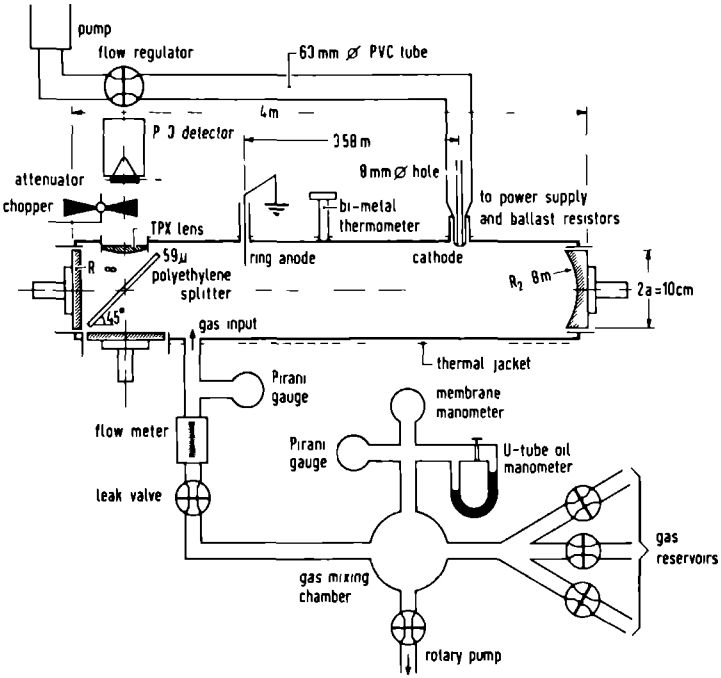

Fig 1 The schematic diagram of the setup used in this experiment

the experimental setup is shown in fig 1 The gaseous components were separately admitted into the mixing chamber where the pressure of each constituent gas as well as the total pressure of the mixture could be controlled by a Heraus Diviac membrane manometer, oil manometer and a Pirani Balzers gauge type TPG 022, respectively The fore-pressure in the gas mixing chamber was kept constant at 17 torr during all the measurements Another rotary pump AEG 71 N, connected to the outlet of the mixing chamber and provided by a regulating valve, facilitated the maintenance of the constant forepressure and prevented the pressure in the laser tube to increase due to the excessive gas quantity Another vent of the mixing chamber was coupled to the variable Leybold 17317 fine leak valve The mixture was then passed through the Brooks R 2-15A flow meter in order to measure the total flow, and subsequently admitted to the laser tube near the anode end The DK 25 Leybold pump was used to pump the gas through the 8 mm central hole drilled in the cathode, and through a 5 m long PVC pipe (53 mm inner diameter) connected to it The pumping line was terminated by an flow regulator which provided additional flow control, if required

The external temperature of the Duran 50 glass tube (94 mm inner diameter, with 3 mm thick wall) was measured near the anode end by means of a bi-metal thermometer placed in direct contact with the outer wall of the discharge tube In order to reduce the heat dissipation the 1 mm thick aluminum shield has been wrapped around the laser tube When the laser was run at about 105°C external (the temperature inside the laser discharge tube was not measured, but it is believed to be 30–40°C higher) no polymer deposit has been found on the inner walls after 300 hours of operation for all of the investigated mixtures A tentative expla-

nation of this effect is that the inner wall temperature is higher than that of the gas itself, thus preventing the condensation and the formation of the polymer crust. We have observed that the laser output is in general strongly affected by the discharge tube temperature, and that the maximum output for the particular mixture is obtained at a temperature slightly lower than 105°C external, as measured under the protective buckler. These observations agree with the results published elsewhere [12,14]. We have also noticed, that the temperature associated with the highest output power is dependent on the gaseous mixture used as an active medium.

3. Results

In fig. 2 is plotted the laser output power contained in the TEM_{00} mode at 337 μm versus the percentage of hydrogen added to the nominal mixture at the specified discharge conditions (0.6 A stabilized, stationary striations, pressure 1 torr, outer wall temperature 105°C and flow rate of 390 cm^3/min air at STP, i.e. approximately 11 lit/min air at working pressure). The methane–ammonia mixture CH_4–NH_3 in 1 : 4 proportion has been found to produce the highest output power, and has therefore been chosen as unity (the absolute maximum at the given conditions was about 18 mW as detected by a Molectron P-3-00 detector). For the accurate measurement of the detected voltage, the signal from the pyroelectric P-3-00 detector has been fed into a Philips GM 6012 tube voltmeter. The meaning of the diagram shown is best illustrated by an example. In case of the CH_4–NH_3 1 : 4 mixture, the points corresponding to the abscissa values of 0.50 and 67 should be interpreted as the following volume ratios of the three gases involved: CH_4–NH_3–H_2 = 1 : 4 : 0, 1 · 4 : 5 and 1 : 4 . 10, respectively. Fig. 2 clearly shows the laser power reduction for all basic mixtures when hydrogen is supplied, with the exception of the ethylene–nitrogen C_2H_4 N_2 1 : 1 gaseous mixture. The cursively written numbers at the points of maxima refer to the atomic C : H : N concentrations in the appropriate mixture. At the top of the C_2H_4–N_2–H_2 diagram, the C and N concentrations are comparable and that of hydrogen is four times that large (i.e. C : H : N = 1 : 4 1), which is higher than the value reported by Schotzau [7], A similar form of the curve as for C_2H_4–N_2–H_2 has been

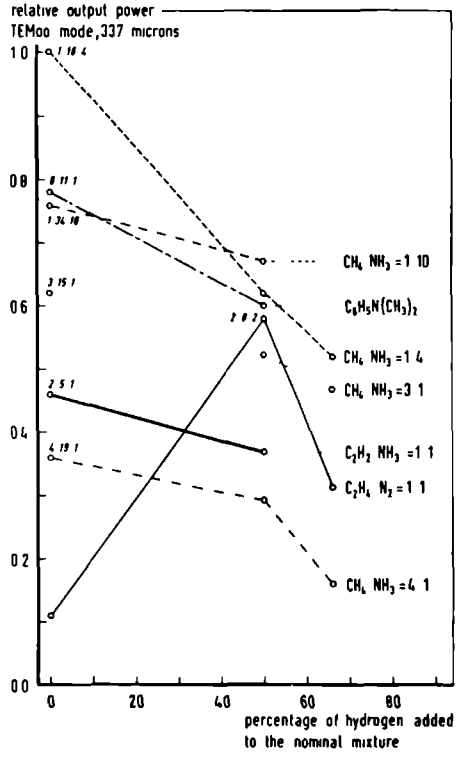

Fig 2. Relative output power contained in TEM_{00} mode at 337 μm, plotted versus the percentage of the added hydrogen, for the several mixtures, at given discharge conditions.

confirmed by investigating the ammonia–acethylene NH_3–C_2H_2 2 : 1 mixture, in which the C, H and N concentrations obey the same ratio (not drawn in fig. 2, however). The variation of the mixture composition by the hydrogen addition has altered the mode suppression factor defined as the ratio of powers in the TEM_{00} and TEM_{10} modes. For example, this ratio increased from eight for pure dymethylamine $C_6H_5N(CH_3)_2$ to fifteen for the $C_6H_5N(CH_3)_2$–H_2 1 . 1 mixture. On the contary, the same parameter for C_2H_4–N_2 dropped from thirteen to nine for the C_2H_4–N_2–H_2 1 : 1 : 2 medium with accompanying considerable boost of the output power level. We sup-

pose that the variation of the mode suppression ratio is to be attributed to a change in the ambipolar diffusion coefficient and consequently to affection of the laser gain in the radial direction [15] Chemical excitation and surpression of HCN laser modes has recently been reported for some other laser active mixtures [16]

Our results relate to one particular set of pressure and flow values, both choosen as to ensure high power output, and at a typical current value of 0 6 A One would normally anticipate, that the data expected to be obtained if this experiment is repeated at another set of discharge parameters, would be the scaled version of our results [13] In summary, we conclude that hydrogen as a buffer gas added to the basic fuel of a HCN laser, produces an increase of the output power only in mixtures of relatively low hydrogen concentration Apparently, most of the mixtures with higher gain factors that we have investigated, possess already the hydrogen concentrations required for the optimum out put power level

Acknowledgements

The authors want to express their appreciation to Mr E G H van Leeuwen for his invaluable suggestions and extraordinary assistance during the course of the entire experiment, as well as to Mr P Claus for designing the current stabilization unit Gratitude is to Messrs F P van der Meer, F S de Boer, G v Lieshout, A Th Diels, S Geertsen and Th C Oor for the steady and most enthusiastic collaboration

References

[1] S F Dyubko, V A Svich and R A Valitov, Sov Phys Tech Phys 13 (1969) 1596
[2] S F Dyubko, V A Svich and R A Valitov, Sov Phys Tech Phys 14 (1969) 855
[3] B Adam, U Zimmerman, H J Schotzau and F K Kneubuhl, Conference Digest, Intern Conf on Submillimeter Waves and Their Applications, Atlanta, Ga (USA), (1974) p 78
[4] H J Schotzau, H J Mahler and F K Kneubuhl, Phys Lett 38 A (1972) 286
[5] H J Schotzau and F K Kneubuhl, Z Angew Math Phys 23 (1972) 11 a
[6] H J Schotzau and F K Kneubuhl, Appl Phys 6 (1975) 25
[7] H J Schotzau, Ph D Thesis, ETH Zurich (Switzerland, 1973)
[8] R Volk, Phys Lett 42 A (1972) 321
[9] G Morris, C Brand and H Jacobs, J Quant Elect IEEE QE-6 (1970) 180
[10] W Muller and G Flesher, Appl Phys. Lett 8 (1966) 217
[11] K Yoshihiro and C Yamanouchi, Rev Sci Inst. 45 (1974) 767
[12] P Belland and D Veron, Opt Commun 9 (1973) 146
[13] D D Bicanic and A Dymanus, Inf Phys 14 (1974) 153
[14] S Ono, K Hotta and Y Shibata, Paper pres at 8th Conf Microwave and Optical Generation and Amplification (Kluwer, Deventer, The Netherlands, 1970)
[15] J D Cobine, Gaseous Conductors - Theory and Applications (Dover Publications Inc New York, 1958) p 236
[16] H J Schotzau and F K Kneubuhl, Phys Lett 46 A (1974) 415

Infrared Physics 1976 Vol 16 pp 601 604 Pergamon Press Printed in Great Britain

IMPROVED CW POWER CHARACTERISTICS OF HCN LASER SYSTEM AT 337 μm

D D Bicanic and A Dymanus

Fysisch Laboratorium Katholieke Universiteit Toernooiveld Nijmegen The Netherlands

(*Received* 24 *December* 1975)

Abstract An extensive experimental investigation of the CW output power characteristics of several striated HCN laser systems has been performed at given pressure flow rate and discharge tube temperature with regulated currents ranging from 0 3 to 0 8 A Some of the laser media studied have been found to produce output power levels higher than generally expected for popular gaseous fuel mixtures

INTRODUCTION AND EXPERIMENTAL

A low pressure CW electrical discharge through gaseous mixture containing vapor compounds of C, H and N atoms which thus synthesizes HCN molecule, has been found to produce stimulated emission at numerous submillimetre wavelengths Although originally encountered in the pure hydrogen cyanide discharge, active gas mixtures can have virtually any composition provided they contain the C, H and N atoms [1] However, moderate c w output power levels and low efficiency at 337 μm presently obtainable with striated HCN laser systems are mainly due to the inherently low unsaturated gain factors of the active media [2 3 4] Therefore, a series of extensive investigations have been initiated to further improve the laser performance [5 6 7]

This communication describes an experiment in which several gases mixed in various proportions have been tested and compared for power performance when used as active media at 337 μm under identical discharge conditions Detailed descriptions of the laser set-up used in this experiment have been described previously [8 9 10] and will be omitted here The gases were fed into the mixing chamber and then admitted into the laser resonator near the anode end The total pressure and the flow of the particular mixture, both chosen to maximize the output power, were kept constant during all the measurements, and the submillimetre power contained in the fundamental transverse mode was measured as (i) function of the regulated laser current and (ii) function of the external temperature of the laser tube (around which the thin Al shield has been wrapped) at the given current value The usage of the shield disposed of the formation of the brownish paracyanogen polymer on the inner walls of the discharge tube and thus assured stable Q factors and output powers

RESULTS AND CONCLUSIONS

We have studied about forty different gas mixtures, each one containing vapours of one, two or more of the following constituents ammonia NH_3, dimethylamine $C_6H_5N(CH_3)_2$, methane CH_4, nitrogen N_2, carbon monoxide CO, ethylene C_2H_4, acetylene C_2H_2 and diethylether $(C_2H_5)_2O$ respectively The working pressure in the laser tube and the actual flow were approximately 1 torr and 11 l/min of air when reduced to standard temperature The external temperature of the Duran 50 laser tube (2 5 mm thick walls), measured by means of a bimetal thermometer placed under the protective buckler, was about 105 C Figure 1 (where the numbers written above the curves refer to the ratio of the atomic concentrations of carbon, hydrogen and nitrogen respectively) shows the normalized output power in the TEM_{00} mode detected at 337 μm for some of the media investigated plotted versus the regulated laser current

In general, the results of our measurements relevant to the output power measured under the discharge conditions specified above, may be summarized as follows

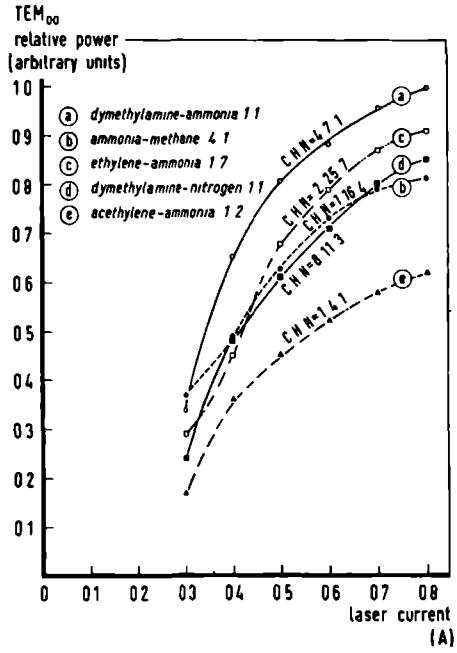

Fig 1 The TEM_{00} mode relative power at 337 μm plotted vs the laser current for some of the investigated media The remaining parameters of the striated discharge are as follows pressure ~1 torr flow 11 l/min air at standard temperature and external tube temperature 105 C

(i) The most significant result is the increase in power by about 30% observed for $C_6H_5N(CH_3)_2$–NH_3 1 1 [curve (a) in Fig 1] and likewise C_2H_4–NH_3 1 1 [curve (c) in Fig 1] mixtures, when compared to the power levels currently accessible with NH_3–CH_4 4 1 blend [curve (d) in Fig 1] We have already reported that this latter mixture yields higher output than the popular CH_4–N_2 1 1 blend[9 11] besides producing cleaner discharges

(ii) Using pure dimethylamine $C_6H_5N(CH_3)_2$ as the flowing vapor we have obtained CW laser action at 337 μm with output power being at higher currents ($\geq$0 4 A) roughly 70% of that of curve (a) shown in Fig 1 No enhancement of the relative power has been observed when methane or nitrogen were used as additive gases to the pure dimethylamine in 1 1 proportion, as the output powers obtained with these three mixtures were practically the same within the limits of experimental error An increase in nitrogen concentration, such as in for example, $C_6H_5N(CH_3)_2$–N_2 1 2 and 1 3 mixtures reduced the output laser power by 15 and 25% when compared to $C_6H_5N(CH_3)_2$–N_2 1 1 blend

(iii) It was quite difficult to get striated discharges when carbon monoxide was one of the initial components in the mixtures NH_3–CO 1 1, CH_4–NH_3–CO 1 1 3, 1 1 1 and 1 4 5 This might be attributed to the development of very volatile nickeltetracarbonyl gas $Ni(CO)_4$ formed by the interaction of the CO with the nickel coated electrode A peculiar effect observed with all the CO mixtures is the lowering of the threshold current to about 0 15 A indicating most likely more efficient populating processes in this current range[12] This resulted in power enhancement at low currents when compared to CO-free mixtures At high laser discharge currents the electron density is high, and the dissociation as well as other de-excitation processes tend to reduce the gain and consequently power drop for the CO enriched media

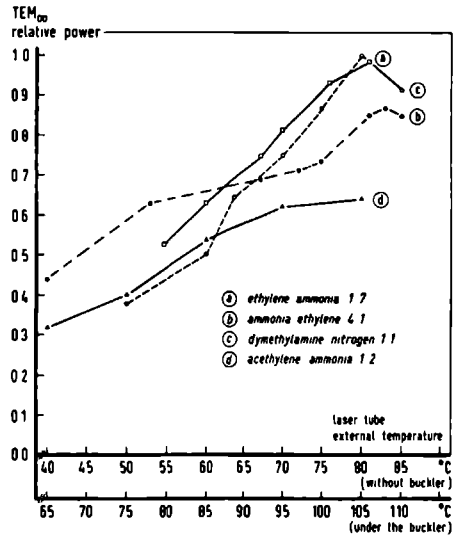

Fig 2 Temperature dependence of the TEM_{00} relative power at 337 μm for few laser media we have studied at laser current 0 6 A pressure ~ 1 torr and flow of 11 l/min air reduced to standard temperature

(iv) If the laser medium contained flowing mixture of diethylether and N_2 or NH_3 in 1 1 proportion, the power was approximately 80% (in the 0 4–0 8 A range) of that associated with the curve (a) in Fig 1 However, the powers observed with these mixtures were far below the values reported by Kotthaus for the same medium [13]

(v) The 1 1 mixture of C_2H_4 and N_2 produced generally low output powers across the entire current range [approximately one order of magnitude less than that of curve (a) in Fig 1] The addition of hydrogen to this medium in 2 1 1 volume proportion secured output powers of roughly 50% of curve (a) By further increasing the hydrogen content to 4 1 1 it was found that the hydrogen–ethylene–nitrogen mixture so formed could yield twice the relative power of the C_2H_4–N_2 alone, under the same discharge conditions Combinations of ethylene and ammonia gases were found to produce substantial output powers, the highest being observed for C_2H_4–NH_3 1 7 blend Lowering of the ammonia percentage in this class media, such as C_2H_4–NH_3 1 4, and 1 1 caused the power drop of 20 and 40% respectively

(vi) Of the mixtures containing the acetylene C_2H_2 the largest power was observed for C_2H_2–NH_3 1 2 blend [curve (e) in Fig 1] Lessening of the ammonia content in this mixture (to C_2H_2–NH_3 1 1 for example) led to reduction of the output power by roughly 40%

(vii) The dependence of the output power on the external temperature of the discharge tube has been observed for all the mixtures which were studied An example of such reliance for the striated positive column at 0 6 A with remaining parameters being already specified above, is shown in Fig 2

In as much as the evidence of the optimum-temperature could be rationalized and its prevalence is quite marked, the great complexity of the volume reactions and the wall processes in the typical HCN laser discharge makes any theoretical predictions disputable Even the tentative conclusion that some of the media we have investigated might *a priori* have higher gain factors than currently thought for the conventional submillimetre media cannot be formulated Instead, one should rather consider the axial field strength in discharge of a particular mixture as being responsible for affecting the optimum concentrations of the plasma energy carriers, i e hydrogen and nitrogen

It is nowadays well established, that just this ratio is determined by the value of the laser discharge current.[14,15]

Acknowledgements We are most grateful to Messrs E G H van Leeuwen, F S de Boer, M J Kaptein, B F J Zuidberg, A Wittlin, P Claus and A Groenen for the received assistance and stimulating discussions in the course of this experiment

REFERENCES

1 CHANTRY, G W, *Submillimetre Spectroscopy* Academic Press, New York (1971)
2 BIRCH, J R & C C BRADLEY, *Infrared Phys* **13**, 99 (1973)
3 STAFSUDD, O M & Y C YEH, *J Quant Electron IEEE QE* **5**, 377 (1969)
4 CORCORAN, V J, W T SMITH & J J GALLAGHER, *J Quant Electron IEEE QE-5*, 292 (1969)
5 VOLK, R *Phys Letts* **42 A**, 321 (1972)
6 BELLAND, P & D VERON, *Opt Commun* **9**, 146 (1973)
7 MORRIS, G, C BRAND, & H JACOBS, *J Quant Electron IEEE QE-6*, 180 (1970)
8 WELLS J S K M EVENSON, L M MATARRESE, D A JENNINGS & G L WICHMAN, *Tech Note* 395, Nat Bur Stds Boulder, Colorado (1971)
9 BICANIĆ D D & A DYMANUS, *Infrared Phys* **14**, 153 (1974)
10 BICANIĆ, D D & A DYMANUS, *Opt Commun* **15**, 175 (1975)
11 FRAYNE, P G *J Phys B* **2**, 247 (1968)
12 DYUBKO, S F & N TOPKOV, *Sov J Quant Electron* **3**, 56 (1973)
13 KOTTHAUS J P, *Appl Opt* **7**, 2422 (1968)
14 SCHOTZAU, H J & F KNELBUHL *Appl Phys* **6**, 25 (1975)
15 SCHOTZAU, H J & S VLPREK, *Appl Phys* **7**, 271 (1975)

C H A P T E R 4

GENERATION OF SUBMILLIMETER-WAVE RADIATION BY SUM AND DIFFERENCE-FREQUENCY MIXING OF HCN LASER AND MICROWAVE KLYSTRON IN METAL-SEMICONDUCTOR DIODES

4.1 Introduction

In the previous two chapters, constructional details and several experiments with the HCN laser have been described. The purpose of this chapter is to introduce metal on semiconductor devices, and in particular point contact (PC) and Schottky barrier (SB) diodes. Small area junction devices have been, and still are being used in experiments requiring mixing or detection of submillimeter radiation. Development of such devices is an active field of both fundamental and applied research.

It has been shown in Chapt. 1 that weak tunable sidebands (computed power levels about 10^{-11}W) can be generated by means of mixing the laser and klystron radiation in bulk media. However, continuous frequency tunability in the submillimeter region can also be achieved by using point contact devices as the non-linear mixing element. Unlike bulk media that have strong absorption bands and require phase matching, PC or SB diodes have no limitations on either input or output frequencies up to their cut-off frequencies.

Following the section in which the general properties of PC and SB diodes at high frequencies are discussed, this Chapter includes a detailed description of the video spectrometer. The last sections deal with the actual generation and reradiation of difference and sum-frequency sidebands, detected directly by means of the method presented in Chap. 1. Finally, generated signals at either sideband were used for high reso-

lution absorption frequency measurements of hydrogen sulphide H_2S and sulphur dioxide SO_2.

4.2 General consideration for PC and SB diodes at high frequencies

While the merits of the PC diodes with cat whisker have been well known ever since the early days of microwave spectroscopy, the SB diode with a planar metal film deposited on a semiconductor substrate has recently emerged to offer a higher level of performance. In general, it is believed that SB diodes have lower series resistance and noise characteristics than the conventional PC diodes. Due to its reliability, wide bandwidth, high response speed, mechanical stability and the strong non-linear behaviour, the SB diode represents the most promising mixer at submillimeter frequencies. Thanks to continual progress in the technology of diode material and micro-forming techniques, further improvements in performance can be anticipated in the future. Recent experiments with SB diodes produced by the novel advanced technique of electron beam lithography con-clearly confirmed their superiority when used as detectors and mixers at submillimeter wavelengths (FET 78, COL 78, KEL 78, WRI 78).

The high frequency behaviour of the diode can be obtained by considering its simplified equivalent circuit, shown in Fig. 4.1. The diode is represented by a voltage dependent barrier resistance R_n shunted by a barrier capacitance C, and both in series with a spreading ohmic resistance r_s. The resistance r_s can be determined from the current-voltage characteristics, or theoretically from the relationship valid for a circular contact area (TOR 48):

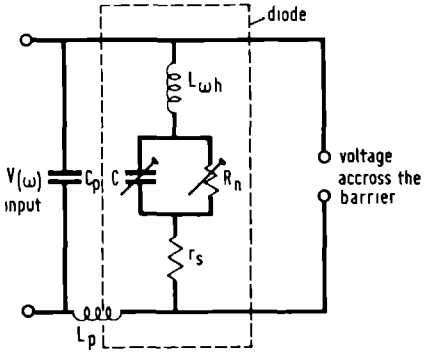

Fig. 4.1 Equivalent circuit of the diode.

$$r_s = 1/4\ \sigma\ a_c \tag{4.1}$$

where σ is the conductivity and a_c is the contact radius. An expression for the capacitance C associated with the rectifying barrier of a PC diode is given by Benson (BEN 69) and reduces at zero bias voltage to:

$$C_o = \pi\ a_c^2\ \{\ \frac{\varepsilon_o \varepsilon N_c\ e}{2\Phi_o}\ \}^{\frac{1}{2}} \tag{4.2}$$

where Φ_o, N_c, e and ε are the "built-in" potential barrier height, majority carrier density, electronic charge and relative dielectric constant of the semiconductor material, respectively. Conley (CON 67) gives for a uniformly doped SB diode the following expression that can be used to determine junction capacitance in the presence of an applied voltage:

$$C^2 = \frac{e\ a_c^4\ N_c\ \varepsilon\ \pi^2}{32(V_B - V_{dc} + \frac{3}{5}\ V_F)} \tag{4.3}$$

where V_F, V_B and V_{dc} indicates Fermi level of the semiconductor, the height of the metal-semiconductor interface and the applied d.c. voltage, respectively. Junction capacitance is related to zero bias capacitance C_o through:

$$C = C_o/(1 - V/\Phi_o)^{\frac{1}{2}} \qquad (4.3a)$$

where V is the fraction of the applied external bias voltage that appears at the diode junction (HEW 67).

The inductance of the whisker L_{wh} may also be considerable at high frequencies. The parasitic capacitive and inductive reactance of the diode package C_p and L_p must be small in comparison with other quantities if their influence is to be neglected.

An important parameter in considering the diode properties is the cut-off frequency given by $f_{co} = (2 \pi C_o r_s)^{-1}$. Using Eqs. 4.1 and 4.2 it is easy to show that

$$f_{co} = \frac{2}{\pi^2} \left(\frac{2 e \Phi_o}{\varepsilon\varepsilon_o}\right)^{\frac{1}{2}} \frac{N_c^{\frac{1}{2}}}{a_c} \qquad (4.4)$$

where μ is carrier mobility of the semiconductor material.

The equivalent circuit in Fig. 4.1 forms a potential dividing network: therefore the voltage accross the junction barrier at some angular frequency ω is lower than the applied signal voltage. For efficient diode performance at higher frequencies it is necessary to keep r_s and C_o as low as possible. In practice this means minimizing the contact dimensions since capacitance is dominated by $a_c^2\pi$. Zero bias capacitance in the order of 10^{-16}F have been reported, and the minimization of the spreading resistance r_s can be achieved by using the material of large

mobility and heavy dope.

Throughout this experiment n-type Te doped GaAs fabricated by Monsanto Company was used as crystal material to produce the PC diode. Its properties are as follows: resistivity $\rho = 0.003\ \Omega$ cm, mobility $\mu = 2500\ cm^2/V\ s$, carrier density $N_c = 8 \times 10^{17}/cm^3$, dielectric constant at 890 GHz $\varepsilon \sim 11$ and barrier height $\Phi_o \sim 0.8$ V. By substituting these values into Eqs. 4.2 and 4.4, a zero bias capacitance of $C_o = 3.2 \times 10^{-15}$ F and a cut-off frequency close to 4 THz are obtained. In these calculations a contact diameter $2\ a_c = 1.2\ \mu$m has been assumed; in Sect. 4.6 it is described how such whiskers have been prepared.

Schottky barrier chips provided by Dr. Harold Fetterman from Lincoln Laboratory, M.I.T.(USA) were used to produce SB diodes. Each chip consists of a matrix of barrier dots electroplated on a GaAs epitaxial layer through a protective quartz surface mask. The diameter of the barriers ranges from 1.5 μm to 7 μm, general description of these diodes can be found elsewhere (CLI 71). A spreading resistance of 10-15 Ω is estimated for this SB diode, and capacitance C_o is approximately 10^{-15}F for smallest diode (contact diameter equals diode size). Scanning electron microscope (SEM) photographs of a Te-doped GaAs crystal surface used to produce PC diode, and of Fetterman's SB diode are shown in Figs. 4.2a and 4.2b under low magnification. Fig. 4.2c shows again the SB diode SEM photograph taken at an angle of 20^o to the normal incidence.

By courtesy of Prof. Koji Mizuno of Tohoku University, Sendai, Japan and Dr. Gerald Wrixon, Department of Electrical Engineering, University College, Cork, Ireland, we have recently obtained several SB chips with diodes of smaller diameters but these have not yet been tested at the time of writing.

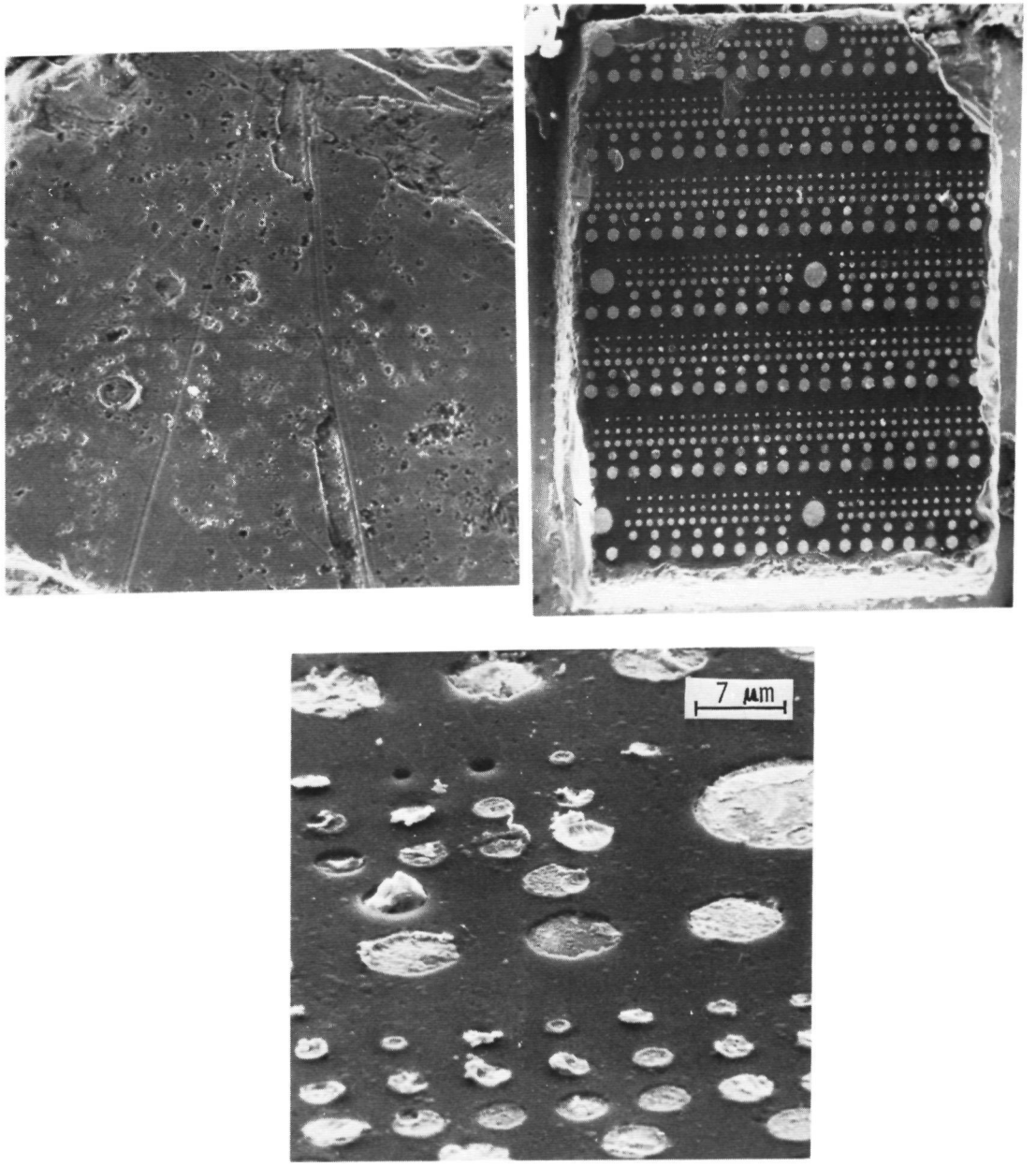

Fig. 4.2 The SEM photographs of:

a: n-type Te doped Monsanto GaAs crystal surface
b: GaAs Schottky barrier diode developed at M.I.T. Diode is soldered eutectically on a golden carrying pen.
c: M.I.T. Schottky barrier diode surface taken at a angle of 20^{o} to the normal.

4.3 The apparatus

In Chap. 1 the experimental set-up using PC or SB diodes as the non-linear element for sideband generation has been discussed without emphasis on technical details. This section provides a complete description of all components of the video spectrometer and detection system.

4.3.1 Physical and mechanical properties of the mixer

The mixer is the heart of the entire apparatus, and a major problem was the choice of a specific mixer that would most efficiently generate and reradiate the submillimeter sideband power. In the course of this experiment a large variety of diode mounts have been developed and tested for video and mixing performance, ranging from completely open (optical) structures to fully closed waveguide mounts (DIJ 71, ZUI 77, BIC 73, BIC 75a). Initially, an open mount mixer was designed for the sideband generation experiment (BIC 73). The output power of a 70 GHz klystron was launched towards the diode junction via an unterminated RG-99/U waveguide. Although such an open-end waveguide is an inefficient radiator of energy, due to impedance mismatch at the end, the emitted power was nevertheless estimated to be a few milliwatts. Klystron radiation should be coupled with the microwave electric field parallel to the whisker antenna. The distance between the open end waveguide and the whisker plane must be adjusted for the maximum absorption of microwave power.

Laser radiation should be coupled quasi-optically, namely by means of a lens that focusses the emergent beam onto the junction. The relative orientation of the whisker and incident electric field of the laser is important in such open type struc-

tures (MAT 70). Therefore a frame, which carried the klystron source and microwave components with the mixer was constructed. The frame could be rotated with respect to the plane of the electric field of the laser, in such a way that relative orientation of the whisker and microwave electric field vector remained unaltered. The same antenna is used for both receiving and emitting the radiation. Detection of radiation reemitted from the diode should then, consistent with directional characteristics predicted by the antenna theory, be attempted along direction of the strongest lobe close to the wire.

Suggested open mount mixer was only tested for video performance at 890 GHz. Focusing the laser power was achieved rather easily, but tuning by means of plane short circuiting plunger was not optimal.

Later in the course of this project, a mixer was designed consisting of three stacked rectangular waveguides, each located in a distinct plane (BIC 75). This mixer resembles a conventional cross-waveguide harmonic generator, to which a third waveguide oriented at 45^{o} to both mixer arms has been added. In the final design, a quasi-optical structure was adopted consisting of a circular waveguide terminated by a horn to collect the laser radiation and sandwiched between two rectangular waveguides (BIC 75).

A cross sectional and exploded view of the final mixer is shown in Fig. 4.3 and 4.4, respectively. The three waveguide system was preferred to an open mount as it enabled independent tuning of three relevant frequencies. The klystron radiation was transmitted through a rectangular silver coated RG-99/U waveguide [inner dimensions $a_1 \times b_1$ = (3.099 x 1.549)mm and cut-off frequency 48.37 GHz] in the fundamental mode. The ra-

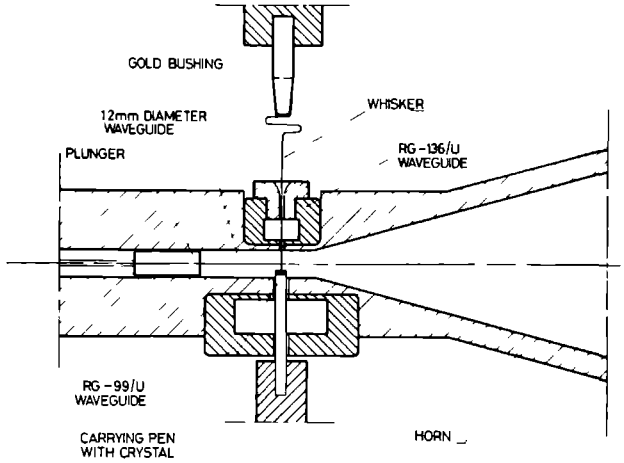

Fig. 4.3 The cross sectional view of the triple arm mixer developed in the course of this experiment.

diation at the sideband frequency was propagated through RG-136/U waveguide [a_1 x b_1 = (1.75 x 0.85)mm and cut-off frequency 85.7 GHz] oriented with the longitudinal at 90^o with respect to the axis of the klystron waveguide. Note that RG-136/U is several times oversized for submillimeter wavelengths,since the waveguide for the fundamental mode at 337 μm should heve dimensions of (0.254 x 0.127)mm. In addition to technical difficulties associated with fabrication ad mounting such a small waveguide, its power attenuation is prohibitive. In general power attenuation increases with wavelength for a given size of the waveguide, and decreases with increase in waveguide dimension for given wavelength (MAR 67). Attenuation (assuming a perfect surface finish) in oversize rectangular waveguide RG-136/U is about 15 dB/m at 337 μm. However, an addition of 80 dB/m is calculated, using relations of Laredo (LAR 64) for fundamental waveguide at 337 μm. A priori excitation

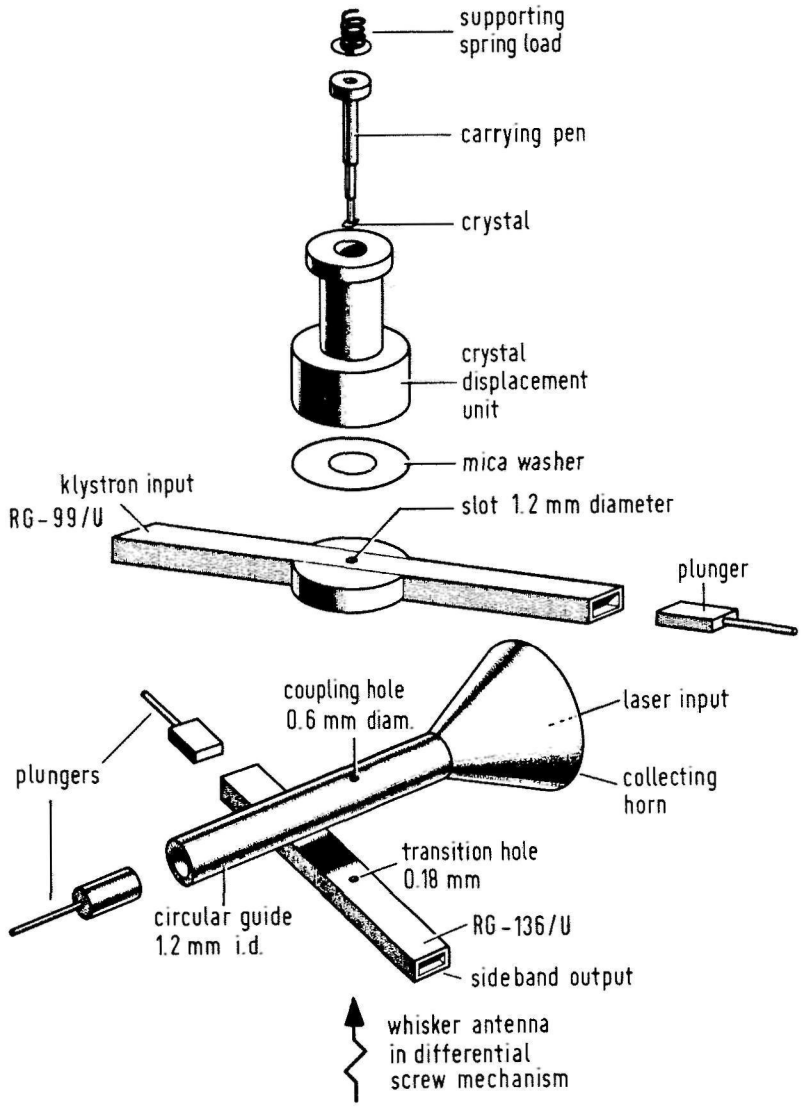

Fig. 4.4 Exploded view of three level mixer used for submillimeter sideband conversion experiment.

of the fundamental mode in an oversize waveguide is not anymore guaranteed. Analysis of resonance condition shows that RG-136/U waveguide can support eight different modes at the most intense HCN laser frequency.

The circular waveguide has an inner diameter of 1.2 mm and served as the input arm for the HCN laser power. Laser radiation is coupled into the junction by means of a lens which focusses the submillimeter radiation onto a copper horn which terminates the circular waveguide. The conically shaped horn formed an integral part of the circular waveguide, as both were electroformed as a single unit. The horn was designed to match the input radiation with a minimum of reflection loss. It is 42 mm long with a 23 mm circular aperture at its mouth and terminated by a smooth transition to the 1.2 mm diameter waveguide. In order to maximize power density at the junction plane, the diameter of circular waveguide was chosen to be comparable to the spot size formed by the focusing lens (see Sect. 2.3.1). The shape of the horn was designed to fit the envelope of the intensity distribution pattern formed by the F/1.8 lens (TPX material, 70 mm diameter and 130 mm focal length). The three waveguides were soldered together producing a compact wafer unit (Fig. 4.5) that could be easily mounted (or demounted).

A pointed metalic wire (tungsten for SB and gold-copper alloy for PC diodes) 50 μm thick acting as a receiving and emitting antenna, was passed through a common hole drilled through the three waveguides. This whisker was several millimeters long ($\sim$ 10 mm measured from the crimp to the tip) and was welded to a nickel post held in a differential screw mount with anti-backlash spring. To assist the alignement, the whisker passes through 0.06 mm diameter gold bushing prior to

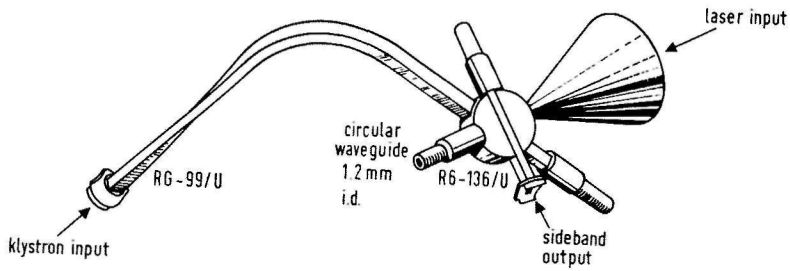

Fig. 4.5 The compact unit containing three soldered waveguides. The twist/90^0 bend in the RG-99/U klystron input arm was needed to satisfy matching requirements imposed by the geometry of the interacting fields.

entering the output waveguide of the mixer. The hole between the middle and the output waveguide has a diameter of 0.18 mm. It was established experimentally that mixer performance with a coupling hole of this diameter was better than with initially used 0.7 mm diameter hole, although no final conclusion can be drawn with respect to overall improvement that might eventuall result by trying other hole diameters. The wall thickness between two adjacent waveguides was reduced to about 0.1 mm. Great care has to be taken not to create a structure that is too fragile and susceptible to mechanical shocks. Reduction of wall thickness was necessary, after sufficient evidence has been collected in preliminary experiments indicating occurrence of large coupling loss for 1 mm thick walls.

To produce a point contact diode the whisker antenna linking two top waveguides was brought in contact with a prepared semiconductor crystal surface. Feeble contact was usually made with

the crystal protruding roughly one third of the middle waveguide. The crystal was soldered eutectically to a 0.5 mm diameter golden pen, mounted concentrically in a 1 mm diameter brass post that completely protrudes into the RG-99/U waveguide and functions as a antenna for microwave radiation. A hole of 0.6 mm diameter, slightly larger than the pen's own dimension, served as coupling slot between the upper wall of RG-99/U and the circular waveguide. Wall thickness between these two waveguides was also milled down to 0.1 mm. Finally, a 1.2 mm diameter hole was drilled in the 1 mm thick bottom wall of the microwave waveguide to allow the insertion of the brass post. An insulating mica washer acting as the microwave choke was inserted, as the leakage into this part of the mixer must be small. The bottom section of the mixer is a near duplicate of early harmonic generator developed in this laboratory (HUI 66). The IF impedance matching section used successfully by van Dijk and Zuidberg was not used in the mixer (DIJ 71, ZUI 77). The brass post displacement unit, that could be adjusted externally provides a convenient method for the coarse adjustment of the crystal penetration depth in the middle waveguide. Supporting spring load exerts slight force in upward direction and provides connection with the NBC connector. Equidistant, small holes drilled in the base of the post permit the rotation of the crystal without changing the penetration depth.

As seen in Fig. 4.4 all mixer arms were terminated by short circuiting plungers that could be accurately repositioned for independent impedance matching in each arm of the mixer. Care was taken to work with plungers that display good symmetry about their axis over the entire region accessible to the electromagnetic field. Since it has been observed that performance of the

plunger is dependent on its surface condition, cleaning from time to time was required.

For the optimum coupling of submillimeter radiation to the diode, the mixer unit was oriented with the whisker parallel to the electric field of the laser radiation. As shown in Sect. 2.3.2 the output laser beam is polarized in the plane perpendicular to that containing beam splitter. The condition for required mutual parallelism of the microwave electric field and the whisker, was in view of above laser field geometry, fulfilled by inserting twist/90^{o} bend section in the RG-99/U waveguide run. Figure 4.6 shows the photograph of complete mixer unit.

4.3.2 The monochromator

A system that could resolve faint sidebands from spectrally close but more intense laser radiation was considered indespensible for the success of this experiment. A modified version of the microwave grating monochromator developed by the Solid State Physics Group of Prof. Wyder for the identification of higher harmonic generated by a 100 GHz klystron was constructed and used for this purpose (KOR 78). The term monochromator is reserved here for selecting device; spectrometer includes the source and detector as well.

Basically, the monochromator shown in Fig. 1.2 within the dotted line consists of an input RG-136 waveguide flange to which a parabolic horn is attached, followed by a diffraction grating, spherical mirror, metal mesh and lightpipe that guides the selected radiation through the exit slit to the absorption cell and detector. After initial spatial collimation by the parabolic horn, the composite beam is falling on the grating.

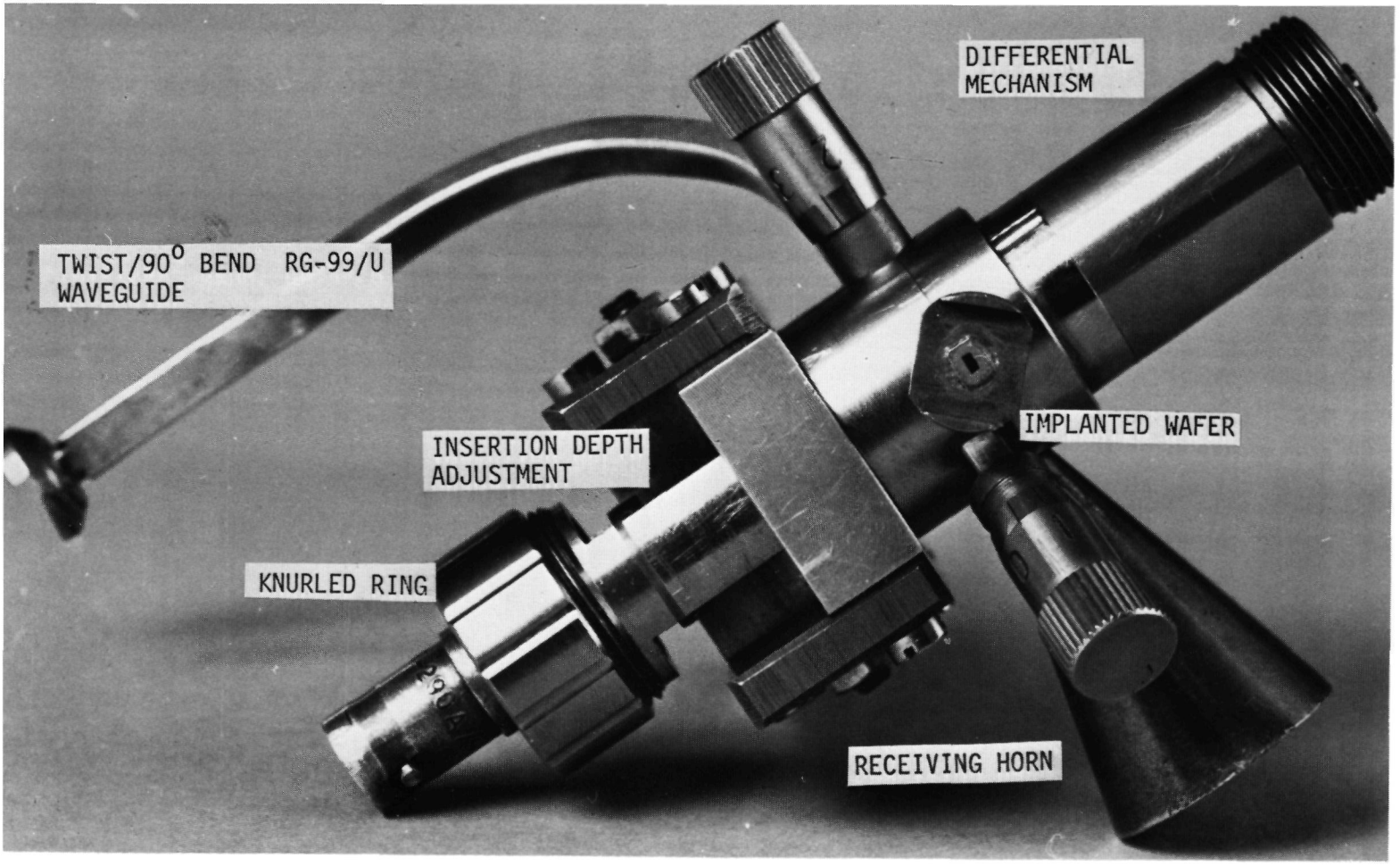

Fig. 4.6 The photograph of the assembled triple arm mixer. By means of an suitable foot, the entire mixer could be fastened to the base plate thereby forming an integral part of the monochromator.

Various spectral components are spatially separated by the grating and collected by the mirror that refocusses them to the entrance of the exit lightpipe. The function of the metal was to provide large rejection at the laser frequency, without affecting significantly the generated sidebands. Black painted screen with circular aperture that equals the size of the exit lightguide diameter was stretched across the short side of the monochromator wall to prevent off axis signals, propagating otherwise than through the hole from reaching the detector. Monochromator components were contained in an aluminum box with inner dimensions of 540 mm x 192 mm and 9 mm thick walls. The inside of the apparatus was coated with the antireflecting material and could be operated at reduced pressures if required to eliminate absorption by water vapor. All optical components used in the monochromator were of high accuracy and precision.

4.3.3 Parabolic horn reflector

The output RG-136/U waveguide of the mixer, down which the desired sideband is propagating, was via an short section of identical waveguide connected to the input horn of the monochromator. This auxilliary section includes also an twist/90^{o} bend to provide the coupling between mixer and monochromator with input slit oriented perpendicularly to the symmetry axis of RG-136/U mixer arm.

The horn has a fixed aperture and serves primarily to collimate the beam incident on the diffraction grating. Overall distance between center point on parabolic surface and horn throat was 100 mm. Dimension of parabolic surface is large compared to the wavelength used (MAL 63).

Frequent need for mounting/demounting of the mixer unit,

and the small spot diameter of the focused laser radiation required the possibility for accurate spatial repositioning of the mixer. This was realized by rigidly locking the foot of the mixer into the closely fitting massive base, as shown in Fig. 4.7. The base itself was bolted into the aluminum plate carrying the microwave equipment, which was in turn fastened to the monochromator bottom. The latter (weight $\sim$ 30 kg) rested on 15 mm thick aluminum support plate 650 mm x 500 mm, that could be displaced by heavy duty X-Y-Z stack of translation stages. Turning on the micrometer heads of X-Y-Z stack secured precise, smooth and quick search for laser spot size location, as the entire set-up moved as a whole without affecting the mutual orientation of both electric fields with respect to whisker configuration (see Fig. 4.8).

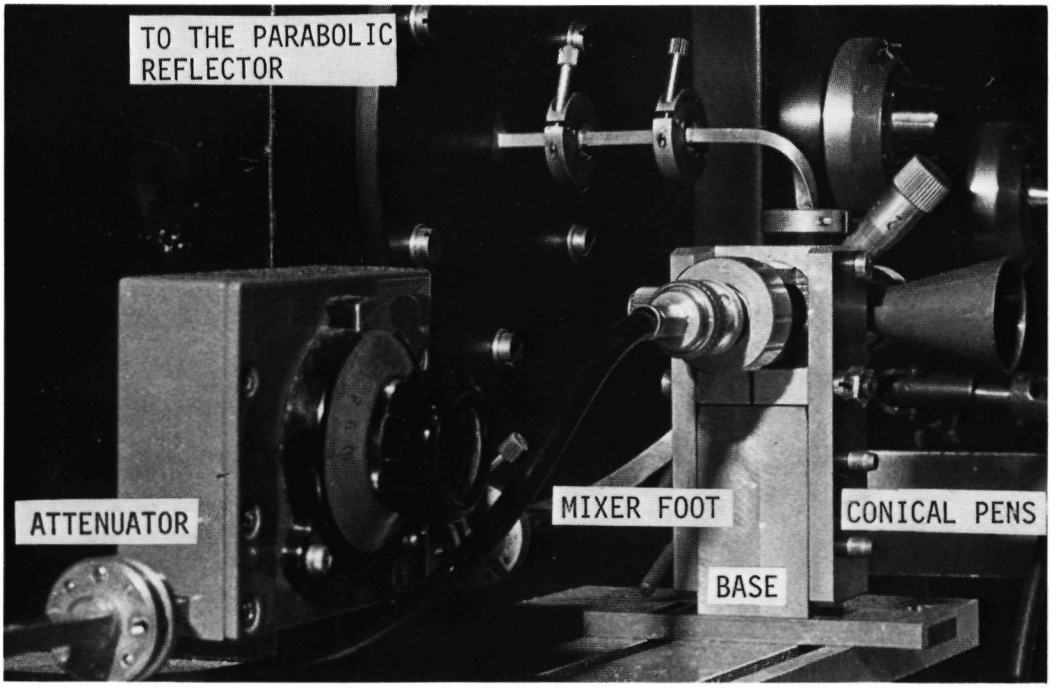

Fig. 4.7 Detailed photograph showing the mixer mount to the carrying plate and the monochromator input slit.

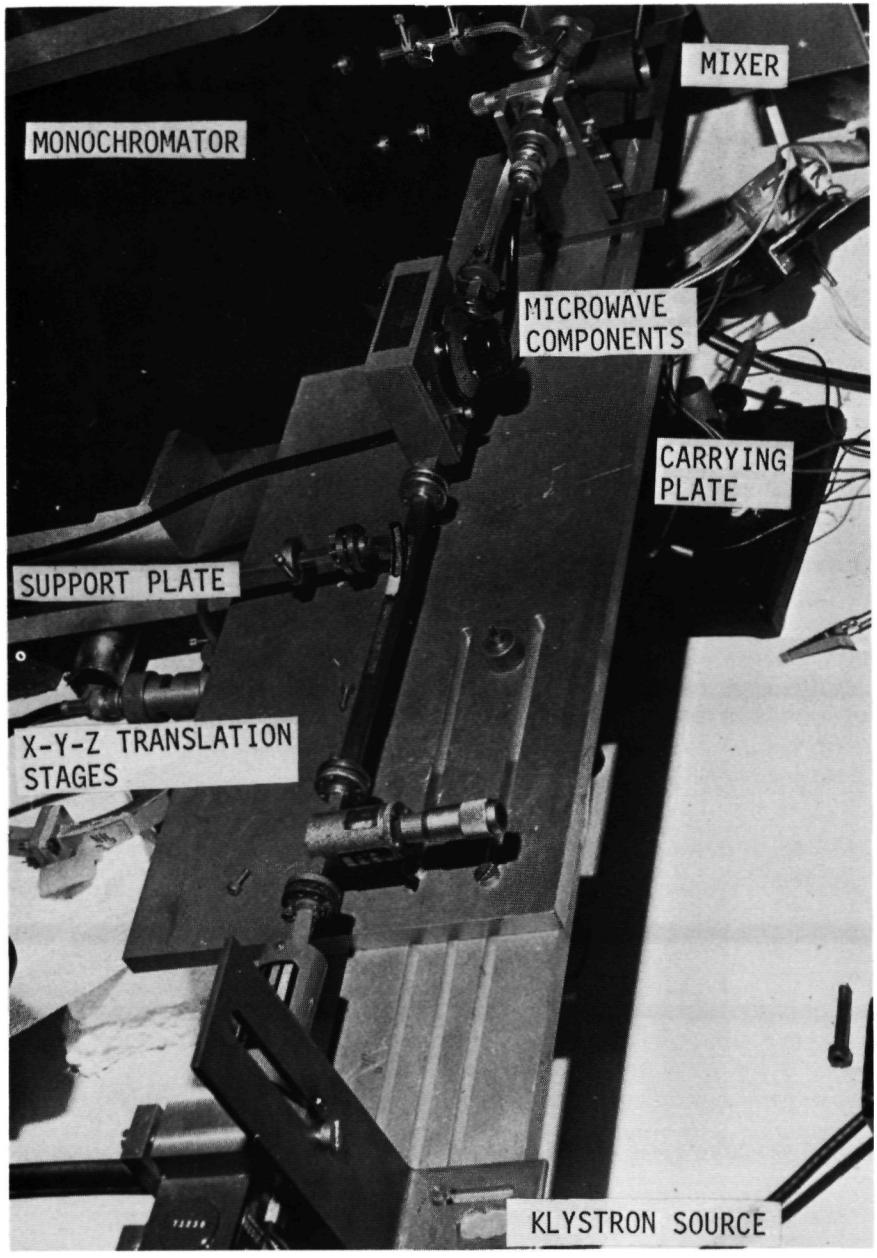

Fig. 4.8 The part of the apparatus.

4.3.4 Reflection grating and the mirror

About 200 mm away from the parabolic horn, the collimated beam was incident on the plane reflection grating used as diffractive element. The 35-57-310 certified precision aluminum grating with groove spacing d_{gr} = 0.33 mm and ruled area of 63 mm x 63 mm was obtained from Bausch and Lomb. It is essentially an echelette grating with rectangular facet set at 31^{o} blazed angle to the average grating plane. Blazed wavelength λ_B is 344 μm in the first order. To mount the grating in the spectrometer it was necessary to frame it in an adapting holder of larger dimensions. The free, unruled area of the holder was blackened by the same material as the inside of the spectrometer in order to prevent unwanted spurious effects. The grating rotates on fixed ball bushings coplanar with the parabolic horn. Radiation reflected from the grating due to periodic error in groove spacing, or scattered radiation originating from random error in groove placement is considered to be negligible. An echelette grating is only effective for wavelength that vary roughly over factor of two. Relatively coarse grating ($d_{gr} > \lambda_B$) rough rule of thumb is that in first order the efficiency drops to half its maximum at $\frac{2}{3}\lambda_B$ and again at $\frac{3}{2}\lambda_B$ on the other side of the blaze peak. With a grating $d_{gr} \sim \lambda_B$ the efficiency at peak of blaze is smaller, but the useful wavelength range is greater (LOW 72). For this grating first order efficiency exceeding 90% has been calculated by the author at the wavelengths to be generated.

The grating was scanned by means of a bar with rack and pinion drive. Drive knob drum uniformly divided, and attached to the bar was provided with counting dial to indicate complete revolutions. For automatic motor drive, the shaft of the rigid

lever arm could be coupled to gear mechanism of a precise Elkmehanic motor, if required. Transmission gear ratio of the grating drive mechanism is such, that one full revolution on the dial knob produces $2^{o}42'$ angular displacement of the grating.

When the first order wavelength and the groove spacing are comparable, theoretical resolving power $R = \Delta\lambda/\lambda$ based on Rayleigh criterion equals the number of grooves. For this grating with 3 grooves per millimeter and which is 63 mm across, the theoretical resolving power is 1 part in 189, which corresponds to resolution of 4.7 GHz at 890 GHz laser frequency. The resolving power has not been determined experimentally.

Without an absolute wavelength scale, spectra lines observed with grating spectrometer are useless, and hence calibration of the system was required. The HCN laser line at 890 GHz provided a convenient "calibration" frequency. Two positions of the grating were taken as references: (1) position T_0 corresponding to 90^{o} incidence, i.e. zeroth order diffraction for which grating appears as a plane mirror for all wavelengths, and (2) position at which maximum laser signal was transmitted by the monochromator. From grating equation that relates the wavelength, groove spacing and direction of incident and diffracted beam for first order operation, the angular difference between two grating positions could be evaluated and compared with that measured in practice (see Sect. 4.4).

The diffracted beam was focussed by the aluminum 150 mm diameter, 240 mm focal length spherical mirror, mounted 160 mm away from the grating. The axis of this F/1.6 mirror lies in the same plane as the axis joining the middle portion of the grating and the parabolic horn. The mirror condenses the radiation on a brass lightpipe (13 mm diameter) that serves as the

exit slit of the monochromator and transfers energy further towards the detector. The mirror was adjusted for maximum energy transmission at the laser frequency, and the total radiation path from input slit to the output lightpipe of the monochromator was about 750 mm.

4.3.5 Metal mesh filter

The large disparity in power expected at the sidebands and the laser carrier frequency required use of a system capable of high supression at the frequency of the laser. The original idea was to use two gratings behind each other. One of them if blazed at the wavelength to be detected would act as fore-filter reflecting most of the incident energy into the desired order. With grating having for example two grooves per millimeter at 25^{o} blaze angle, a bandwidth of 60 GHz (2 cm^{-1}) at half height could be expected at 890 GHz (MOE 74). Two of such gratings might be sufficient to adequately resolve sideband and carrier frequency separated by about 70 GHz.

Later, our attention turned to metalic meshes whose reflection and transmission properties are frequency dependent. Such meshes are thought to be superior to the filters relying on selective absorption in medium. However, the use of a single metal mesh is believed insufficient to meet all the imposed requirements. The best commercially available band stop filters, made of several layers of special metal meshes, have low peak transmission and bandwidths much too broad for application in this spectrometer.

A filter with narrow passband and high transmission at the sideband frequencies but a large rejection factor at the laser frequency was necessary. A filter, that possesses these proper-

ties has been designed for this experiment by Dr. Reinard Ulrich of the Max Planck Institut für Festkörperforschung in Stuttgart, West Germany (ULR 76). The filter, F/370/II, was fabricated by Garching Instrumente (Garching, West Germany) and consists of four self supported inductive copper meshes accurately spaced in the stainless steel frame. The calculated curve at normal incidence at the lower sideband (∿ 820 GHz) is shown in Fig. 4.9. It was not possible with reasonable means to design a filter which passes simultaneously the upper (∿ 960 GHz) and the lower sideband (∿ 820 GHz) and still has high rejection at the laser carrier frequency. The filter is designed for second order operation, which means that spurious passbands will occur at multiples of the first order (410 GHz and 480 GHz in the above example). A filter (design frequency f_o = 812 GHz)

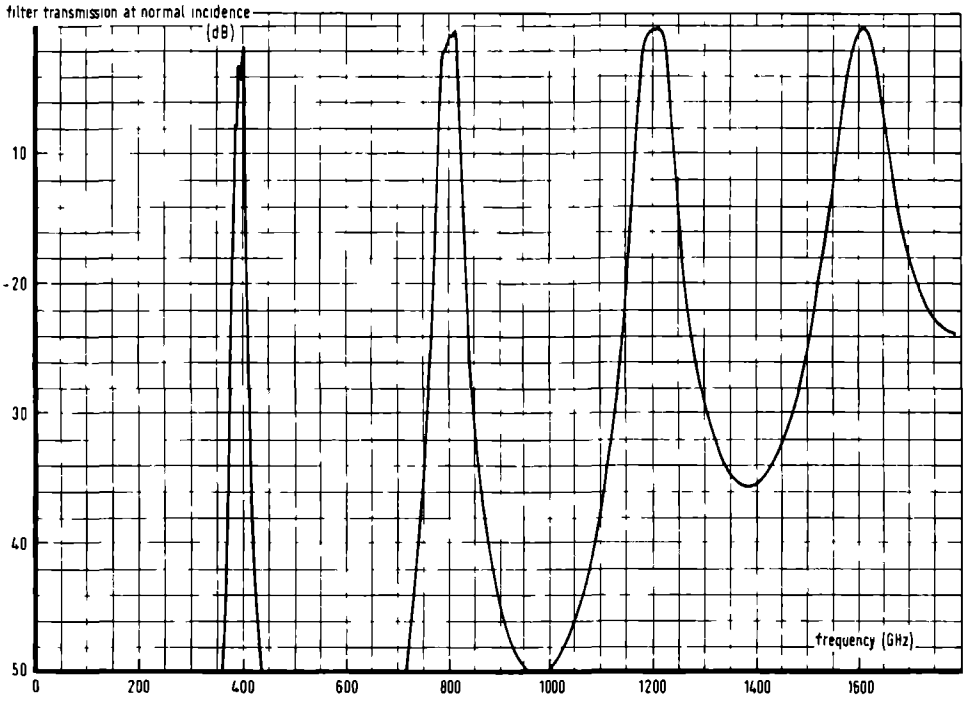

Fig. 4.9 Transmission characteristics of metal mesh filter F370/II developed for this experiment (after Ulrich).

operating at the lower sideband was preferable because of the higher attenuation contrast between this sideband and the laser frequency (ULR 76). Effective pass (3 dB bandwidth is 42 GHz at 812 GHz) and stopbands for the filter operating in second order at 820 GHz are also indicated in Fig. 4.9. The ideal transmission curve of F370/II metal mesh filter around the laser frequency is depicted in Fig. 4.10. Actual performance is slightly inferior due to the difficulty of meeting the stringent mechanical tolerances, so that the true transmission curve will lie within the shaded area in Fig. 4.10. This diagram, indicates that one could expect attenuation of approximately 42 dB at 890 GHz and only 1.5 dB at 820 GHz sideband frequency. In practice, values of 34 dB at almost normal incidence have been measured at 890 GHz.

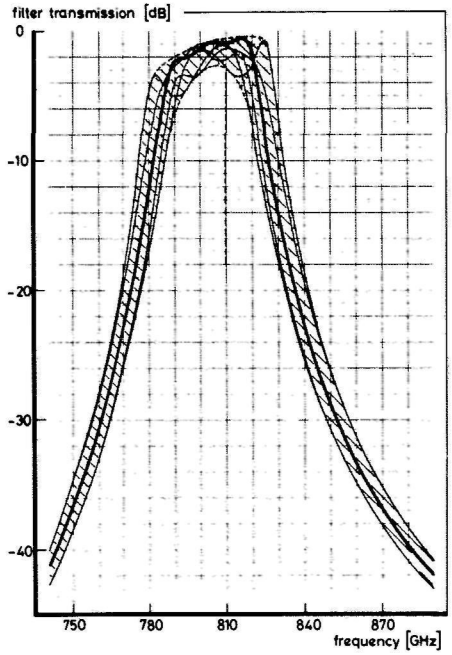

Fig. 4.10 The ideal (computed) transmission of filter F370/II around the design frequency (difference-frequency sideband). Shadowed region indicates extreme limits due to the mechanical tolerances (after Ulrich).

Although going to higher order of operation will add more decibels to the attenuation factor, the bandwidth will decrease correspondingly (ULR 76). Moreover mechanical tolerances become increasingly severe and the adjustment of center frequency of the filter with sufficient accuracy becomes very difficult. As a result, the center frequency may considerably deviate from the specified design frequency, producing high attenuation just at the design frequency. Because of all these difficulties and considerable filter sensitivity to small tilts or radiation at oblique incidence, Dr. Ulrich strongly discourages operation of the filter in orders higher than second. If one filter of this kind does not produce sufficient suppresion at laser frequency, two of F370/II in series will be capable of $\sim$ 70 dB attenuation, but care has to be taken to prevent possible interferences between individual filters. Our estimate that one mesh filter in conjunction with the monochromator should provide adequate an solution to the problem, was later experimentally verified. The mesh in its stainless steel frame was mounted in the 80 mm x 80 mm perspex plate for ease of manipulation as shown in Fig. 4.11. In the monochromator, mesh assembly was placed just in front of the shielding screen and the entrance of the exit lighpipe. The clear diameter of the filter was 25 mm. The perspex plate was clamped firmly in a holder bolted to the bottom of the monochromator. Holder is adjustable in height, and it can be rotated in vertical plane enabling the experimentalist to find optimal position of the mesh filter with respect to the axis of the lightpipe.

4.3.6 Lightpipe, absorption cell and detection system

The straight brass lightpipe, 13 mm in diameter and 220 mm

Fig. 4.11 Front view of the metal mesh filter F370/II.

long, is actually an greatly oversized waveguide without mode discrimination at the sideband frequencies and served to transfer the radiation to the absorption cell and/or to the detector. Transmission of the lightpipe, that receives radiation from F/1.6 optical system is $\sim$ 88% at 337 μm calculated from the expression given by Ohlmann (OHL 58).

A simple 300 mm long absorption cell was made from brass tubing of the same diameter as the lightpipe. The output end of the exit lightpipe was connected to the input of absorption cell by means of a quick type coupling. Teflon film 1 mm thick, that served as vacuum seal was clamped between the coupling. The cell was provided with two ports for admission and exhaustion of the gas to be studied. With a Leybold D2 rotary pump in series with a diffusion pump, the cell could be evacuated to about 5×10^{-4} Torr prior to the admission of desired gas. Attenuation of the evacuated cell at 820 GHz was found to be 30%.

Three types of braod band submillimeter detectors have been used in the course of this experiment: a room temperature and low noise IR 50 Golay cell from Oriel Optik GmbH, and two liquid He cooled detectors namely Putley RPY 23 detector from Mullard and germanium bolometer fabricated by Queen Mary College Ltd (henceforth abbreviated QMC).

Each of these detectors required construction of a specific lightpipe to establish the path for efficient transmission of radiation between the absorption cell and the detector entrance. A tapering section 65 mm long, was used to couple Golay cell (with quartz window) as integral part of the monochromator. The size and the orientation of dewar vessel of Putley detector required different approach. A coupler consisting of U - formed gold coated brass tube (13 mm diameter) has been used. The tube with total length of 1500 mm makes use of two mirrors positioned at 45^{o}, introducing change of direction in horizontal and vertical plane respectively. One end of the tube is connected tightly to the absorption cell by means of a flange and the other end is inserted loosely onto the polyethylene seal mounted at the entrance of condensing copper lightpipe of the detector. Transmission of 85% for the entire lightpipe has been measured.

Finally the QMC detector was connected directly to the absorption cell (or monochromator) via a tapered cone affixed by means of a flange. The other end of the taper was loosely inserted in the window opening of the detector of roughly the same diameter. Two stacked micro-positioners in combination with precision scissor laboratory jack were used for translation of the platform carrying the detector along the three orhtogonal axes.

When using the Golay cell, the radiation was amplitude modulated by a blackened, two vaned chopper driven by 10 Hz

synchronous motor and detected with a lock-in amplifier. The chopper was mounted outside the monochromator box (between the laser lens and the mouth of the mixer horn) rather than close to the exit lightpipe. The amount of heat developed by rotating vanes, and reaching the detector was found substantial in this latter case. With the chopper placed between the mixer mouth and the laser lens (there was only very little room there anyway) the influence of incident background radiation including ambient thermal fluctuations and proximity of the laser enveloppe was less pronounced.

With the two liquid He cooled detectors, the chopping speed was selected according to response time of detectors. Radiation was modulated at 1 kHz for the Putley and 120 Hz for the QMC detector by impressing a square wave voltage on the top of the d.c. bias of the mixer.

Basic performance data for three detectors used were collected from manufacturer's specification sheets, and are shown in Table 4.1. However, inferior N. E. P. performance for Putley (4x) and QMC bolometers ($\sim$ 50x) has been experimentally observed.

Type detector	Responsivity (V/W)	Frequency range (GHz)	Chopping frequency (Hz)	Noise equivalent power N.E.P.
Oriel IR 50	1.5×10^6	7500-300	1 - 30	typical $\sim 10^{-11}$ W at 1 Hz bandwidth chopping frequency 11 Hz, and black body temperature $500^{o}K$
Mullard RPY 23	82	2000-30	up to few thousand	$2.75 \times 10^{-11} W/Hz$
Queen Mary College Ltd. germanium bolometer	62×10^3	7500-60	10-200	$5 \times 10^{-13} W/Hz^{\frac{1}{2}}$

Table 4.1 Relevant parameters of three submillimeter detectors used in the course of this experiment.

4.4 The "calibration" of the monochromator

Prior to the initial search for sideband frequency signals it was necessary to "calibrate" the monochromator i.e. to find relation between the wavelength and angular setting of the echelette grating (and thus control knob read off scale) corresponding to the first order diffraction for that wavelength. As not more but one of the two strong HCN laser transitions could be selected as the "source", the term calibration (in the strict sense) is not applicable here. Term interpolation seems more appropriate, since we have experimentally determined two end "calibration" points, and then used grating equation to obtain the values lying between these margins. Studying the relationship:

$$\lambda = 2\, d_{gr} \cos\alpha_i \cos\theta_d \qquad (4.5)$$

where α_i is the incident angle completely determined by the geometry of the monochromator (here $\alpha_i \sim 23^o$), it is seen that direct proportionality exists between the operating wavelength and the first order angle of diffraction θ_d. Consequently, there are two possibilities to calibrate the monochromator: (1) determine experimentally $\Delta\theta_d$ for the laser lines at 337 μm and 311 μm (from the difference of two micrometer positions on the drive knob used to tilt the grating) corresponding to $\Delta\lambda$ and compare it with $\Delta\theta_d$ calculated from Eq. 4.5; or (2) use a single source, such as for example 337 μm line of HCN laser, but rotate the grating to the position for which zeroth order diffraction requirement is satisfied. In such position, called T_0, $\theta_d = 90^o$, and hence the echelette appears as a plane mirror for all the wavelengths. Thus again, by measuring the difference in angles between the first order diffraction and T_0 position, it is

possible to deduce a correlation between rotation of the grating and corresponding readings on the drive knob. Knowing that one full revolution on the knob corresponds to $2^{o}42'$ echelette rotation, and using the grating equation 4.5 it is possible via (1) or (2) to interpolate for all other wavelengths λ and to obtain the calibration curve of the apparatus.

Approach (2) was used in this experiment. The calibration was performed with 337 μm laser radiation using Golay cell detector with the known response and mounted on the exit lightpipe of the monochromator. The presence of point contact was not absolute necessary, as the calibration could also be performed by optimizing on pure "leakage" signal from the laser. The parabolic horn and the mirror inside the monochromator were both aligned for maximum energy transmission of the spectrometer at this frequency. The validity of the calibration curve was then checked with another laser line or alternatively by utilizing higher order harmonics produced from 70 GHz klystron. In this latter case, diode contact has actually been produced, but laser radiation was prevented from reaching the junction. The angular setting of the grating at which maximum transmission of a particular harmonic was observed, agreed well with data from the interpolation curve.

4.5 Overall insertion loss of the spectrometer

An experimental investigation was carried out in order to get an estimate of overall insertion loss of the spectrometer at 890 GHz. This figure includes the sum of losses due to coupling mismatch of the laser signal through the mixer horn, transition loss through the coupler hole in the common wall between the circular and output mixer waveguides, attenuation loss along

the connecting waveguides and finally transmission loss of optical components inside the spectrometer.

The measurement was performed with the mixer mounted on the entrance slit of the monochromator, with the crystal and whisker being brought into their conventional positions in the middle waveguide. First, measurements were made with the whisker not contacting the crystal surface; the measurement were repeated with a spring loaded contact established in order to find out whether there is any contribution due to the reradiation of the fundamental laser frequency by the diode.

Plungers of the circular and the harmonic waveguide were adjusted to produce maximum detector output with grating positioned for first order diffraction at 337 μm. Since we were primarily interested in the ratio of power detected behind the monochromator to the input laser power, it was necessary to construct a system capable of monitoring the amount of incident laser power at any desired time, without displacing the spectrometer. An aluminum holder that could be fitted to lens adapter in such a way that the axes of both coincided proved a satisfactory design. Two slits cut at 45^{o} along both side walls of the holder allowed insertion of a metalized plane mirror that reflected laser radiation 90^{o} to its original direction of propagation. A "Molectron" pyroelectric detector with calibrated responsivity was used to measure laser power in this plane. The magnitude of the laser signal in this reference plane was found to be 65% of the maximum signal obtained with same detector on the optical axis when placed in focal plane with all other experimental conditions and plunger adjustments unaltered.

While searching for desired sideband frequencies, this system proved very useful, as it allowed one to check rapidly

whether or not the laser resonator was detuned due to thermal drift. Also the possibility for inadvertent renewing of the contact was thereby eliminated.

The total measured insertion loss(with whisker contact established in SB diode) was about 20 dB (factor 100). However, this figure is only approximate as it is critically dependent on fairly arbitrary factors which determine the diode performance.

De Kort, using nearly identical monochromator, found a transmission loss of approximately a factor of 2 around 800 GHz due to the optical components inside the monochromator (without the mixer thus) in his harmonic generation experiments (KOR 78). In de Kort's instrument, the surfaces of the horn and mirror are true parabolas, which produced a factor of 2.5 improvement in internal monochromator transmission compared to our apparatus. The effect of the grating size that should match the cross sectional dimension of expanded beam should also be considered. The Bausch and Lomb echelette used in our spectrometer has ruled area which is only 35% of that used by de Kort. As the parabolic horn was designed for use with the larger grating, an additional loss could be anticipated. In view of these arguments, overall insertion loss measured for our spectrometer could possibly be reduced by a factor five by improving the monochromator.

Another cause of the large overall insertion loss figure is likely the collecting efficiency of the mixer horn. By removing the plunger of the circular waveguide, and placing the pyroelectric detector behind the open end of revealed by the removed plunger, the waveguide a transmission of 25-30% of 890 GHz laser signal has been measured. There was no fixed connection between the entrance cone of the pyroelectric detector

and the open termination of the circular waveguide receiving the laser radiation, so the signal detected represented only a lower limit of the collecting efficiency. (This is true, because any additional collecting optics would only contribute to the signal enhancement). The errors involved are therefore unknown, but the tendency is obvious.

It should be however noted, that the overall insertion loss figure has been determined with all three plungers positioned to maximize the laser signal at the detector behind the spectrometer. The collecting efficiency under the normal operating conditions, where matching of the laser radiation to the mixer mount is of the crucial importance may be considerably different.

The waveguide run connecting the output mixer waveguide to the input slit of the monochromator was found to have transmission of 90% at 890 GHz.

The 20 dB loss figure makes no distinction between loss occurrence in the mixer itself from the total insertion loss of the spectrometer.

Finally, we have tried to separate the reradiated contribution to the signal at 890 GHz from pure leakage reaching detector at the same frequency. The whisker was lifted off the crystal surface but still functioned as an antenna. Measurements were also repeated with the whisker being completely removed from the mixer mount. In all cases, the plungers were optimized for maximum signal at detector. The measurements established that reradiated power represented a small fraction ($\sim$ 1%) of the 890 GHz leakage signal, and the attempt to produce the sidebands to produce the sidebands with the present set-up could begin.

4.6 Preparation of diodes

The prefabricated M.I.T. SB diodes were used in the geometrical arrangement normally encountered with conventional PC diodes, i.e. by lowering the tip of the tungsten whisker into the depression containing metal deposit. The point contact diodes, on the other hand, were produced by establishing a spring loaded feeble contact between the gold-copper alloy whisker and the crystal mounted on the carrying pen.

Whiskers of 7-10 mm average length (measured from the top to the crimp close to the welding point on the chuck) and tip of small area ($\sim 2 \times 10^{-9}$ cm^2), such as the one shown in Fig. 4.12a (before contact) were prepared from 50 μm diameter tungsten or alternatively gold-copper wire by the self terminating d.c. electropolishing technique. A dilute aqueous solution of potassium hydroxide was used as the etching liquid for the tungsten wires, whereas the gold-copper whiskers were etched in an aqueous solution of NaCN + K_4 [$Fe(CN)_6$] (MAR 67).

Inspection under SEM typically revealed a flattened top whisker diameter of about 0.5 μm (Fig. 12 b). The evidence of a large number of experimental trials, has shown that whiskers with a long relatively sharply pointed tip contour (typically 150 μm in length see Fig. 4.12a)showed the best performance. Contacts, made with such whiskers were not very susceptible to the mechanical dammage and survived sometimes for a period of several weeks before renewing was required. They could also withstand a substantial levels of microwave and laser power before burning out as indicated by deterioration of the I-V characteristics.

The shape and dimensions of the whisker spring soldered to the nickel chuck differ from those commonly used in this labora-

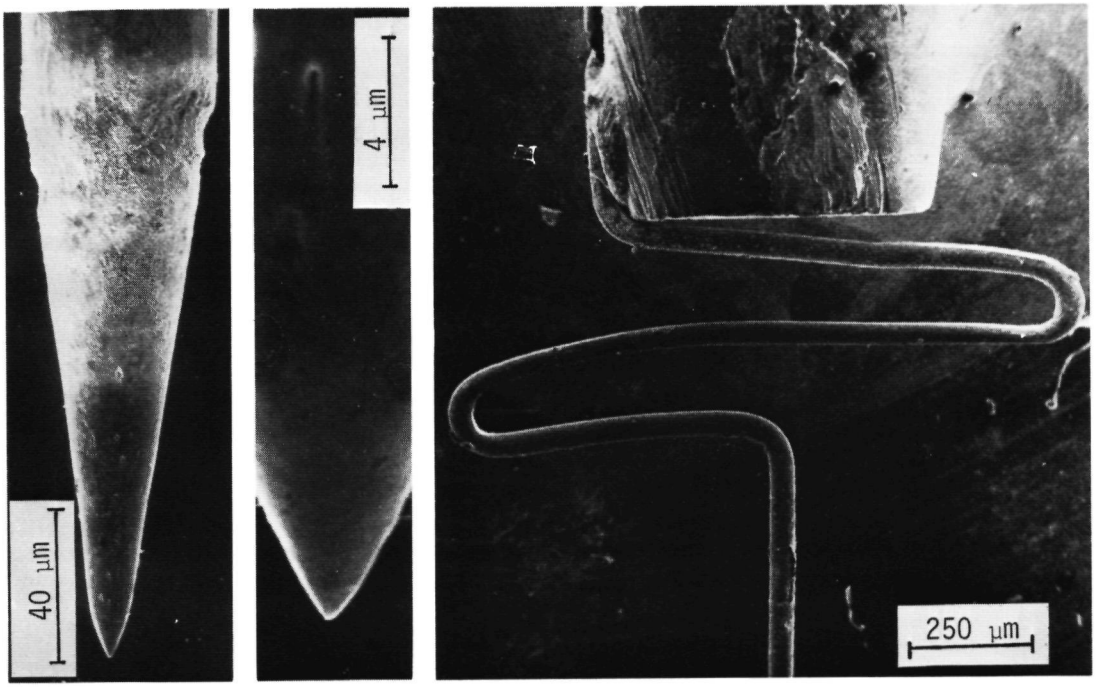

[a] [b] [c]

Fig. 4.12 The SEM photographs of:a) whisker dimensions;
b) tip of the whisker;
c) spring load of the whisker.

tory in the past years. After the whisker was bent in the crimping jig, the length and the radius of curvature of the loop were made larger than previously (Fig. 4.12c). This resulted in a double-loop structure which provided outstanding spring action, mechanical stability and better degree of controlling the adjustable contact force.

Another novelty developed in the course of the experiment was the device used for mounting of the crystal material to the gold carrying pen (LEU 78). The new technique efficiently replaced the somewhat clumsy older method that used random size diode chips and relied too much on the individual skill of the experimentalist and good deal of luck as well.

The apparatus shown in Fig. 4.13 consists essentially of two basic parts- (1) thermally well insulated heating block element made of boron nitride connected to power supply capable of 14V a.c. and 4 A with tantallum wire leads, and (2) the pivot arm adjustable in height that accomodated a long stainless steel rod by which the small frictional force required for the eutectic soldering process could be exerted. The straight, short section of 0.5 mm diameter gold wire that functions as a carrying pen was placed in a central hole in the top surface of the heating block. A shallow square notch made in the bottom

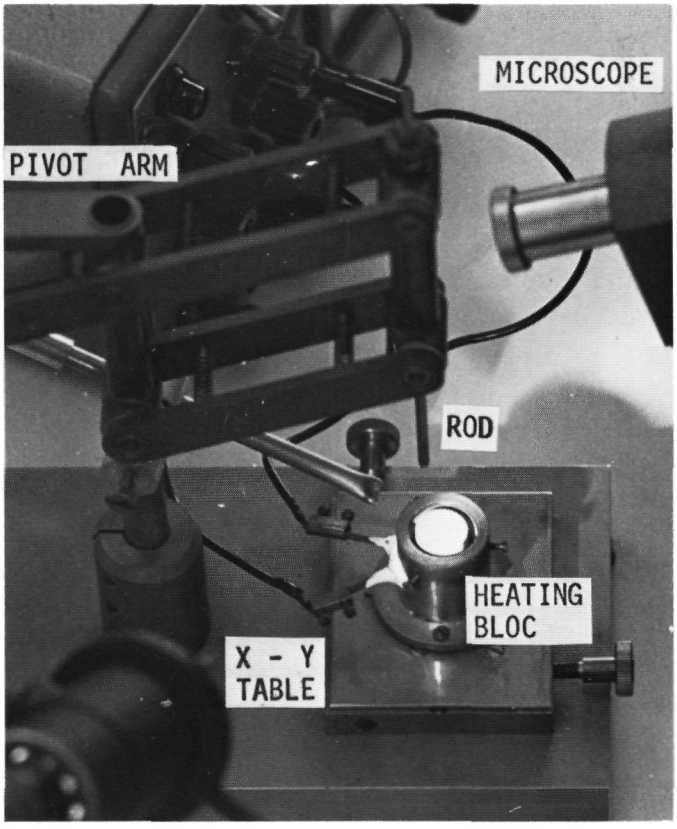

Fig. 4.13 The apparatus used for mounting of the crystals to the carrying pen.

surface of the rod was filled with a small amount of silicon grease and accepted the crystal chip (cut previously to dimensions of 0.5 mm x 0.5 mm with a diamant saw). The rod carrying the chip and the gold pen were brought in contact by displacing the micrometers of a X-Y translation stage bolted to the heating block assembly. At elevated temperature, close to the eutectic point ($\sim 460^{o}$C for gold/crystal interface) the rod is gently rotated back and forth by hand in small steps. The whole process is observed through the a stereo microscope, and once the interface is softened the power supply is turned off and a stream of cold air is switched on. The temperature of the carrying pen was continuously monitored with a thermocouple in order to prevent overheating. The excessive area of crystal is removed by fine and paper polishing. After wipping off the grease and rinsing in alcohol the mounted crystal chip is ready for use.

Besides simplifying the process of mounting the crystal and reducing the time interval required for reaching the desired temperature, this new technique also guarantees that the crystal surface will be perpendicular to the axis of the gold pen. Due to the improved motion and temperature control, the risk for accidental "loosing" of the crystals is practically eliminated, which is very important considering limited supply of the precious diode material.

4.7 Generation of difference-frequency sideband near 820 GHz

4.7.1 Current-voltage d.c. characteristics of SB diode

The separation between the whisker and the prepared crystal surface in the circular mixer waveguide is viewed through the microscope. When the whisker is almost touching the surface, the

mixer assembly is mounted as shown in Fig. 4.8 and the actual contact is produced by turning the differential screw mechanism in the presence of incident laser or klystron power. The current-voltage (I-V) characteristics of the diode was displayed on the oscilloscope during this operation.

Experience gathered with a large number of SB and PC diode suggests that the shape of the I-V characteristics gives a qualitative prediction of the diode performance as a mixer. However, it should be emphasized that good d.c. characteristics is necessary but not a sufficient condition for good mixer performance.

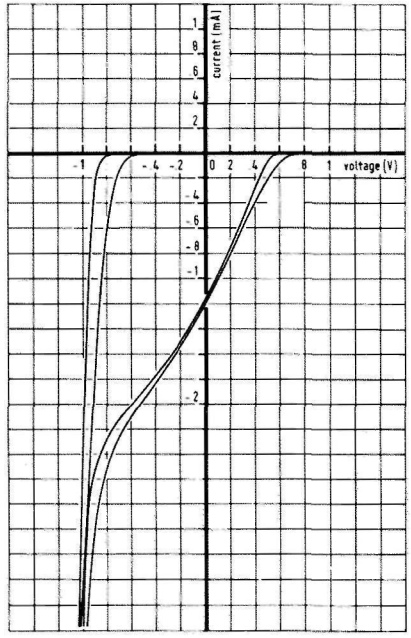

Fig. 4.14 The current-voltage (I-V) characteristics of the M.I.T. SB diode.

a) no power incident to the diode;
b) laser power only (30 mW) at 890 GHz;
c) klystron power only (120 mW) at 70 GHz;
d) irradiated by 30 mW laser power and 120 mW klystron power simultaneously.

Fig. 4.14 (curve a) shows a typical I-V characteristics of SB diode in the absence of laser and microwave power. The shape displayed is an average one, sufficient for sidebands generation. The diode characteristics features low reverse leakage current (few μA), and good non-linearity evidenced by an sharp knee in the backward region close to -0.8 V. The saturation current for the diode is about 2 μA. The non-linearity in the forward direction occurs at voltages exceeding 4 V and is not shown in the above figure. Under the typical operating conditions of in the presence laser or klystron power the shape of the I-V characteristics changed as shown by curves b and c in Fig. 4.14, respectively. With both sources of radiation delivering power to the diode, curve d in Fig. 4.14 is obtained.

The I-V characteristics of the conventional GaAs PC diode displays at negative voltages a reverse breakdown point of less pronounced non-linearity. All the recordings in the text hereafter are obtained with the M.I.T. SB diode.

The peak electric field of the klystron radiation across the smaller dimension of the RG-99/U waveguide oscillating in the TE_{10} mode was calculated to be 7.2 kV/m at input power level of 120 mW around 70 GHz. However, in calculating the electric field of the laser radiation, it was necessary to assume that all the power emitted by the laser was collected by the horn and reached the junction. Then, the peak electric field of the laser at 337 μm can be determined from the total power emitted by the laser and the ultimaze size to which the laser beam can be focused by the given lens. For the F/1.8 T.P.X. laser lens producing the spot size of 1.5 mm diameter, the time average energy flow at, say 30 mW laser power, is 1.7 W/cm^2 and consequently 3.6 kV/m is obtained for the value of laser electric field.

4.7.2 Rectification at 890 GHz and other useful checks to assess the diode quality

The magnitude of the rectified diode crystal current in the presence of the 890 GHz laser radiation provided a quantitative measure of the diode performance when used as a detector of submillimeter radiation.

The author has studied the video responsivity and the effect of the d.c. bias voltage on the rectified signal while using 8 m the HCN laser as the radiation source and SB diode in the mixer. It is interesting to note that sizeable variation of rectified and sideband signals (that arise from even order terms in expansion of I-V characteristics) with applied d.c. bias has been observed with metal-on-metal diodes in the infrared region (SAN 72).

In present experiment maximum video responsivity of 5 V/W has been obtained. This is somewhat lower than reported by Zuidberg using the same diode in a similar configuration (ZUI 77). The rectified voltage for a typical barrier contact is a strongly peaked function of the applied bias, as seen in Fig. 4.15, with a maximum of 125 mV for 25 mW of incident laser power(from which the above quoted 5 V/W has been derived) chopping mechanically at 20 Hz. For comparison, Mizuno obtained a responsivity of 2 V/W using his own SB diodes (MIZ 75).

With reduced laser power, the video signal was proportionally decreased, but the shape of the rectified signal-d.c. bias curve was the same as shown in Fig. 4.15. Similar measurements performed later at a higher laser frequency (964 GHz) showed that the rectified signal is nearly independent on frequency for a given coupling configuration.

Larger video signals could be obtained when microwave power

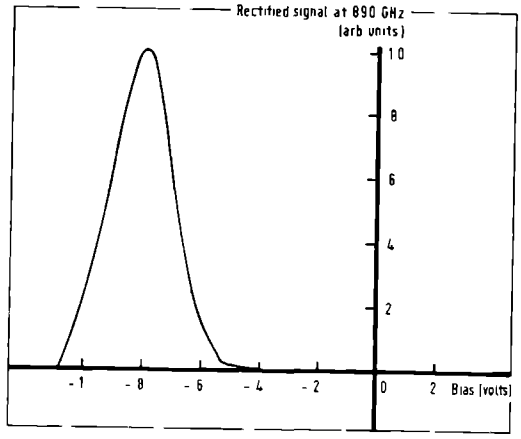

Fig. 4.15 Rectified signal obtained with M.I.T. SB diode at 890 GHz (laser power 30 mW) plotted versus the bias voltage. Maximum responsivity is 5 V/W.

was applied to the diode at a given bias voltage. A shift of threshold bias voltage (the bias voltage at which diode power absorption is first discernible) towards the zero bias voltage on the I-V characteristics has been generally observed.
The shape of the curve corresponding to Fig. 4.15 became broader, but the maximum in rectified signal appears at the same negative value of the bias voltage. No signal has been observed for a positive bias up to 0.5 V.

The shape of the curve shown in Fig. 4.15 suggests that the application of bias modulation to the diode between the points corresponding to maximum and minimum rectified signal should aid considerably in the search for sideband signals. The amplitude modulation (100%) of the sideband signal is produced by a bias voltage that swings between zero and the voltage that yields maximum rectified signal. Modulation at positive bias voltage is preferred to the negative bias value close to

-1 V, as in this latter case the diode could be damaged.

With the diode mount optimally matched to the incident laser beam diode currents of few tenths of a milliamp have been obtained from good SB and PC contacts. Sometimes, values close to or exceeding 1 mA have been measured. The optimization of the present experimental set-up particularly with respect to the focal point of the laser radiation is quite tedious requiring frequent readjustement of many parameters, but it pays off the effort, at last.

The diode absorbed the microwave power well. The intensity of the microwave power incident to the mixer was varied with a precision Hitachi M1502 flap attenuator. With the RG-99/U planger positioned to optimize the absorption of 70 GHz radiation produced by a Varian VRE 2103B8 klystron, the I-V characteristics was typically as shown in Fig. 4.14 (curve c). Klystron power was usually about 120 mW. For the best diode contacts the characteristics (curve c) asymptotically approached the bias voltage axis at larger positive value.

Another useful assesement of the diode quality was obtained by studying its performance as a combination harmonic generator + heterodyne detector. The laser as local oscillator and the twelfth klystron harmonic (produced in the mixer itself) was used as the signal oscillator. The signal to noise ratio of the intermediate frequency signal (about 160 MHz) taken through the NBC connector on the mixer base, amplified in narrow-band amplifier and displayed on the scope served as the criterion. The magnitude of the beat signal could be optimized by adjusting properly the position of plungers in the laser and klystron waveguides. It was consistently observed that careful matching of both klystron and laser inputs were required for good signal

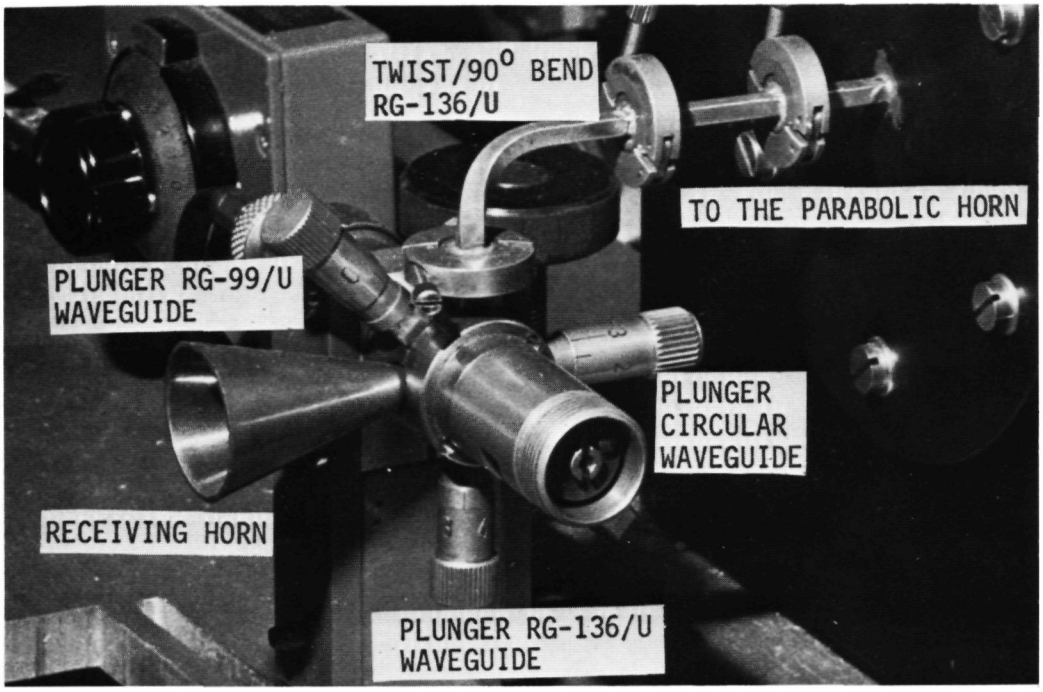

Fig. 4.16 Detail of the experimental set-up showing the three waveguides and connection between the monochromator and the mixer assembly. The plunger in the output waveguide RG-136/U aided considerably in the search of sideband signals.

to noise ratios. The position of the plunger in the 1.2 mm diameter laser waveguide that produced maximum beat and rectified signal coincided, suggesting that best video detectors are also the best mixers. This was indeed confirmed in the frequency mixing of laser and klystron radiation that produced tunable sidebands.

4.7.3 The search for reradiated difference-frequency sideband at 820 GHz

With optimized coupling of laser and klystron to the diode the search for difference-frequency proceeded by adjusting the plunger in RG-136/U output waveguide shown in Fig. 4.16. Because the narrow transmission bandwidth of the metal F370/II mesh filter accepts the 804 GHz emission of the $J(9)_+ \rightarrow J(8)_+$ cascade transition in $(04^0 0)$ vibrational state of the HCN laser, great care had to be exercised to prevent the oscillation of this line. The intensity of this "leakage" transition, if optimized, was 6% of the intensity of the TEM_{00q} mode at 890 GHz. Since 804 GHz line oscillates only whenever the 890 GHz transition is lasing, laser action at the former frequency can be avoided by tuning the plane mirror of the resonance to a position where the resonance conditions for both transitions are not fullfilled simultaneously. Displacement of the output coupling mirror can also assist in quenching the 804 GHz oscillation and prevent it from entering the spectrometer.

When searching for the difference frequency signal the grating was set at the appropriate angular position, and the metal mesh was placed in front of the monochromator lightpipe. Phase sensitive detection was used by applying the on-off (square wave) amplitude modulation to the klystron power from the Wavetek wave generator that also provided reference input for PAR 120 lock-in amplifier.

The difference-frequency signal was easily found. Grating (d_{gr} = 0.33 mm) in series with the mesh filter yielded total rejection factor of 58 dB at 890 GHz at angular setting where maximum transmission of difference frequency signal was expected. In later stages of the experiment the metal mesh filter could be

removed because sufficient suppression of the 890 GHz leakage could be obtained by delicately adjusting plunger positions. Moreover, the true and the "leakage" signals could be distinguished by the opposite phase in the lock-in amplifier.

Maximum voltage amplitude of the 820 GHz sideband signal was equivalent to $\sim 10^{-7}$ W power (based on the known responsivity value for QMC detector) detected after transmission through the monochromator and the evacuated absorption cell. This value was later confirmed by using calibrated Golay cell IR 50 and RPY 23 Putley detectors. Further improvement in sideband signal intensity could be obtained by using more klystron power, but at the risk of contact burnout.

Spectral purity of the generated sideband was checked with an Fabry-Perot interferometer placed between the monochromator lightpipe and the detector. Insertion of the interferometer introduced a transmission loss of a factor of 2.5 at 820 GHz. Analysis of the positions of interference maxima shown in Fig. 4.17 demonstrated that the signal was indeed originating from

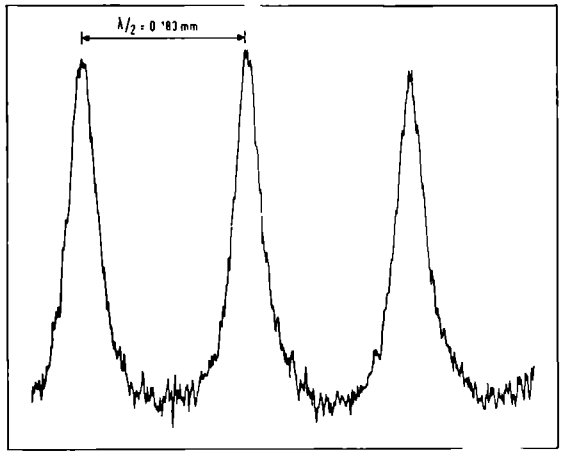

Fig. 4.17 Fabry-Perot interferogram of 820 GHz difference-frequency sideband signal.

the non-linear mixing process of the laser and fundamental klystron frequency. The signal dissappeared if laser or microwave power were prevented from reaching the diode thereby verifying that the signal is not due to 804 GHz "leakage" or high order klystron harmonics.

4.7.4 Reradiated difference-frequency signal strength as a function of external bias, and laser and klystron power levels

Figure 4.18 shows the relative strength of the reradiated signal at 820 GHz as a function of the d.c. bias applied to the SB diode. The curve was measured at typical working conditions (30 mW laser power, and 120 mW klystron power) and the maximum

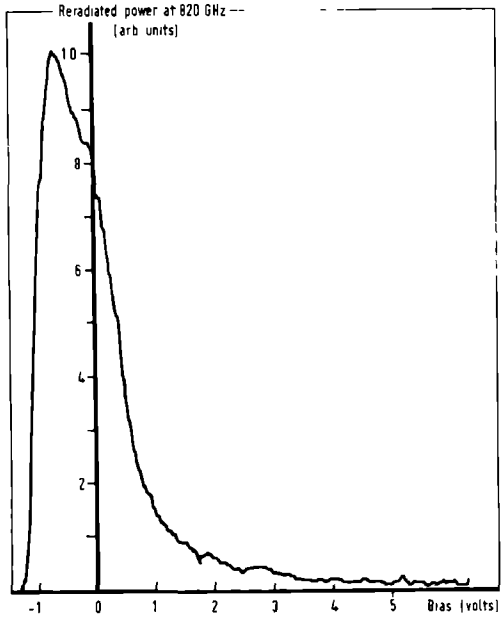

Fig. 4.18 The relative strength of the reradiated power at 820 GHz sideband versus the bias voltage. The power levels of laser and klystron were 30 mW and 120 mW, and the maximum corresponds to strength of 5×10^{-8} W at 820 GHz.

peak corresponds to 5 x 10^{-8}W. As in the case of rectified signal at 890 GHz (see Sect. 4.7.2) reradiated power is strongly dependent on the external bias. Substantial increase of the reradiated power signal (this was varying from contact to contact) could be obtained at about 0.8 V negative bias (corresponding to the reverse knee of the diode) when compared to the zero bias. This is consistent with the observations described in Sect. 4.7.2 indicating clearly that the optimization of the non-linearity with the appropriate matching is of vital importance for sideband generation. All the measurements that have been discussed in this section were obtained with M.I.T. SB diodes. With conventional Te doped GaAs PC diodes, typically three to five times less sideband power was obtained.

Reradiated power at 820 GHz was been studied as a function of laser and klystron power. If the klystron power is maintained at a constant level of 120 mW and the laser power is varied by detuning the resonator, a linear variation of sideband power on the laser power is found (see Fig. 4.19).

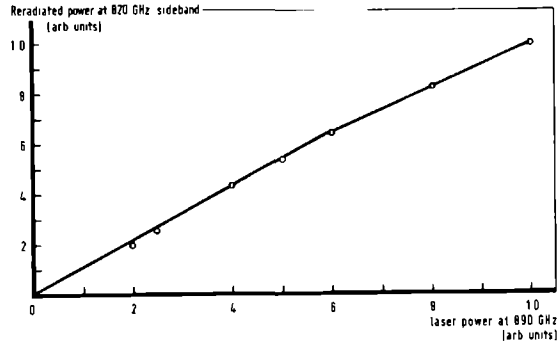

Fig. 4.19 The relative strength of the reradiated power at 820 GHz as a function of the laser power (890 GHz) at constant microwave power of 120 mW(70 GHz). At maximum laser power 30 mW, the magnitude of reradiated difference-frequency sideband power is 5 x 10^{-8}W.

Such linear dependence indicates the absence of saturation effects within the accessible range of submillimeter power. The klystron power was kept constant in the above measurements, and 120 Hz bias modulation has been applied to the diode. The maximum laser power (mark 1.0 on the horizontal axis in Fig. 4.19) of 30 mW yielded 5 x 10^{-8}W at the 820 GHz sideband.

Quite a different dependence was observed (Fig. 4.20) when klystron power was varied at a constant laser input power level of 30 mW. Initially, reradiated power at the 820 GHz sideband increases rapidly with microwave power. At about 100 mW klystron power the curve begins to flatten off gradually. This behaviour could be expected because the lower frequency microwave power is much more efficiently absorbed by the diode than is the laser power. Currents of approximately 1 mA could readily be generated by incident klystron power alone.

In Fig. 4.20, the 5 x 10^{-8}W at 820 GHz is obtained with 40% (120 mW) of the maximum available power from the klystron. Additional increase in reradiated power results if more microwave power is allowed to reach the diode.

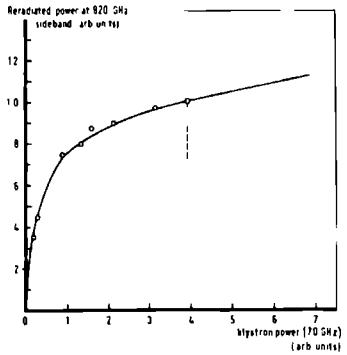

Fig. 4.20 The relative reradiated power at lower sideband (820 GHz) versus relative klystron power (∿70 GHz) at constant laser input of 30 mW at 890 GHz. At 120 mW klystron power (dotted line), an typical operating point, the magnitude of reradiated power is 5 x 10^{-8}W.

4.8 Spectroscopic application using difference-frequency signals

4.8.1 General considerations and brief historical review

The spectral coverage of the spectrometer is determined by the HCN laser emission frequencies and the range of microwave frequencies efficiently absorbed by the mixer diode. The present mixer has been designated for microwave frequencies of (68-74) GHz. This is determined principally by the RG-99/U waveguide used to transmit microwave power to the diode junction. On the most intense, 890 GHz laser emission line, the spectral coverage on the lower sideband is (816-822)GHz. Clearly, lower and upper frequency limits are fixed by the tuning range of the klystron. In principle, the useful operating range can be extended to lower or higher frequencies by replacing the RG-99/U waveguide in the mixer with another waveguide of appropriate dimensions. Alternatively, it is possible to use klystrons or carcinotrons of higher frequency with the present mixer but care has to be taken with regard to possible multimoding effects.

The best and final check to verify the origin of the generated difference-frequency sideband was to perform absolute frequency measurements in absorption on selected gases. The asymmetric rotors hydrogen sulphide H_2S and sulphur dioxide SO_2 were chosen for the measurements. Calculated frequencies associated line strengths for H_sS (based on rotational constants from the microwave spectrum) were published by Helminger et al. (HEL 73). Lovas (LOV 78) from National Bureau of Standards, Washington D.C. has recently computed line positions and intensities around 1 THz for SO_2. Using the technique of Fourier transform spectroscopy, John Fleming at the National Physical Laboratory, Teddington, England has measured absorption frequencies

of H_2S and SO_2 in the 300 GHz - 1200 GHz range (10 cm^{-1} - 40 cm^{-1}) with an accuracy of 90 MHz (0.003 cm^{-1})(FLE 74, FLE 77).

Other molecule worth studying are CO, NO, N_2O and NO_2. Available microwave data for the CO molecule have been analyzed by Lovas to calculate line position in the submillimeter region (LOV 74). Lovas (LOV 74a) also reviewed NO data providing sufficient information to allow the measurements at submillimeter frequencies. Predictions based on the extensive measurements of N_2O molecule by Krupnov's group demonstrate a large number of transitions in our frequency range of interest (AND 76). No predictions of submillimeter transition frequencies have yet been made for NO_2, but extensive microwave and infrared studies are in progress now at National Bureau of Standards, Washington D.C. (LOV 78). All of the molecules mentioned above have been studied experimentally by Fleming (FLE 74), who recently also performed precise submillimeter spectroscopy of freons and ozon and investigated the isotope effects in water and hydrogen sulphide (FLE 77).

4.8.2 Measurements on sulphur dioxide SO_2 around 820 GHz

Since the rotational constants of SO_2 are smaller than those of hydrogen sulphide, a much more dense absorption spectrum is anticipated for this molecule. Using microwave data Kivelson (KIV 54) obtained the following values of the rotational constants for SO_2: A_o = 2.027 cm^{-1}, B_o = 0.344 cm^{-1} and C_o = 0.293 cm^{-1}. The corresponding values for H_2S are 10.39 cm^{-1}, 9.04 cm^{-1} and 4.72 cm^{-1}(FLE 74). As SO_2 is a near prolate asymmetric rotor (Wang's prolate asymmetry parameter is -0.0146) transitions of the type $\Delta J = 0$, $\Delta K_{-1} = 1$ ("Q" branch) producing series of strong, closely spaced absorption lines dominate the

submillimeter spectrum. These absorptions have been observed in low resolution (7.5 GHz(0.25 cm^{-1}) by Stone (STO 62). Apart from the work of Krupnov (KRU 73) and Fleming (FLE 74) there appears to be no other report of the submillimeter spectrum of SO_2. Using Fourier transform spectrometry, Fleming observed a large number of lines, including several Q branches between 743 and 1190 GHz (25 cm^{-1} to 40 cm^{-1}), but the line positions could not be given to an accuracy better than 0.6 GHz (0.02 cm^{-1}) (FLE 74, FLE 76). A large number of SO_2 transitions (about 30) at frequencies accessible to the present spectrometer have been predicted by Lovas (LOV 78). His data based on microwave data up to J = 28 include also the line intensities.

A search for the SO_2 spectral lines was concentrated around 820 GHz where three transitions have been predicted (LOV 78): $18_{11,7} \leftarrow 17_{12,6}$ at 818.376570 GHz, $19_{5,15} \leftarrow 18_{4,14}$ at 820.150172 GHz and $23_{12,12} \leftarrow 22_{,13,9}$ at 821.060734 GHz.

The required frequencies were generated from the lower sideband of the most intense HCN laser emission line (890.760 GHz) mixed with the output of a (67-73)GHz Varian VRE 2103B8 klystron. Klystron power delivered to the diode was about 120 mW(maximum power available from klystron was $\sim$ 300 mW). The klystron was stabilized by locking its frequency to a K band (OKI 24V10 A) intermediate klystron, which was in turn locked to a frequency standard. The same technique has been used previously in the experiments of Zuidberg and van Dijk (ZUI 77, DIJ 71). The complete diagram of the video spectrometer and the klystron stabilization scheme used for absorption frequency measurements is shown in Fig. 4.21. A search for the absorption line was performed by scanning the Schomandl frequency decade ND30 M synthesizer while maintaining the klystron lock. The HCN

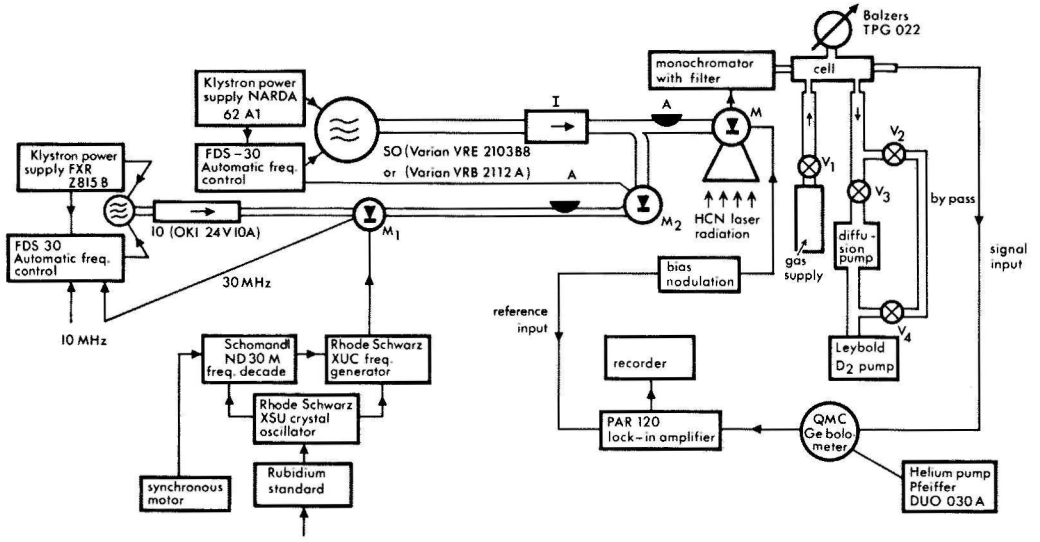

Fig. 4.21 Diagram of the complete high resolution spectrometer. SO-signal oscillator (E or W band klystron); IO - intermediate oscillator (K band klystron); I - isolator, M - triple arm mixer; M_1/M_2 mixer diodes; A - calibrated attenuator.

laser was operated in the striated free-running mode, without any stabilization. The sulphur dioxide gas was supplied by Matheson Gas Products with a quoted purity at 99.9%. The QMC bolometer was used to detect the difference-frequency signal after passing through the absorption cell.

Figure 4.22 shows a recorder trace of the $19_{5,15} \leftarrow 18_{4,14}$ SO_2 absorption line at a pressure of 0.04 Torr in the absorption cell. The line was recorded at ambient room temperature and the monochromator was not evacuated. There is a transmission "window" between 603 GHz and 990 GHz for which the attenuation by atmospheric water vapour absorption could be neglected. The integration time of the lock-in amplifier used to record the line

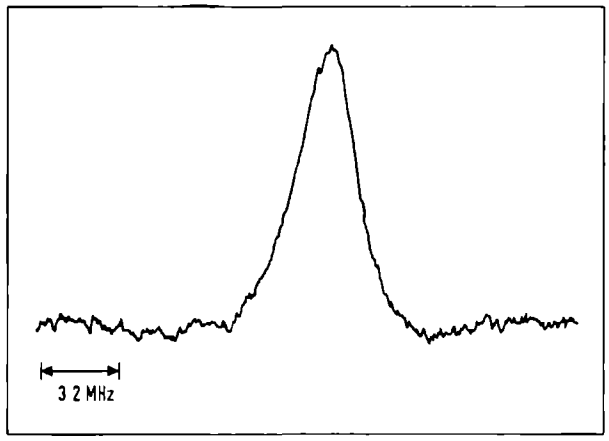

Fig. 4.22 Recorder trace of the $19_{5,15} \leftarrow 18_{4,14}$ transition of sulphur dioxide SO_2 at 820.151(2) GHz.

shape shown in Fig. 4.22 was 1 second.

The peak of the absorption line is found to have frequency 820.151(2) GHz which is in agreement with the frequency 820.150172 predicted by Lovas (LOV 78), but departs considerably from 821.19 GHz (27.373 cm^{-1}) measured by Fleming (FLE 74). The observed halwidth at half maximum is 1.2 MHz. At this frequency the calculated Doppler halfwidth of SO_2 is 636 kHz at room temperature. According to the simple theoretical approach about of Sugden (SUG 65) halfwidth of the line due to the pressure broadening is about 400 kHz at 0.04 Torr. Contributions of other sources to the line broadening in the present experimental conditions could be neglected, so that the expected total halfwidth of the theoretical line shape (convolution of Doppler and collision broadening) is 0.8 MHz. The measured halfwidth agrees fairly well with that expected from the calculations.

The uncertainly in the measured SO_2 frequency is larger than normally encountered in microwave absorption measurements.

The HCN laser was operated in an unstabilized free-running mode under working conditions that guaranteed high output power. However, it is not easy to set the laser exactly on the top of the laser gain profile at 890.760 GHz. Just this uncertainty and thermal drift of the laser frequency sets a limit to the experimental uncertainty in the measured frequency. Of course, frequency stabilization of the HCN laser would remove this source of uncertainty.

4.8.3 Measurement on hydrogen sulphide H_2S around 800 GHz

All strong transitions of $H_2{}^{32}S$ below 800 GHz have been observed in the laboratory (HEL 73). The strong $5_{4,2} \leftarrow 5_{3,3}$ transition (slightly above 800 GHz) with a line strength of 2.461 appeared as very suitable for testing the spectrometer. The predicted frequency was 800.855957 GHz with an estimated uncertainty of 1.629 MHz (HEL 73).

The Varian VRB 2112 A klystron with (86-92) GHz tuning range was used at microwave input arm of the mixer. Its output power was about 100 mW at desired frequency of 89.904 GHz. Hydrogen sulphide gas (99.5 % pure) was supplied by Matheson Gas Products Company.

The experimental technique was the same as described in Sect. 4.8.2. Instead of amplitude modulating the microwave power, the external bias modulation to the diode was applied. Modulation took place between the two points on I-V characteristics (across its zero point) corresponding to the minimum and maximum of the reradiated sideband (see Fig. 4.18). This modulation technique produced the same result as the on-off square wave modulation of the microwave power.

Figure 4.23 shows the measured H_2S line at a pressure of

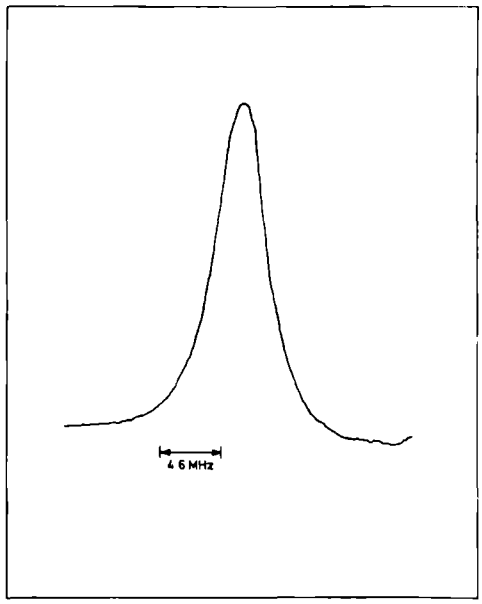

Fig. 4.23 Recorder trace of $5_{4,2} \leftarrow 5_{3,3}$ transition of H_2S at 800.853(2)GHz.

0.07 Torr in the absorption cell and at room temperature. The measured frequency is 800.853(2) GHz (BIC 78). This value assumes 890.760 GHz for the laser frequency. The observed half-width at half absorption maximum is 2.1 MHz, compared to the theoretically expected value of 1.1 MHz (Doppler broadening 850 kHz and collision broadening 700 kHz). The measured frequency agrees well with predicted one (LOV 78), but is in poor agreement with the value 797.65 GHz (26.84 cm^{-1}) reported by Fleming (FLE 74).

A slight asymmetry of the line shape is clearly seen in Fig. 4.23. It is most likely caused by the resonating character of the mixer and the monochromator, and can be regarded as an instrumental background effect. These uncontrolable resonant effects can occur in the mixer containing the waveguide stack

and along the signal path from the input to the output slit of the monochromator. However, it was possible to reduce their effect by substracting (in a computer of average transients, for example) the lock-in signals recorded with and without gas in the absorption cell.

The good signal to noise ratios obtained with SO_2 and H_2S has proved the feasibility of developed technique for high resolution spectroscopic application.

4.9 Generation of sum-frequency sideband near 1 THz

Extension of the present technique to the region above 1 THz via sum-frequency sideband generation was the logical step to follow the successful results obtained with the lower sideband. The (958-964) GHz part of the submillimeter spectrum can be covered using the 890 GHz laser transition and 70 GHz klystron. Using the weaker laser transition at 964 GHz would shift the operating range to (1032-1038) GHz without the need to replace the klystron.

First the magnitude of the reradiated sum-frequency sideband originating from 890 GHz laser and 70 GHz klystron radiation was studied because of the higher power available at 890 GHz. Because of its high rejection at the sum frequency (see Figs. 4.9 and 4.10) the metal mesh filter F370/II cannot be used at 960 GHz. The situation is further complicated by possible oscillation on the cascade laser transition $J(11)_- \rightarrow J(10)_+$ doublet levels of (1 1^1 0) vibrational state at 968 GHz that oscillates simultaneously with the 890 GHz transition. The intensity of the 968 GHz emission is about 1 % of that at 890 GHz under most favourable conditions for 968 GHz. Fortunately the 968 GHz leakage could be distinguished from the generated sum-frequency

sideband by its opposite phase after phase sensitive detection which simplified the optimization of the "true" sum-frequency signal at 960 GHz. In practice, minute displacements of the resonator and output coupling mirror, as well as adjusting the position of plungers proved sufficient to quench oscillation in the laser on the cascade transition.

The sum-frequency was quickly found and its origin was checked by the same sequence of tests used previously with the difference-frequency sideband. The magnitude of the reradiated signal was 60% (3×10^{-8}W) of that obtained with difference-frequency with the same SB diode modulation method and frequency and the same amount of laser and klystron power. Both, sum and difference-frequency sideband reradiated power was measured with the QMC bolometer, which contrary to RPY 23 Putley detector, has the same response at both frequencies.

Dependence of the reradiated sum-frequency power on the applied bias voltage was very similar to that observed with the same SB diode at 820 GHz (see Fig. 4.18). The maximum and the zero of reradiated power appear at about - 0.7 V and -1.3 V respectively, as in Fig. 4.18. The variation of reradiated power as a function of klystron or laser power also resembled the shape of the curves plotted in Fig. 4.19 and 4.20.

In closing this section we conclude that the present technique appears almost equally effective at the 960 GHz sum-frequency sideband, as it does at the 820 GHz difference-frequency sideband.

4.10 Generation of sum-frequency sideband at 1.037 THz

Results obtained at the 960 GHz sum-frequency sideband were sufficiently encouraging to suggest extension of this

technique to frequencies above 1 THz. No high resolution frequency measurements have been performed by this, direct generation technique in this frequency range.

Using the conventional triple arm mixer with an M.I.T. SB diode and whiskers of the same length and contact radius as reported previously, an attempt was made to generate the sum-frequency sideband at (964 + 73)GHz = 1.037 THz. The power available in the 964 GHz (311 μm) line, for this HCN laser was approximately 30% of the maximum attainable power at 890 GHz: The F370/II metal mesh filter could not be used at this sideband frequency.

After first optimizing the plunger position for maximum rectified signal at 964 GHz and then irradiating the diode with the usual amount of microwave power, the reradiated signal was easily found with good signal to noise ratio. The power at the 1.037 THz sum-frequency sideband was 50% of that obtained on the 820 GHz sideband using the same diode contact, klystron power, modulation type and frequency and the same detector. This figure does not account for smaller amount of laser available at 964 GHz, from which efficient operation at frequencies above 1 THz must be deduced.

The functional dependence of the reradiated power at 1.037 THz on the applied d.c. bias and klystron and laser power levels was very similar to the curves obtained with the same SB diode shown in Fig. 4.18, 4.19 and 4.20 respectively. Maximum reradiated signal occurred at the negative bias voltage required for largest video signal at 964 GHz, suggesting again that the best detector was also the best mixer. If measurements are repeated with new diode contacts the general shape of the reradiated power-external bias plot remains the same, but it is

shifted to larger negative voltages, depending on the form of the I-V characteristics.

4.11 Spectroscopic application - the measurement on sulphur dioxide SO_2 at 1.037 THz

In the tables of Lovas (LOV 78) six transitions are predicted within the spectral range of the available sum-frequency sidebands that could be generated by mixing 964 GHz and (67-73) GHz klystron. The only SO_2 frequencies measured above 1 THz are those obtained at low resolution by Fleming (FLE 74, FLE 77).

The sum-frequency near 1.037 THz was measured by locking the Varian VRE 2103B8 klystron to a frequency standard via an intermediate (OKI 24V10 A K band klystron using the same experimental apparatus shown in Fig. 4.21. Since absorption is generally strong, the initial search for an absorption line was performed simply by sweeping the klystron slowly across its mode ($\sim$ 150 MHz) with a ramp voltage applied to the reflector. The output of the detector was connected to the Y-input, and the ramp voltage (by suitable potential dividing network) to the X - input of the recorder.

Once the approximate frequency of an absorption line (evidenced as the absorption line (evidenced as the abrupt change in output signal in X-Y contour) was observed, the reflector voltage was fixed, and the line was recorded by sweeping the ND30 M Schomandl decade of the frequency lock system shown in Fig. 4.21.

Figure 4.24 is a recording of the SO_2 transition near 1.037 THz at a pressure of 0.05 Torr. This transition is assigned to $9_{9,1} \leftarrow 8_{8,0}$ transition and the predicted frequency is 1036.800539 GHz with an uncertainty of 206 kHz(LOV 78).

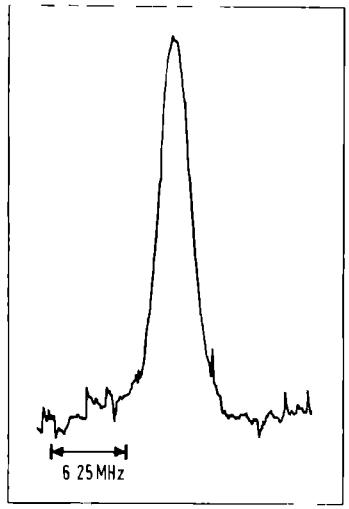

Fig. 4.24 Recorder trace of the $9_{9,1} \leftarrow 8_{8,0}$ transition of sulphur dioxide SO_2 at 1036.803(1) GHz.

The measured line peak frequency is 1036.803(1), GHz if 964.3134 GHz is assumed for laser carrier frequency. At 0.05 Torr and room temperature, pressure and Doppler halfwidth is 500 kHz and 803 kHz, respectively giving about 1 MHz for the total halfwidth due to both contributions. The observed halfwidth of the line 1.5 MHz agrees quite well with that predicted. The principal uncertainty in the measured line frequency arises from the uncertainty in the frequency of the unstabilized laser emission. at 964 GHz.

This measurement demonstrates clearly that for spectroscopic measurement above 1 TH sufficient power can be obtained by the fundamental mixing of laser and klystron in the present spectrometer. The measured absorption line of SO_2 is the highest transition frequency ever measured by a microwave generation technique. Other molecules such as asymmetric rotors H_2S, NO_2 and linear molecules as CO, NO and N_2O for example, remain yet

to be studied. The genrated radiation has the same properties as conventional microwaves, prooving thus that the microwave techniques can be successfully used above 1 THz mark. We believe that minor modifications on the microwave input side of the three waveguides mixer will permit further extension to still higher frequencies. Further improvements in sensitivity may result by switching to heterodyne detection or the use of another mixer design (see Chap. 5). Work on this matter is in progress (HEU 78).

C H A P T E R 5

CLOSING REMARKS AND FUTURE OUTLOOK

Although much experimental work has been done, the possibilities to improve the overall efficiency of this technique are far from being exhausted. We expect that the performance of the spectrometer, resulting in increased power levels at generated sidebands, may be improved by some modifications proposed below.

i) The coupling of the laser radiation to the diode structure is certainly not optimal. As one may see from the results presented in Chap. 4, the coupling of the laser signal to the mixer is of vital importance for the efficient generation and remission of the sidebands. An independent attempt was made using a triple arm mixer with the circular waveguide 0.6 mm in diameter instead of 1.2 mm; all other mixer components were the same as described in Sect. 4.3.1. This alteration caused a deterioration in performance (to about 40%) at the 820 GHz sideband. Only a very few measurements were performed in the early phase of the experiment with larger horn dimensions and a broader central waveguide, so at the moment little can be said about optimal dimensions. Since there are many different ways in which mixer assembly can be made, further investigation in this direction is probably worth the effort.

ii) In view of the rigorous requirement for the proper matching of the laser radiation to the diode mount, it is questionable whether reduction of the spot size without further modification in the mixer construction, would be advantageous for the system. For the purpose of reducing the spot

size utilization of silicon for the laser lens material is strongly suggested. This hard and easy to polish homopolar crystal does not absorb heavily ($\alpha < 0.5$ cm^{-1}) in the sub-millimeter band and has a constant refractive index 3.3 from 12 μm to 400 μm (CLM 70). An immediate advantage of using silicon instead of TPX or polyethylene as the laser lens material, is the higher power density achievable at the site of the diode due to the inherently smaller spot size obtainable with a silicon lens. Because of the considerable disproportion in the size of contact dimension and the spot size of the laser radiation in the junction plane, larger power flow reaching the diode, and possibly more pronounced non-linearity can be expected. By the courtesy of Philips Laboratory, Lent, The Netherlands, a slice of n-type, dislocation free silicon (resistivity 20 Ω cm) has been obtained (HOE 75). A plano-concave lens, 50 mm in diameter, 5 mm thick with 110 mm radius of curvature and 48 mm focal length has been designed here and manufactured in United Kingdom by Rofin Optics. With these constructional parameters, a spot size diameter of 0.85 mm was expected and verified by experiment. Transmission of the lens was measured to be 40% at 890 GHz. Due to the lack of time this silicon lens was never tried with the present mixer configuration. However, despite the considerable transmission loss, the experiments should be repeated.

iii) The major advantage of the three waveguide mixer is the possibility to tune the generating and the generated signals almost independently. However, even in the present type mixer, difficulties were experienced because the matching in one waveguide always affected to some extent the matching

in another waveguide. Since there are reasons enough to expect that further improvements are possible, future mixer designs may be considerably different from that used at present. In the triple arm mixer generated sidebands are extracted through the top waveguide; however the sideband power must also be available in the middle, laser waveguide. To eliminate this source of loss the present mixer could be adapted rather easily to a design using only one waveguide (PRE 76). Such a single level mixer consists of the diode placed in RG-99/U 70 GHz fundamental waveguide accepting the laser radiation, and a 70 GHz directional coupler functioning as the input arm for the microwave signal, as shown in Fig. 5.1.

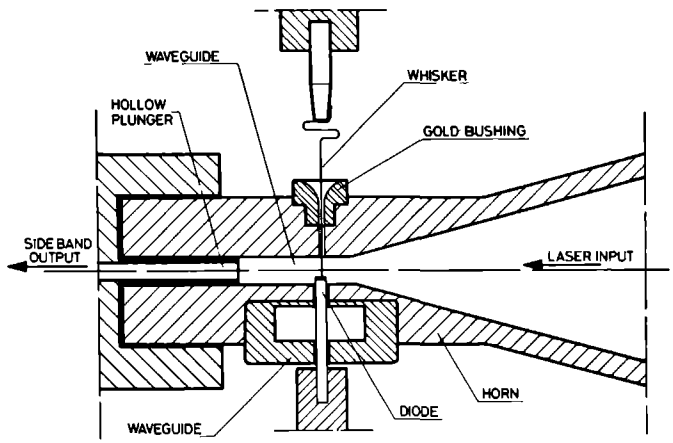

Fig. 5.1 Two level mixer

The coupling of the laser signal to such an oversize waveguide through a suitable horn would not be much of a problem in this configuration. The rectangular RG-136/U wave-

guide extending behind the junction, functions as the part of the 70 GHz short circuit by maintaining the distance between the "plunger" and the diode at approximately quarter wavelength at 70 GHz (see detail diagram in Fig. 5.1). Obviously in such design, lacking an sliding plunger, the independent tuning of laser and reradiated signals is not possible. Some degree of tuning could be obtained by displacing the complete mixer assembly with respect to the laser along the axis of the lens. Another option is to maintain a separate waveguide for the microwave input and to use the 1.2 mm diameter waveguide for receiving the laser radiation and propagating the sideband signals, thereby eliminating the third waveguide. Matching the microwave power is just as efficient as in the current mixer, but some other method has to be utilized to tune 890 GHz and reradiated signals. Preliminary experiments obtained with two waveguides mixer indicate power drop to 40% of the value at 820 GHz, but this result cannot be treated with any degree of finality and more measurements are required. One important advantage of single and/or double level mixer designs described above is that whiskers of considerably shorter effective length can be used. With present mixer, metalic antennas as long as 10 mm have been used, and the reactance of such a wire is certainly quite large at submillimeter frequencies. For comparison the commercially available MC 10890 borad band submillimeter detector from EMI Varian, uses a 0.25 mm long whisker with the SB diodes (PRE 76).

Using of corner reflector diode mount, instead of three waveguide stack mixer, offers another possibility

for future improvements. Recently, Fetterman et al. used a quasi optical configuration approach to design a corner reflector SB diode mixer, and obtained tunable laser sideband radiation of $\sim 10^{-7}$ W (FET 78). Such non-resonant mixer structure has another strong point in its favor, namely the actual completing of the diode contact can be observed under the microscope. This possibility is not present in the triple arm mixer where producing of the diode contact is still a matter of luck, and clearly the reproducibility is not guaranteed. Van den Heuvel (HEU 78) in Nijmegen, is currently constructing an open type device in the continuation of efforts to optimize the mixer design.

iv) Further improvement in overall efficiency could be obtained by using larger gratings, each blazed for maximum efficiency in the frequency range of interest. To enhance the reflectivity, silver or gold may be used as grating coating. Replacing the condensing mirror of the monochromator by a parabolic surface and matching the mouth of the collimating horn to the size of the grating might aid in reducing the insertion loss as already discussed (see Sect. 4.5). Finally, using a longer absorption cell is suggested.

v) The large majority of the experimental data published in this thesis were obtained with the M.I.T. SB diode. Diodes of different barrier sizes have been obtained by Prof. Mizuno (1 μm diameter) and Dr. Wrixon (2 μm diameter) are yet to be studied intensively. In the course of the experiment we have also tested silicon doped GaAs PC diode Physical properties of this material produced by Laser Diode Laboratories Inc. are as follows: ρ = (0.0021 - 0.0013) Ω cm (compared to 0.003 Ω cm for tellurium),

μ = (1917 - 1436) cm^2/V s and N_d = (1.4 - 3) x $10^{18}/cm^3$, as quoted by the manufacturer. The Si doped crystals exhibit interesting peculiarity in the form of I-V characteristics, namely the reverse knee is closer to the origin than for an ordinary PC or SB GaAs diode. Although the shape of the characteristics is not as non-linear as in the case of an average SB diode, absorption of klystron and laser power was very good. Substantial diode currents, exceeding 400 μA, without bias were obtained readily with 890 GHz radiation incident onto the diode, mounted in the triple arm mixer. It may be expected that the non-linearity nearer to the origin, will amply compensate for the less pronounced asymmetry of the I-V characteristics.

vi) Finally the utilization of a heterodyne system in place of direct broad band technique to detect the generated sidebands will definitively increase the sensitivity and the frequency selectivity of the spectrometer. The 890 GHz laser and the 70 GHz klystron radiation are coupled to the PC or SB diode in the first mixer (triple arm mixer for instance) and the composite beam of the generated frequencies is sent through the same filtering unit as described with the video system of Fig. 1.2. The possible output frequencies from the first mixer are determined from (z_1 890 $\pm$ z_2 70) GHz with z_1 and z_2 being integers 0, 1, 2, ... etc. The same laser (via a diplexer) or another HCN laser at 890 GHz is used to provide the local oscillator power for mixing in the second stage at another mixer M_2 (also an PC or SB diode). Mixer M_2 would be essentially a semi-closed structure (similar to M_1) and the coupling of the signal and the local oscillator powers

could be achieved by the appropriate lenses and horns. Slight modification of heterodyne detector designed by Zuidberg (ZUI 76, ZUI 77, ZUI 78) would be an excellent choice to be used for M_2. The output frequencies of first mixer beat with the local oscillator powers at 890 GHz and 70 GHz in second mixer to give out an intermediate frequency in the MHz range that could be further processed in the usual way. The application of the phase sensitive detective would reduce the effective noise bandwidth thereby improving the detection sensitivity (BRU 74, PRE 76).

Although such system is frequency selective and potentially much more sensitive than the video system, practical difficulties in dealing with the circuits of this kind may not be undersetimated. It was mainly for this reason that the relatively simpler video detection system was chosen above the more sophisticated heterodyne technique.

* * * * * * * *

Observations of H_2S and SO_2 transitions in the THz region with essentially quasi microwave techniques, the first of this kind ever performed, demonstrates the feasibility of the sideband generation technique for high resolution spectroscopy. Half-widths of 2 MHz (Doppler limited range) have been measured which represents a resolving power of 5×10^6. The encouraging results obtained so far suggest the advisability of further pursuing the development of this methode. Since the entire subject is still in an elementary state of development, just moved from the experimental to the application stage, no final conclusion can be made at the present time about how much may be gained in the immediate future.

Nevertheless, we expect that the continuous progress in the technology of tunable microwave sources, lasers and diode materials will lead to the possibility of producing monochromatic reradiated sidebands of considerably higher power levels. As essentially any klystron or carcinotron can be used to produce continuously tunable sidebands at the fixed frequencies of any discharge or optically pumped submillimeter laser, the development of the technique described in this thesis may be regarded as a practical route towards the definitive surmounting of the submillimeter barrier.

REFERENCES

AGE 68 G.V. Ageev, R.P. Bašuk, A.S. Bebčuk, N.S. Voidetskaja, D.A. Gromov, N. Solovljeva and A.V. Česnokov in "Proceedings of Second Symposium on Non-linear Optics", R.V. Hohlov (Ed.) p. 211, Nauka, Novosibirsk (1968)

AND 73 B.A. Andreev, A.V. Buremin, E.N. Karyakin, A.F. Krupnov and S.M. Shapiro, Jour. Mol. Spec. 62, 125 (1973).

BAR 74 A.S. Barker Jr., Bell Telephone Laboratories, Holmdel, New Jersey (USA), Priv. Comm. (1974).

BEC 70 R.E.J. Becklake and M.A. Smith, Rad. Elect. Eng. 39, 161 (1970).

BEE 62 W.R.J. Bennett, Appl. Opt. Suppl. 1, 24 (1962).

BEL 73 P. Belland and D. Veron, Opt. Comm. 9, 146 (1973).

BEN 69 F.A. Benson (Ed.), "Millimeter and Submillimeter Waves", Iliffe Books Ltd., London (1969).

BER 63 D. Belincourt, Phys. Rev. 129, 1009 (1963).

BIĆ 73 D.D. Bićanić, Quart. Rep. 39, 174 (1973).

BIĆ 74 D.D. Bićanić and A. Dymanus, Infr. Phys. 14, 153 (1974).

BIĆ 74a D.D. Bićanić, Quart. Rep. 42, 9 (1974).

BIĆ 74b D.D. Bićanić, Quart. Rep. 44, 23 (1974).

BIĆ 74c D.D. Bićanić, Quart. Rep. 43, 15 (1974).

BIĆ 74d D.D. Bićanić and G.E. Copeland, Appl. Phys. 5, 133 (1974).

BIĆ 75 D.D. Bićanić, Quart. Rep. 47, 57 (1975).

BIĆ 75a D.D. Bićanić, Quart. Rep. 49, 89 (1975).

BIĆ 75b D.D. Bićanić and A. Dymanus, Opt. Comm. 15, 175 (1975).

BIĆ 75c D.D. Bićanić, Quart. Rep. 46, 37 (1975).

BIĆ 76 D.D. Bićanić and A. Dymanus, Infr. Phys. 16, 601 (1976).

BIĆ 78 D.D. Bićanić, B.F.J. Zuidberg and A. Dymanus, Appl. Phys. Lett. 32, 367 (1978).

BIR 73 J.R. Birch and C.C. Bradley, Infr. Phys. 13, 99 (1973).

BON 74 E. Bonek and H. Korecky, Appl. Phys. Lett. 25, 740 (1974).

BOS 66 D.R. Bosomworth, Appl. Phys. Lett. 9, 330 (1966).

BOY 64 G.D. Boyd and H. Kogelnik, Bell Syst. Tech. Jour. 43, 2873 (1964).

BOY 71 G.D. Boyd, T.J. Bridges, M.A. Pollack and E.H. Turner, Phys. Rev. Lett. 26, 383 (1971).

Footnote: The abbreviation Quart. Rep. that appears in the list of references stands for Quarterly Report of the Atomic and Molecular Research Group Fysisch Laboratorium, Katholieke Universiteit, Nijmegen, The Netherlands. These reports, are written in English, if not stated otherwise and are available on request.

BOY 72 G.D. Boyd, T.J. Bridges, C.K.N. Patel and E. Buchler, Appl. Phys. Lett. 21, 553 (1972).

BOY 73 G.D. Boyd and M.A. Pollack, Phys. Rev. B. 7, 5345 (1973).

BRA 72 C.C. Bradley, G. Edwards and D.J.E. Knight, Rad. Elect. Eng. 42, 321 (1972).

BRA 72a C.C. Bradley, Infr. Phys. 12, 287 (1972).

BRI 70 T.J. Bridges, G.D. Boyd and M.A. Pollack, Proceedings of Symposium on Submillimeter Waves, p. 157, Polytechnic Institute of Brooklyn, New York (1970).

BRU 74 G. Brunt, EMI Electronics Ltd. Research and Development, Wells (Great Britain), Priv. Comm. (1974).

CHA 68 T.Y. Chang, N. van Tran and C.K.N. Patel, Appl. Phys. Lett. 13, 357 (1968).

CHB 65 J.E. Chamberlain, G.W. Chantry, E.D. Findlay, H.A. Gebbie, J.E. Gibbs, N.W.B. Stone and A.J. Wright, Infr. Phys. 6, 195 (1965).

CHY 69 G.W. Chantry, H. Ewans, J.W. Fleming and H.A. Gebbie, Infr. Phys. 9, 31 (1969).

CHY 71 G.W. Chantry, "Submillimeter Spectroscopy", Academic Press, London (1971).

CLI 71 B.J. Clifton, W.T. Lindley, R.W. Chick and R.A. Cohen, Proceedings Third Biennial Cornell Electrical Engineering Conference, p. 463, Ithaca, New York (1971).

CLM 70 P.D. Coleman and G. Sherman, Proceedings of Symposium on Submillimeter Waves, Polytechnic Institute of Brooklyn, p. 694, New York (1970).

COB 58 J.D. Cobine, "Gaseous Conductors", Dover Publications, New York (1958).

COL 76 M. Mc. Coll, D.T. Hodges and A. Garber, paper presented at Second International Conference on Submillimeter Waves and Their Applications, San Juan, Puertorico (1976).

COL 78 M. Mc. Coll, D.T. Hodges, A.B. Chase and W.A. Garber, Conference Digest of Third International Conference on Submillimeter Waves and Their Applications, p. 243, Guilford, Great Britain (1978).

CON 67 J.W. Conley and G.D. Mahan, Phys. Rev. 161, 681 (1967).

COR 69 V.J. Corcoran, R.E. Cupp and J.J. Gallagher, IEEE Jour. Quant. Elect. QE-5, 424 (1969).

COR 70 V.J. Corcoran, Appl. Phys. Lett. 16, 316 (1970).

CUB 51 T.K. Mc Cubbin Jr., Prog. Rep. Office of Naval Research (1951).

DAN 74 E.J. Danielewicz and P.D. Coleman, Appl. Opt. 13, 1164 (1974).

DYU 73 S.F. Dyubko and N. Topkov. Sov. Jour. Quant. Elect. 3, 56 (1973).
DIJ 71 F.A. van Dijk, Ph. D. Thesis, Katholieke Universiteit, Nijmegen (1971).
EVE 71 K.M. Evenson, J.S. Wells, L.M. Mataresse and D.A. Jennings, Jour. Appl. Phys. 42, 1233 (1971).
FAH 61 J. Fahrenfort, Spectrochim. Acta 17, 698 (1961).
FET 78 H.R. Fetterman, P.E. Tannenwald, B.J. Clifton, R.A. Murphy, C.D. Parker, W.D. Fitzgerald and N.R. Erickson, Appl. Phys. Lett. 33, 151 (1978).
FLE 74 J.W. Fleming, NPL Report Mat. Appl. 34, National Physical Laboratory, Teddington, Great Britain (1974).
FLE 77 J.W. Fleming, IEEE Trans. Instr. Meas. IM-25, 286 (1977).
FOX 61 A.G. Fox and T.Li, Bell Syst. Tech. Jour. 40, 453 (1961).
FUL 71 D.W.E. Fuller and B.O. Baker, Proceedings of the Joint Conference on Infrared Technics, p. 115, Reading, Great Britain (1971).
GAR 68 C.H.B. Garrett, IEEE Jour. Quant. Elect. QE-4, 70 (1968).
GEB 64 H.A. Gebbie, N.W.B. Stone and F.D. Finlay, Nature, 202, 169 (1964).
GLA 24 A. Glagolewa-Arkadiewa, Nature (London) 113, 640 (1924).
GOR 64 W. Gordy and G. Jones, Phys. Rev. 135, A295 (1964).
GRE 66 W.R. Gretsch, Proc. IEEE 54, 1528 (1966).
GUS 74 T.K. Gustafson and T.J. Bridges, Appl. Phys. Lett. 25, 56 (1974).
HAD 67 A. Hadni, "Essentials of Modern Physics Applied to the Study of Infrared", Vol. 2, Pergamon Press, oxford (1967).
HAG 04 E. Hagen and H. Rubens, Phil. Mag. 7, 157 (1904).
HAR 73 W.L. Harries, Physics Department, Old Dominion University, Norfolk, Virginia (USA), Priv. Comm. (1973).
HAT 73 T. Hattori, Y. Homa, A. Mitsuishi and M. Tacke, Opt. Comm. 7, 229 (1973).
HEA 68 H.G. Heard, "Laser Parameter Measurements Handbook", John Willey and Sons Inc., New York (1968).
HEL 73 P. Helminger, F.C. de Lucia and W.H. Kirchoff, Jour. Phys. Chem. Ref. Data 2, 215 (1973).
HEU 78 F.C. van den Heuvel, Fysisch Laboratorium, Katholieke Universiteit, Nijmegen, Priv. Comm. (1978).
HEW 67 Hewlett-Packard Associates, Application Note 907 (1967).
HOC 67 D. Hocker, Phys. Rev. Lett. 26A, 255 (1967).
HOD 77 D.T. Hodges and M. Mc Coll, Appl. Phys. Lett. 30, 5 (1977).

HOE 75 G. Hoekstra, Philips Research Laboratories, Lent, The Netherlands, Priv. Comm. (1975).
HUI 66 C. Huiszoon, Ph.D. Thesis, Katholieke Universiteit, Nijmegen (1966).
ISO 75 S. Isomura, National Institute for Metal Research, Tokyo, Japan, Priv. Comm. (1975).
JAM 67 D.J. James and J. Ring, Jour. de Phys. C2, 28, 150 (1967).
JOH 69 C.J. Johnson, G.H. Sherman and R. Weil, Appl. Opt. 8, 1667 (1969).
KAM 70 I.P. Kaminow, T.J. Bridges and M.A. Pollack, Appl. Phys. Lett. 16, 416 (1970).
KEL 78 W.M. Kelly and G.T. Wrixon, Conference Digest of the Third International Conference on Submillimeter Waves and Their Applications, p. 245, Guildford, Great Britain (1978).
KIM 70 M.F. Kimmit, "Far Infrared Techniques", Pion Limited, London (1970).
KIV 54 D. Kivelson, Jour. Chem. Phys. 22, 904 (1954).
KLE 62 D.A. Kleinman, Phys. Rev. 126, 1977 (1962).
KOG 66 H. Kogelnik and T. Li, Appl. Opt. 5, 1550 (1966).
KON 67 S. Kon, M. Yamanaka, J. Yamamoto and H. Yoshinaga, Jap. Jour. Appl. Phys. 6, 612, (1967).
KOR 78 K. de Kort, Fysisch Laboratorium, Katholieke Universiteit, Nijmegen, Priv. Comm.
KOT 68 J.P. Kotthaus, Diplomaarbeit, Technische Hochschule München, West Germany (1968).
KRU 73 A.F. Krupnov,"Broad-Band Microwave Spectroscopy in millimeter and submillimeter wave range", Radiophysical Research Institute, Gorky, Soviet Union (1973).
KUH 74 J. Kuhl and W. Schmidt, Appl. Phys. 3, 251 (1974).
LAR 64 S.J. Laredo, Proc. Inst. Elect. Eng. 111, 1417 (1964).
LEN 66 B.A. Lengyel, "Introduction to Laser Physics", John Willey and Sons Inc., New York (1966).
LEU 78 E.G.H. van Leeuwen, Fysisch Laboratorium, Katholieke Universiteit, Nijmegen Priv. Comm. (1978).
LEV 66 A.K. Levine, "Lasers", Marcel Dekker Inc., New York (1966).
LID 67 D.R. Lide and A.G. Maki, Appl. Phys. Lett. 11, 62 (1967).
LLE 67 F. Llewellyn-Jones, "Ionization and Breakdown in Gases", Methuen and Co. London (1967).
LOE 67 E.V. Loewenstein and A. Engelsrath, Jour. de Phys. C2, 8, 153 (1967).
LOV 74 F.J. Lovas and P.H. Krupenie, Jour. Phys. Chem. Ref. Data 3, 245 (1974).

LOV 74a F.J. Lovas and D. Tiemann, Jour. Phys. Chem. Ref.Data 3, 609 (1974).

LOV 78 F.J. Lovas, United States Department of Commerce, National Bureau of Standards, Washington D.C. (USA) Priv. Comm. (1978).

LOW 72 E. Loewen, "Diffraction Handbook", Bausch and Lomb Inc., Rochester (1970).

MAL 63 K.B. Mallory, R.H. Miller and P.A. Szente, IEEE Trans. Micr. Theory Techn. MTT-11, 433 (1963).

MAR 67 D.H. Martin (Ed.), "Spectroscopic Techniques for Far-Infrared, Submillimeter and Millimeter Waves", North Holland Publishing Co., Amsterdam (1967).

MAT 70 L.M. Matarrese and K.M. Evenson, Appl. Phys. Lett. 17, 8 (1970).

MID 65 J.E. Midwinter and J. Warner, Brit. Jour. Appl. Phys. 16, 1135 (1965).

MIZ 75 K. Mizuno, R. Kuwahara and S. Ono, Appl. Phys. Lett. 26, 605 (1975).

MOE 74 K.D. Moeller, Farleigh Dickinson University, Teaneck, New Jersey (USA), Priv. Comm. (1974).

MOR 70 J.M. Moran, IEEE Jour. Quant. Elect. QE-6, 93 (1970).

NIC 23 E.F. Nichols and J.D. Tear, Phys. Rev. 21, 587 (1923).

NIE 69 G.T. Mc Nice and V.E. Derr, IEEE Jour. Quant. Elect. QE-5, 569 (1969).

NIK 77 D.N. Nikogosyan, Kvant. Elekt. 4, 5 (1977) (in Russian)

NOB 73 P.W. Noble, ICI, Imperical Chemical Industries Ltd. Plastics Division, Welwyn Garden (Great Britain) Priv. Comm. (1973).

NOW 75 T. Nowicky, Inrad, Interactive Radiation Inc., Technical Note 501 (1975).

NYE 60 J.F. Nye "Physical Properties of Crystals", Clarendon Press, Oxford (1960).

OHL 58 R.C. Ohlmann, Richards P.L. and M. Tinkham, Jour. Opt. Soc. Amer. 48, 531 (1958).

ORL 64 L.M. Orloff, Proc. IEEE 52, 173 (1964).

ONO 70 S. Ono, K. Hotta and Y. Shibata, Proceedings of Eighth Conference on Microwave and Optical Generation and Amplification, p. 21-24, Kluwer, Deventer (1970).

PRE 76 B.E. Prewer, EMI Electronics Ltd., Research and Development, Wells, Great Britain, Priv. Comm. (1976).

RAD 75 H.E. Radford, IEEE Jour. Quant. Elect. QE-11, 213 (1975).

ROS 76 M. Rosenbluch, R.J. Temkin and K.J. Button, Appl. Opt. 15, 2635 (1976).

ROS 73 D. Röss, "Lasers, Light Oscillators and Amplifiers", Academic Press Inc., London (1973).

SAN 72 A. Sanchez, S.K. Singh and A. Javan, Appl. Phys.Lett. 21, 240 (1972).
SAU 77 K. Sauter and G.V. Schulz, IEEE Trans. Micr. Theory Techn. MTT-25, 468 (1977).
SHA 72 L.E. Sharp and A.T. Wetherell, Appl. Opt. 11, 1737 (1972).
SHE 76 Y.R. Shen, Prog. Quant. Elect. 4, 207 (1976).
SHE 77 Y.R. Shen (Ed.), "Non-linear Infrared Generation", Topics in Applied Physics Vol. 16, Springer Verlag, Berlin (1977).
SMA 73 J.G. Small, Physics Department, Massachusetts Institute of Technology, Cambridge, Massachusetts (USA), Priv. Comm. (1973).
SMA 74 J.G. Small, Ph.D. Thesis, Massachusetts Institute of Technology, Cambridge, Massachusetts (USA) (1974).
SOC 67 V. Sochor and E. Brannen, Appl. Phys. Lett. 10, 232 (1967).
STA 69 O.M. Stafsudd and Y.C. Yeh, IEEE Jour. Quant. Elect. QE-5, 377 (1969).
STO 63 N.W.B. Stone, Ph. D. Thesis, University of London (1963).
SUG 65 T.M. Sugden and C.N. Kenney, "Microwave Spectroscopy of Gases", Van Nostrand Co. Ltd., London (1965).
SVI 71 V.A. Svich and S.F. Dyubko, Sov. Phys. Tech. Phys. 10, 812 (1971).
TAC 75 M. Tacke, Max Planck Institut für Festkörperforschung, Stuttgart, West Germany, Priv. Comm. (1975).
THO 33 J.J. Thompson, "Conduction of Electricity through Gases", Cambridge University Press (1933).
TOR 48 H.C. Torrey and C.A. Whitmer, "Crystal Rectifiers", Mc Graw-Hill Book Co. Inc., New York (1948).
TRA 72 K. Tradowsky, "Lasers", Prisma Technica 48, Het Spectrum, Utrecht (1972).
TUR 71 R. Turner and T.O. Poehler, Jour. Appl. Phys. 42, 3819 (1971).
ULR 76 R. Ulrich, Max Planck Institut für Festkörperforschung, Stuttgart, West Germany, Priv. Comm. (1976).
VAL 72 R. Valitova (Ed.), "Technics of Submillimeter Waves", Soviet Radio, Moscow (1972) (in Russian).
VAN 76 J. Vanderkooy and C.S. Kang, Infr. Phys. 16, 627 (1976).
VOL 72 R. Volk, Phys. Lett. 42A, 321 (1972).
WEL 71 J.S. Wells, K.M. Evenson, L.M. Matarrese, D.A. Jennings and G.L. Wichman, Technical Note 395, National Bureau of Standards, Boulder, Colorado (USA), (1971).

WIT 76 A. Wittlin, Polish Academy of Sciences, Warsaw Poland, Priv. Comm. (1976).

WRI 78 G.T. Wrixon, Conference Digest of Third International Conference on Submillimeter Waves and Their Applications, p. 208, Guildford Great Britain (1978).

YAJ 70 T. Yajima and N. Takeuchi, Jap. Jour. Appl. Phys. 9, 1361 (1970).

YAM 70 M. Yamanaka, H. Yoshinaga and S. Kon. Jap. Jour. Appl. Phys. 7, 250 (1970).

YAM 78 M. Yamanaka, M. Wakamiya, M. Takada and H. Yoshinaga, Conference Digest of Third International Conference on Submillimeter Waves and Their Applications, p. 61, Guildford, Great Britain (1978).

YOS 74 K. Yoshihiro and C. Yamanouchi, Rev. Sci. Instrum. 45, 767 (1974).

ZER 65 F. Zernike and P.R. Berman, Phys. Rev. Lett. 15, 999 (1965).

ZER 73 F. Zernike and J.E. Midwinter, "Applied Non-linear Optics", John Willey and Sons. Inc., New York (1973).

ZUI 76 B.F.J. Zuidberg and A. Dymanus, Appl. Phys. Lett. 29, 643 (1976).

ZUI 77 B.F.J. Zuidberg, Ph. D. Thesis, Katholieke Universiteit Nijmegen (1977).

ZUI 78 B.F.J. Zuidberg and A. Dymanus, Appl. Phys. 16, 375 (1978).

Summary

This thesis describes the development and the results of new technique for the generation of continuously tunable submillimeter radiation. The non-availability of sources capable of substantial emission is the main reason that the submillimeter region of the electromagnetic spectrum (100 - 1000) μm has been only marginally explored in the past. In general the amounts of submillimeter power that can be obtained either from an ordinary incandescent source, or by harmonic generation of microwave frequencies is much too weak for many practical applications.

The development of powerful infrared CO_2 lasers allowed the indirect generation of submillimeter radiation by frequency mixing two slightly different frequencies of two lasers in a suitable acentric crystal. The reradiated difference-frequency lies then in the submillimeter spectral region. In recent years a large number of discharge and optically pumped submillimeter-wave lasers emitting at many discrete frequencies have also become available.

Although high power output, spatial and temporal coherence are prominent advantages that make a laser very attractive spectroscopic spurce, the extent of the tuning range that can be achieved is ultimately by width of the Doppler broadened gain profile of the laser emission line. Since Doppler width in submillimeter is only a few MHz and few hundred MHz in infrared, only quasi tunable radiation could be obtained with above mentioned techniques.

Many application, spectroscopy in particular welcome continuously tunable coherent source of the submillimeter radiation. Using a metal-semiconductor point-contact and Schottky barrier diode as a mixer, we have successfully produced submillimeter sidebands by frequency mixing the radiation of a HCN laser and that of microwave klystron. The tunability of the klystron (several GHz) is thereby simply transformed to the submillimeter region, and the intense generated sidebands at both sides of fixed frequency HCN laser are continuously tunable within the tuning range of the klystron. In such way, an interesting analogy is established between the generating radiations on one side, and the generated radiation on the other side. The usability of this technique has been verified by carrying out the high resolution absorption spectroscopic studies of H_2S and SO_2 in the Doppler limited region.

In addition to a brief historical review Chapter 1 contains an outline of submillimeter sidebands generation experiments in bulk crystals used as the non-linear medium. Characteristic

features of the 8 m long high power output HCN laser operating in the continuous mode, used as the initial submillimeter source for sideband frequency conversion, are discussed in Chapter 2. All experimental attempts aimed at obtaining the highest attainable amount of power on a single transition of HCN laser are summarized in Chapter 3. After reviewing basic considerations concerning the high frequency performed of point contact diodes, Chapter 4 includes a detailed description of the triple arm mixer, which is the heart of the apparatus for the generation of tunable sidebands. Remaining components of the spectrometer are also discussed in extenso. The chapter is completed by several sections dealing with the generation of sum and difference-frequency sidebands of 890 and 964 GHz laser emission lines. The strength of reradiated signals was sufficient to allow high resolution absorption frequency measurements on H_2S and SO_2. The first of this kind ever performed at such high frequencies. Finally, the last Chapter presents closing remarks and suggests a number of possibilities to improve the performance of the present system. Since, in principle, any arbitrary submillimeter (or optically pumped) laser and microwave source (klystron or carcinotron) can be used, this method opens a new way towards the practical generation of continuously tunable submillimeter - wave radiation.

Samenvatting

Dit proefschrift beschrijft de resultaten van een onderzoek dat binnen enkele jaren leidde tot de ontwikkeling van een nieuwe techniek om submillimeter straling te genereren met continu afstembare frequentie. De voornaamste reden waarom in het verleden relatief weinig onderzoek is gedaan in het submillimeter gebied van het elektromagnetisch spektrum (100 - 1000 μm) is het gebrek aan stralingsbronnen met een vermogen van enige betekenis. In het algemeen is het submillimeter vermogen dat een zwarte straler afgeeft, of dat men kan verkrijgen door de generatie van microgolf frequenties te zwak voor vele praktische toepassingen.

De ontwikkeling van sterke infrarood CO_2 laser bood een nieuwe mogelijkheid om indirekt submillimeter straling te genereren, gebaseerd op niet-lineaire interakties in acentrische kristallen. In diverse experimenten werden twee enigszins verschillende frequenties van twee CO_2 lasers gemengd in een geschikt niet-lineair kristal met de mengprodukt hun verschilfrequentie, de submillimeter straling. De opkomst en voortdurende technische verbetering van talrijke submillimeter en optisch gepompte lasers gedurende de laatste jaren resulteerde in een groot aantal sterke laser lijnen welke nu beschikbaar zijn voor experimenten.

Hoewel zijn hoge vermogen en coherentie een laser erg aantrekkelijk maken voor spektroscopische doeleinden, blijft zijn afstembaarheid beperkt tot de breedte van de verbrede gain profile ter plaatse van de emissie-frequentie van de laser. Aangezien de Doppler-breedte in het submillimeter gebied slechts enkele MHz bedraagt (hoewel enkele honderden MHz in het infrarood gebied), kon met bovengenoemde technieken slechts stapsgewijze, quasie-verstembare straling verkregen worden.

Echter, vele toepassingen, in het bijzonder de spectroscopie, vragen om continu afstembare submillimeter straling. Met behulp van een metaal-halfgeleider diode als mixer hebben wij met succes de generatie aangetoond van submillimeter zijbanden door de frequentie van een HCN laser te mengen met die van een microgolf klystron. Aangezien het afstemgebied van het klystron (enkele GHz breed) daarbij wordt overgeplaatst naar de krachtig gegenereerde zijbanden aan weerszijde van de vaste HCN laser frequentie, zijn deze ook continu afstembaar binnen het afstemgebied van klystron. Op deze wijze is er een interessantie analogie tot stand gebracht tussen de genererende bronnen enerzijds en de gegenereerde bron anderzijds. De kracht van deze techniek is bewezen met een spektroscopische studie van de gassen H_2S en SO_2 met een, hoewel door de Doppler verbreding begrensd, hoog

oplossend vermogen.

Behalve een kort historisch overzicht bevat Hoofdstuk 1 ook de beschrijving van een experiment met betrekking tot de generatie van submillimeter zijbanden in bulk kristallen als niet-lineair medium. De karakteristieken van een 8 m lange HCN laser met een hoog continu vermogen, welk als primaire submillimeter bron voor de generatie van zijbanden werd gebruikt, worden in Hoofdstuk 2 nader bekeken. Alle experimentele pogingen om het hoogst mogelijke vermogen te verkrijgen uit een enkele HCN laser overgang zijn samengevat in Hoofdstuk 3. Na een beschouwing met betrekking tot het gedrag van een punt-contact diode bij hoge frequenties vervolgt Hoofdstuk 4, overigens het meest uitgebreide hoofdstuk, met een gedetailleerde beschrijving van de drievoudige mixer, het hart van de opstelling voor zijbanden generatie. Hoofdstuk 4 eindigt met enkele secties waarin de generatie wordt behandeld van de beide zijbanden van zoveel de 890 als de 964 GHz laserlijnen. Het vermogen van de uitgestraalde zijbanden was voldoende om de frequenties van absorptie lijnen van H_2S en SO_2 met hoog oplossend vermogen te kunnen meten. Het laatste hoofdstuk tenslotte bevat conclusies en somt enkele mogelijkheden op om de werking van het huidige systeem te verbeteren.

Aangezien in principe elke submillimeter laser (al dan niet gepompt) em microgolf bron (klystron of carcinotron) gebruikt kan worden, opent de gepresenteerde methode nieuwe wegen naar een praktische en continu afstembare stralingsbron in het submillimeter gebied.

Curriculum vitae

The author of this thesis was born on March 13,1943 in city of Zagreb(Croatia) Yugoslavia. He graduated from "II Gimnazija Braća Ribar", Zagreb in 1961 and enrolled as a fresman in the the Faculty of Sciences of the University of Zagreb the same year. In 1966 he received there a Eng. Phys. degree (bachelor degree in technical physics) for the thesis entitled "Magnetic susceptibility measurements of Hg [$Co(CNS)_4$] and hemoglobine by the Faraday method"", completed at the Institute for Atomic Physics Research "Ruder Bošković" in Zagreb. In 1967 he was appointed research associate at the Insitute for Aerodynamical and Thermodynamical Research IAT in Zagreb. A year later he left for the United States of America to go on to work for a M.Sc. degree of the Old Dominion University at Norfolk, Virginia. In 1969 he joined the Modern Optics and Spectroscopy Laboratory in Norfolk, where he carried out research on plasma diagnostics of the argon ion laser under a NASA Langley Research Center grant. After election to Sigma Pi Sigma honor society, the author obtained his M.Sc. degree from Old Dominion University for a thesis entitled "Spectroscopic measurement of the electron temperature in the tenuous argon ion laser plasma" in 1971. After graduation he worked as a teacher at Norfolk Academy and instructor at Old Dominion University Physics Department. In the same year he received a Ph.D. fellowship from the Department of Physics and Astronomy at the University of Oklahoma at Norman, to continue the work on argon ion lasers with Prof. R. St. John. Late in 1971, the author returned to Europe, and took up a post in Department of Atomic and Molecular Physics, Fysisch Laboratorium, Katholieke Universiteit, Nijmegen, The Netherlands. There he has worked under the guidance of Prof. A. Dymanus on the construction of continuously tunable coherent source of submillimeter radiation and the extension of high resolution spectroscopy beyond 1 THz mark.

S T E L L I N G E N

I

De methode van generatie van kontinu afstembare zijbanden via het opmengen van laser en klystron straling in punt-contact diodes opent de mogelijkheid tot het verrichten van hoog-oplossend vermogen spektroskopie door het gehele submillimeter gebied.

Dit proefschrift

II

Het belang van de reële waarde van de stabilitietsfaktor g bij de bepaling van de totale verliesfaktor van submillimeter laser resonators is vaak miskend.

III

De faktor welke door Baldwin wordt gebruikt voor het omrekenen van de tweede order susceptibiliteit vanuit het gerationaliseerde MKS naar het niet-gerationaliseerde CGS stelsel is onjuist.

G.C. Baldwin, "An Introduction to Nonlinear Optics", Plenum Press New York (1969) blz. 83

IV

De suggestie van Alexander et al. dat er vier onafhankelijke intensiteiten gemeten kunnen worden door variatie van polarisatie indien laser bundel, moleculaire bundel en de detektie richting loodrecht op elkaar staan is onjuist.

M.H. Alexander, P.J. Dagdigian and A.E. DePristo, Jour. Chem. Phys. 66, 59 (1977)

V

Bij zeer jonge kinderen met een hersenletsel moet men zo vroeg mogelijk beginnen met neurofysiologische bewegingstherapie om het ontstaan van pathologische bewegingspatronen te voorkomen. De integratie van deze sensomotorische aanpak in het dagelijks leven is een eerste vereiste voor het slagen van deze therapie.

VI

Bij spiertraining van been- en heupspieren dienen behalve warming-up oefeningen, óók rek- en onstspanningsoefeningen toegepast te worden ter voorkoming van blessures bij plotselinge start- of stopakties.

VII

Bij bevolkingsonderzoek op borstkanker door middel van mamographie mag worden aangenomen dat het aantal gespaarde levens meer dan honderd maal groter is dan het aantal doden geinduceerd door de gebruikte straling.

J.H.C. Hendriks, Symposium Stralingsgevaar, Enschede (1978)

VIII

Het introduceren van niet-authentieke interpretatieve finesses en dynamische nuances in het choreographie-repertpoire van sommige folkloristische dansgroepen wijst op een gebrek aan respekt voor de rijke culturele erfenis van zuidslavische volken.

IX

Het behandelen van het zeer jonge neuromotorisch gehandicapte kind door de ouders levert onder bepaalde omstandigheden ongunstige effekten op die voorkomen hadden kunnen worden als bij het aanmeldings- en vervolgonderzoek meer aandacht besteed zou zijn aan het niveau en de wijze van interaktie tussen de ouders en het kind.

J. de Moor, wordt gepubliceerd

X

Het kan verwacht worden dat jaarlijks terugkerende sportevenement(en) die openstaan voor alle werknemers en studenten de algemene verhoudingen tussen de verschillende afdelingen zullen verbeteren, en bij zullen dragen tot vorming van tradities binnen de Faculteit Wiskunde en Natuurwetenschappen te Nijmegen.

XI

Het is wenselijk dat er meer bekend wordt over aan patiënten toegediende straling zowel kwalitatief als kwantitatief. Dat kan geschieden door i) aanschaffing en gebruik van meetapparatuur binnen Röntgen Diagnostiek Afdelingen of ii) kontrole door de overheid.

XII

Bij de chronische fatigue klachten is het vaak zeer moeilijk somatische en psychische faktoren afzonderlijk te waarderen. De onderzoeker moet er op bedacht zijn dat het lang niet altijd om een of-of kwestie gaat, maar om een en-en kwestie.

XIII

Zestig percent van alle sportblessures worden veroorzaakt door onoplettendheid van de sporters.

R. Hendriksen, RKZ Hilversum
wordt gepubliceerd

XIV

Een hulpbehoevende kan het best geholpen worden door hem jou te laten helpen.

XV

Mochten op een dag de sociale verschillen tussen de mensen verdwenen zijn, dan blijven er toch nog, gelukkig, de verschillen over.

Nijmegen, 20 december 1978 *D.D. Bićanić*